Deconvoluting the Resident Mesenchymal Stromal Cell Niche for AT2 Stem Cells in Homeostasis and Disease in Adult Murine Lung

Inaugural Dissertation

Submitted to the

Faculty of Medicine

In partial fulfilment of the requirements for the

PhD-Degree of the Faculties of Veterinary Medicine and Medicine

Of Justus Liebig University Giessen

By:
Sara Taghizadeh

Of

Chaboksar, IRAN

Gießen 2022

From the Department of Internal Medicine II

Director / Chairman: Prof. Dr. Werner Seeger

of the Faculty of Medicine of the Justus Liebig University Giessen

First Supervisor and Committee Member: Prof. Dr. Saverio Bellusci

Second Supervisor and committee Member: Prof. Dr. Reinhard Dammann

Committee Member (Chair): Prof. Dr. Klaus Schlüter

Committee Member: Prof. Dr. Xin Sun

Date of Doctoral Defence: 27.09.2022

Declaration

“I declare that I have completed this dissertation single-handedly without the unauthorized help of a second party and only with the assistance acknowledged therein. I have appropriately acknowledged and referenced all text passages that are derived literally from or are based on the content of published or unpublished work of others, and all information that relates to verbal communications. I have abided by the principles of good scientific conduct laid down in the charter of the Justus Liebig University of Giessen in carrying out the investigations described in the dissertation.”

_____

Sara Taghizadeh

List of figures

List of tables

Abbreviations and Acronyms

ADRP	Adipose differentiation-related protein
AT1	Alveolar epithelial cell type I
AT2	Alveolar epithelial cell type II
AMPs	Alveolar mesenchymal progenitors
ASC	Adult stem cell (aSC)
BASC	Brochioalveolar stem cell
BMP 4	Bone morphogenetic protein 4
BPD	Bronchopulmonary dysplasia
Br	Bronchi
Brl	Bronchiole
CCSP	Club cell secretory protein
COPD	Chronic obstructive pulmonary disease
CLD	Chronic lung disease
E	Embryonic
ECM	Extracellular matrix
EGF	Epidermal growth factor
ESC	Embryonic stem cell
FACS	Fluorescence-activated cell sorting
FEV1	Forced expiratory volume in one second
FGF10	Fibroblast growth factor
FGFR	Fibroblast growth factor receptor
GFP	Green fluorescent protein
GLI1	Glioma-Associated Oncogene 1
HBSS	Hanks balanced salt solution
HYX	Hyperoxia
ID2	Inhibitor of differentiation 2
IPSC	Induced pluripotent stem cell (iPSC)
IVC	Inspiratory vital capacity
LIF	Lipofibroblast

MANC	Mesenchymal alveolar niche cell
MYF	Myofibroblast
NEBs	Neuroendocrine bodies
NF-κB	Nuclear factor 'kappa-light-chain-enhancer' of activated B-cells
NOX	Normoxia
P	Postnatal
PBS	Phosphate-buffered saline
PDGF	Platelet-derived growth factor
PDPN	Podoplanin
PECAM	Platelet endothelial cell adhesion molecule
PFA	Paraformaldehyde
PPARγ	Peroxisome proliferator-activated receptor gamma
PTHRP	Parathyroid hormone-related protein
RA	Retinoid acid
RMC	Resident mesenchymal cell (rMC)
SCGB1A1	Secretoglobin, Family1A, Member 1
SDS	Sodium dodecyl sulfate
SEM	Subepithelial mesenchyme
SFTPC	Surfactant protein C
SFTPB	Surfactant protein B
SHH	Sonic hedgehog
SMM	Submesothelial mesenchyme
3D	Three-dimensional
TAE	TRIS-Acetate-EDTA
TBS-T	TRIS-buffered saline with Tween 20
TGF-β1	Transforming growth factor -β1
TLR	Toll-like receptor
VEGF	Vascular endothelial growth factor
VEGFR	Vascular endothelial growth factor receptor
WNT	Wingless and int

1. Introduction

1.1 The basics of lung development

The respiratory system is comprised of the lung, trachea, associated vasculature, and nerves. The primary function of this system is gas exchange, which takes place in alveolar sacs. This function is orchestrated by many cell types located along a proximal to distal axis.

During embryogenesis in mice, lung development starts at embryonic day 8 (E8) with the specification of the lung domain in the anterior foregut endoderm. Nkx2.1 is the earliest known marker expressed in the lung domain and a transcriptional factor which plays a crucial role in respiratory system formation. It regulates gene expression through cellular and molecular processes such as proliferation, differentiation, migration, and apoptosis (1).

The respiratory tree-like structure starts with two buds, the rudimentary primary bronchi, at E9 out of the ventral foregut endoderm. The trachea is also forming independently in a more anterior position, demonstrating that the trachea and the lung arise from different endodermal progenitors. Two lung buds will elongate to create the two main bronchi and subsequently ramify to give rise to the arborized tree-like structure of the lung. Lung development can be divided into five histologically different stages. The embryonic, pseudoglandular, canalicular, saccular, and alveolar are five stages in the mouse lung. Lung development is divided into two main programs: branching morphogenesis and alveolar differentiation.

The first stage is called the embryonic stage: it is pretty unclear when it ends. Primary buds and trachea form at this stage and are associated with minimal branching of the primary buds.

The second stage of lung development is called the pseudoglandular stage, during which branching morphogenesis is a hallmark event. This stage occurs from E9.5 to E16.5 when branching morphogenesis generates the basic tree-like structure of the lung, including the conducting airways and the numerous terminal bronchioles surrounded by dense mesenchyme. At the same time, epithelial cell progenitors differentiate into basal, neuroendocrine, ciliated, and secretory cells. The mesodermal lung compartment serves as

progenitors for the smooth muscle, lymphatic, endothelial, nerve, and chondrocyte cells. Notably, most of the lung's epithelial and mesenchymal cell types are formed during the late pseudoglandular stage (E13.5-E16.5). Strikingly, any prenatal injurious process (e.g., inflammation due to chorioamnionitis) interfering with normal lung development at that time, could lead to the disturbed formation of these two crucial compartments resulting in impaired pulmonary function postnatally.

The third stage, the canalicular stage, occurs between E16.5 and 17.5. The respiratory bronchioles continue subdividing into smaller units, consisting of a primitive respiratory epithelium competent of gas exchange. This respiratory epithelium arises from the differentiation of distal lung epithelial progenitors. Alveolar epithelial cells type 1 and type 2 arises from stem/ epithelial progenitor cells. Concurrently, the mesenchyme surrounding the epithelium becomes thinner due to mesenchymal cell apoptosis. Furthermore, another characteristic of this stage is the massive formation of a double-layer capillary network. In mice, interstitial fibroblasts containing cytoplasmic lipid droplets (so-called lipofibroblast, LIF) emerge in the mesenchyme.

The fourth stage, the saccular stage of lung development in mice, starts prenatally at E17.5 and ends postnatally at P5. The main events during this stage are the formation of alveolar sacs, surfactant protein production, and further thinning of the mesenchyme to facilitate gas exchange between the intra-alveolar airspace and the capillaries located in the mesenchyme. Furthermore, expansion of the capillary and lymphatic networks continues.

The fifth stage of the development process is the alveolar stage. The main characteristic of this stage is alveolarization or alveologenesis. This process is functionally coordinated by interactions of many cell types, mainly between epithelium, endothelium, and mesenchyme. This stage occurs from P5 to P30. During this stage, the alveolar surface area increases massively at the expense of the mesenchyme through subdividing the alveolar sacs (also called primitive alveoli) into mature alveoli by forming a structure; called “secondary septum.” The alveolarization process requires elastin deposition by the cells located at the tip of these primary septa (1–3).

On 2D sections, these secondary septa elongate to subdivide the alveolar sac into smaller mature alveoli, which is the lung's minimal functional unit responsible for the exchange of CO_2 gas with O_2. At the 3D level, these secondary septa resemble a fishnet structure (4,5).

In mice, this process lasts from P5 to P15, where primary septa still contain a double layer of capillaries. Through this process, the capillary layer will become thinner. A single capillary network allows more efficient gas exchange through microvascular maturation. Secondary crest myofibroblast cells localizing in the mesenchyme at the tip of the emerging secondary septa are responsible for secondary septa formation.

In this study, we used an O_2-exposed mouse model to investigate the impact of hyperoxia (HYX) injury on the lung mesenchyme cells using AT2 stem/progenitor cells proliferation as a read-out.

Newborn mice were exposed to HYX injury between P0 to P8. This treatment leads to an arrest in the alveolarization stage. As mentioned above, in mice, alveologenesis occurs from P5 to P15; the exposition of the newborn to hyperoxia mimics some of the features of bronchopulmonary dysplasia (BPD) phenotype seen in humans.

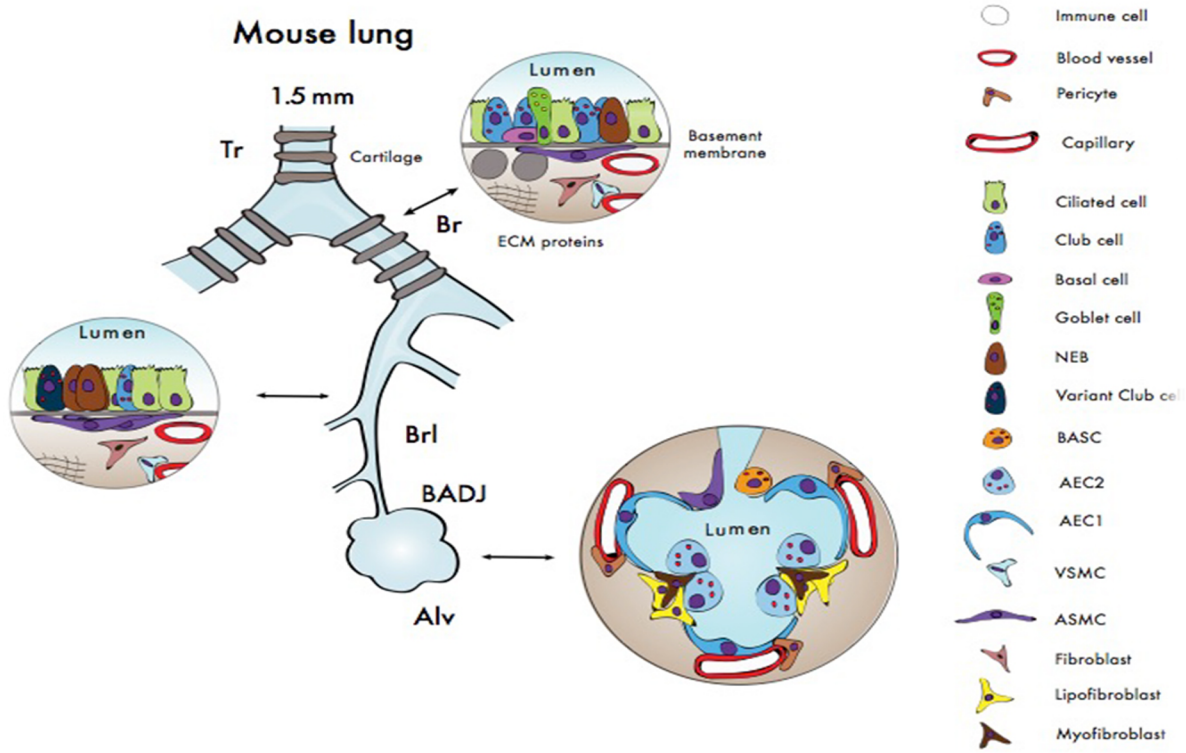

Figure 1: Variety of cell types from proximal to the distal part of the adult lung

The walls of conducting airways consist of pseudostratified epithelium with basal, multiciliated and secretory cells surrounded by supporting smooth muscle, fibroblasts, cartilage, vasculature and neurons extending along the airways. In the mouse, only the pseudostratified epithelium of the trachea (Tr) and bronchi are surrounded by cartilage. The epithelium lining the bronchi (Br) is predominantly composed of mucus-secreting goblet cells, scattered neuroendocrine cells and neuroendocrine bodies (NEBs).

The bronchiolar epithelium (Brl) is lined by club cells and neuroendocrine cells and NEBs. The bronchioles are lined by a simple epithelium that consists multiciliated and club cells, a small number of neuroendocrine cells, NEBs and bronchioalveolar stem cells (BASCs). In the distal alveolar region (Alv), the epithelium is highly vascularised and composed of flat alveolar type 1 cells (AEC1), flanked by cuboidal alveolar type 2 cells (AEC2). BADJ: bronchoalveolar duct junction; ECM: extracellular matrix; PBSMC: parabronchial smooth muscle cell.

1.2 Epithelial-mesenchymal interactions in the distal part

During lung development, specifically during the pseudoglandular stage, many cell types emerge from epithelial and mesenchymal progenitor cells. Multipotent epithelial progenitors expressing $Id2^{+}$ and $Sox9^{+}$ are located at the distal tips in this stage. The subsequent proliferation and differentiation of these progenitors give rise to different epithelial cell types, including club, ciliated, alveolar type 1, and type 2 cells. In parallel, mesenchymal progenitor cells also differentiate into mesenchymal cell types such as smooth muscle cells (SMC), chondrocytes, nerve cells, lymphatic cells, secondary crest myofibroblasts, and lipofibroblasts (6,7). The regulation of this complex process requires involving multiple signaling pathways like the Wnt (wingless and int), Notch, BMP (bone morphogenetic proteins), and Fgf (fibroblast growth factor) pathways. Alveolar epithelial cells (AT1 and AT2) send signal to mesenchyme cells control their proliferation and differentiation during lung development. AT2 signals to lipofibroblasts (LIF) via Parathyroid hormone-related protein (PTHrP) activate the Peroxisome proliferator-activated receptor gamma (PPARγ) pathway (8). This signaling pathway plays a critical role in inducing the LIF phenotype (9). LIFs secrete leptin which stimulates surfactant protein production. It has recently been demonstrated that AT1 cells express key ligands to control mesenchyme cell fate via the Wnt and Shh signaling pathways (10).

These pathways coordinate the epithelial and mesenchymal interactions in terms of branching, patterning, and specification of the lung structure. In particular, Bmp and Wnt signaling play a crucial role in specifying Nkx2.1+ respiratory endoderm progenitors during early lung development. Bmp4, Fgf10, and Shh (Sonic hedgehog) have a complex interplay in forming new branches and outgrowth. BMP4 is expressed in the endoderm, mesenchyme, and distal epithelial buds. Increased Bmp4 expression leads to inhibition of Fgf10 activity. Shh secreted by the epithelium acts through the receptor Patched (Ptch), which is located in the mesenchyme leading to proliferation and differentiation; however, it inhibits Fgf10 expression in the distal tips (11,12).

Fgf10 is a mesenchymal-specific gene expressed in the distal part of the embryonic lung during the early pseudoglandular stage. It acts through the Fgfr2b receptor located at the epithelium. Lineage tracing experiments have shown that a subpopulation of $Fgf10^{Pos}$ cells at embryonic day 12.5 serves as a progenitor for liopfibroblasts (LIF) at later stages of lung

development. Additionally, around 30% of LIF in postnatal lungs express the *Fgf10* gene (13–16). *Fgf10* inactivation leads to complete abrogation of branching and its endogenous changes have been correlated with disease progression and repair after lung injury both in mice and humans (17,18).

An essential stromal cell is represented by the lipofibroblasts (LIFs), rich in lipid-droplets, and can be stained and isolated using the vital dye LipidTox (LT). They express Perilipin 2, Platelet-derived growth factor receptor alpha (*Pdgfra*) and are negative for Acta2, and most importantly, are located close to alveolar type 2 cells (AT2). They are proposed to supply AT2s with the triglycerides needed to elaborate surfactant. Using a co-culture assay of Pdgfrα^{High} mesenchymal cells and AT2s in growth factor-reduced Matrigel, it has been proposed that the LIFs are essential for the maintenance of the proliferation and differentiation of AT2 stem cells (19).

1.3 Heterogeneity in resident mesenchymal cell (rMC) niche

Stem cells have two main properties; self-renewal and differentiation to other cell types, which are necessary during the organogenesis and repair process in the adult organ. The niche is the environment of stem cells in adult tissue that plays a critical role in regulating and maintaining stem cell activity during homeostasis and injury. In the distal part of the lung, alveolar epithelial type 2 cells serve as stem cells in the adult lung. The niche of AT2 cells comprises stromal cells, extracellular matrix (ECM), immune cells, lymphatic, nerves, and capillary networks. The previous section mentioned that the epithelial and mesenchymal interaction is vital during the embryonic and post-natal stages of lung development (20,21).

Alveolar units are composed of two epithelial cell types, type 1 and type 2; however, the mesenchyme population is highly heterogeneous. Lung mesenchymal cells have been identified based on their function, location, and molecular markers. By using a single cell transcriptomic approach, the heterogeneity of the different resident mesenchymal (rMC) populations present in the lung is starting to emerge (22).

McQualter et al. 2009 has defined resident mesenchymal cells as belonging to either the lipofibroblasts or non-lipofibroblasts groups. Stem cell antigen 1 (Sca1) and Thymocyte differentiation antigen-1 (also known as CD90) (Thy1) were used to distinguish between these two groups of rMCs. They also found the LIF population is expressing Pdgfrα marker (23,24). It was already shown that the $Cd45^{Neg}Cd31^{Neg}Epcam^{Neg}Pdgfr\alpha^{High}$ cell population could sustain AT2 stem cell renewal using the so-called alveolosphere *in vitro* assay ($Pdgfra^{+}$ TASCs) (25).

Interestingly, another population of stromal cells, called MANC (Mesenchymal Alveolar Niche Cells), are positive for *Axin2* and *Pdgfra.* This population is also positive for other markers such as *Fgf7, Il6, Wnt and* resides in the vicinity of AT2 cells. They also found the AMPs (Alveolar Mesenchymal Progenitor) population, which is located in the alveolar region and serves as a source of activated myofibroblasts in lung fibrosis (26). In terms of the location of mesenchymal cells in the alveolar area, another subset called Lgr5 positive cells is identified using the 3D organoid model. However, it is unclear whether Lgr5-positive cells play a role similar to the LIFs in the alveolar region (27).

As abovementioned, Fgf10 expression is necessary to form epithelial budding and branching morphogenesis. Both ligands Fgf10 and Fgf7 act through binding Fgfr2b receptor expressed by epithelial cells (28); however, Fgf7 is not playing a significant role in this stage, as demonstrated by the fact that the *Fgf7* KO lungs appear completely normal (29). In our lineage tracing analysis, two waves of expression have been defined: in the first wave, $Fgf10^{Pos}$ cells give rise to alveolar and vascular smooth muscle cells, LIFs, and other subsets. In the second wave, $Fgf10^{Pos}$ cells mainly behave like a progenitor specifically for LIFs (30,31). Recently, another subset of mesenchymal cells, expressing the transcription factor 21 (*Tcf21*), has been found similar to $Fgf10^{Pos}$ cells (32). These different populations have been defined as niches for AT2 stem/progenitor cells. However, it is still unclear how different they are from each other. In the context of lung disease, trans-differentiation of LIFs to activated myofibroblasts (MYF) is considered as one of the most critical mechanisms for the pathogenesis of chronic lung diseases (33).

Travaglini et al. 2020 found the differentiation of pro-LIF into LIF by exploiting single-cell RNA sequencing and identified some novel markers. LIM and calponin homologue domains

1 (Limch1), glycogenin (Gyg), microtubule–actin cross-linking factor 1 (Macf1), microfibril-associated protein 4 (Mfap4), nephronectin (Npnt), Wnt2, collagen type XIII α1 chain (Col13a1), and indolethylamine N-methyltransferase (Inmt), are expressed in the mesenchymal cells across embryonic and post-natal lung development, adulthood, aging and fibrosis in mice. These populations have been defined as LIF because they expressed canonical markers such as *Tcf21, Fgf10, G0s2* (G_0/G_1 switch gene 2). They also found some new markers to define mesenchymal heterogeneity in humans (34).

It is currently challenging to clarify the role of each subset in the healthy lung and disease model because of a high level of heterogeneity in this compartment and the scarcity of specific markers to identify the different mesenchymal subtypes. Li et al. 2018 used Pdgfrα-lineage-labeled cell analysis and showed that this subset contributed to the development of myofibroblasts (MYF) in healthy lungs and of pathological activated MYF in lung fibrosis. In contrast, lineage-labeled cells decreased in the neonatal hyperoxia injury model, and they did not contribute to pathologically activated MYF in the BPD model (35).

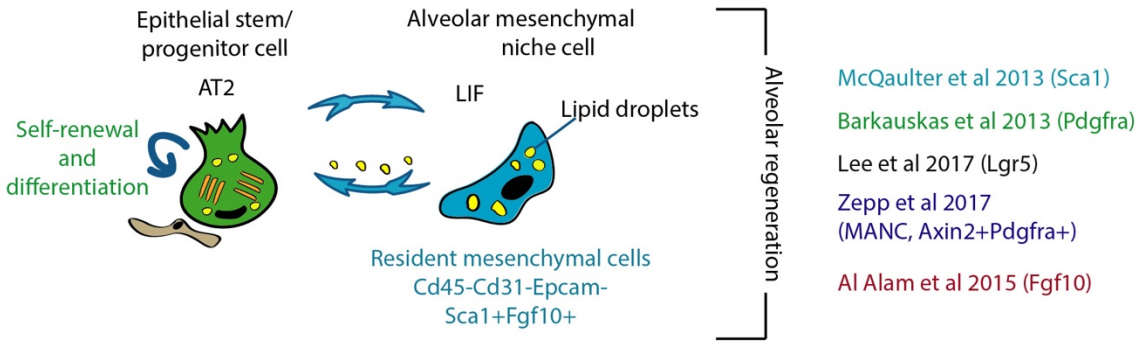

Figure 2: Heterogeneity in alveolar mesenchymal niche cells.
rMC-Sca1$^+$ subset control the proliferation and differentiation of AT2 stem cells. In the alveolar region, lipofibroblasts (LIFs) act as niche cells that provide AT2 cells with the triglycerides needed for the production of pulmonary surfactant. A subset of LIFs is expressing FGF10, which is important for the maintenance and growth of AT2 stem cells. Mesenchymal alveolar niche cells (MANCs) have also been shown to contribute to AT2 cell maintenance. LGR5$^+$ mesenchymal cells also promote AT2 cell growth.

1.4 Bronchopulmonary dysplasia (BPD)

Bronchopulmonary dysplasia (BPD) is characterized by arrested pulmonary development at the saccular stage. BPD is one of the most common form of chronic lung disease (CLD) in neonates. It is defined by the need for supplemental oxygen or ventilatory support for >28 days or beyond 36 weeks post-menstrual age (PMA); the disease can be classified into three different severity grades: mild, moderate, and severe BPD (36,37). The incidence of BPD is reported to be up to 68% in infants born at <32weeks of gestation with a birth weight below 1500 g (38). Prematurity and surfactant protein deficiency are two main triggering factors of BPD. In addition, barotrauma, volutrauma, and oxygen toxicity are negative consequences of supportive care with mechanical ventilation and oxygen supplementation in preterm infants. These factors contribute to the pathology of chronic pulmonary disease companied by arrested lung development, including fewer and larger alveoli with less septation, increased thickness of alveolar septa, and impaired pulmonary vasculature. These infants suffer from life-long respiratory complications like asthma, reduced exercise capacity, early-onset emphysema, and pulmonary hypertension. Based on injury-time point on very early or late stages of lung development, BPD can be defined as old or new BPD. Table 1 summarizes histopathological changes of these two groups of patients. Old BPD is defined as lung disease in infants before implementing exogenous surfactant therapy. In contrast, new BPD is considered lung disease in infants born in the late stage of lung development (canalicular/saccular stage, in humans 23-28 weeks of gestation), where lung development is arrested by postnatal injury. This injury leads to arrest in the lung growth in forming the secondary septation and increasing alveolar surface area at the alveolarization stage. Therefore, impaired alveologenesis with growth arrest in lung development results in prolonged impairment in lung function (39).

The pathogenesis of BPD involves multiple pre-and postnatal injurious hits affecting the development of a premature lung. However, the mechanisms responsible for impaired alveologenesis are still elusive.

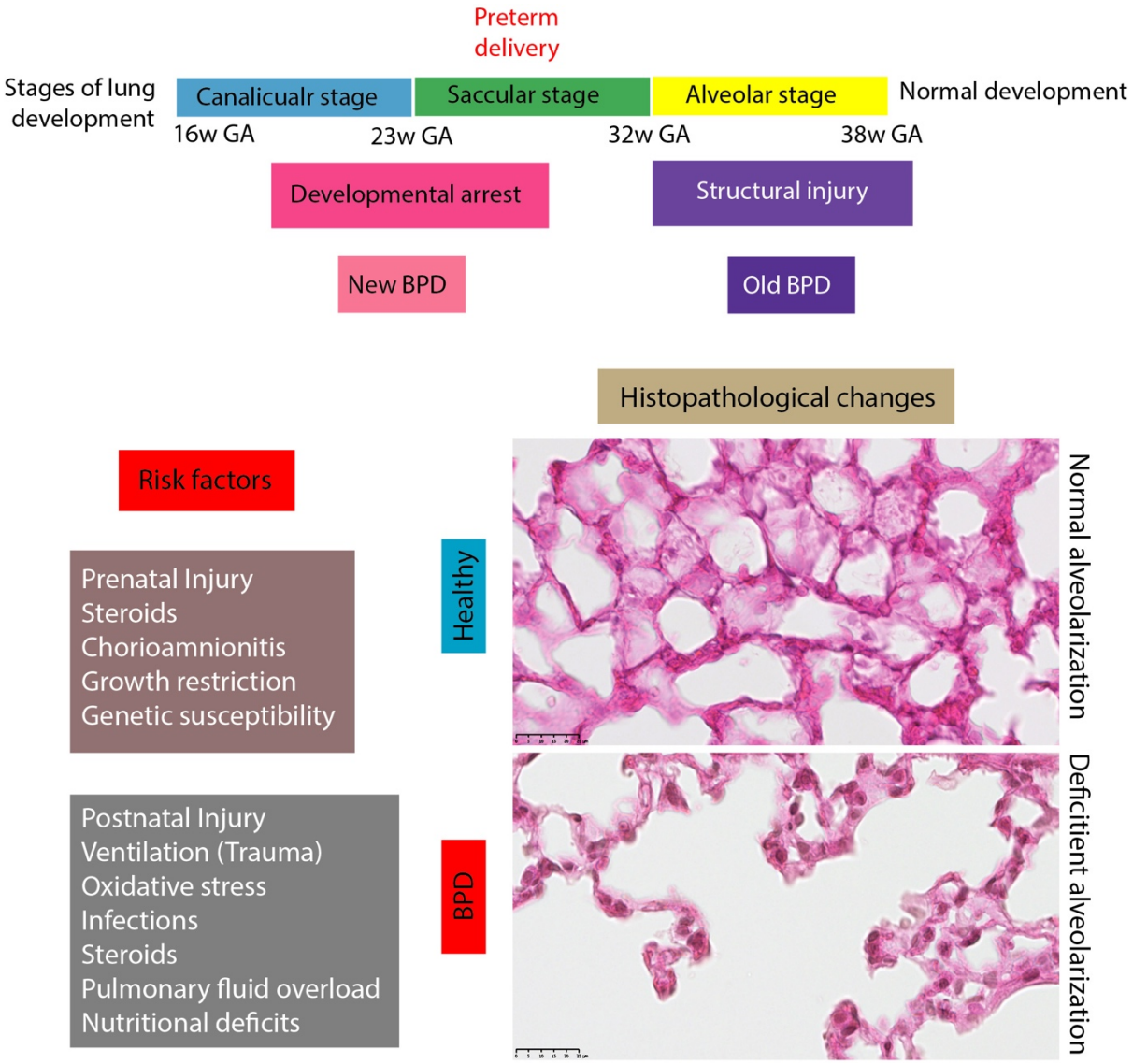

Figure 3: Overview of the multifactorial pathogenesis of BPD.

Multiple risk factors are involved in the pathogenesis of BPD in premature infants. These factors can be divided in pre– and post-natal injuries leading to the development of BPD. The old BPD occurs in premature infants born during the alveolar stage with respiratory distress syndrome that received aggressive mechanical ventilation and high concentrations of inspired oxygen. In contrast, the new BPD occurs in preterm infants born in canalicular or saccular stages with arrested in the lung development.

Table 1. Comparison of old versus new bronchopulmonary Dysplasia (Cerny., et al. Lung 2008)

Old BPD	New BPD
Larger pre-term infants	Extremely premature infants
High ventilation and oxygen needs	Modest ventilation and oxygen
Severe large airway injury	Minimal large airway disease
Interstitial and alveolar edema	Arrested alveolarization
Extensive small airway disease with alternating areas of over inflammation and fibrosis	Minimal small airway disease with less inflammation and fibrosis
Pulmonary artery muscularization	Fewer and abnormal pulmonary arteries

The cellular mechanisms at play during alveologenesis are currently unclear. Still, it is proposed that AT2 cells could mediate the required interactions with the surrounding vascular system and the resident mesenchymal cells to allow the transition from the saccular to the alveolar stage (4). AT2s play a critical role in maintaining efficient gas exchange during homeostasis and serve as progenitor cells for the re-epithelialization of the alveoli after lung injury. In addition, AT2s modify the inflammatory response by secreting different growth factors and cytokines (40).

Fgf10 is a crucial factor expressed by the lung mesenchyme regulating the branching process of the embryonic lung (41). It acts via the tyrosine kinase receptor Fgfr2b. It has been reported to target both the alveolar epithelial progenitor cells to control their proliferation and differentiation (14) as well as resident lung mesenchymal cells (rMC) to control their differentiation along the lipofibroblast lineage (31).

Multiple studies have shown that Fgf10 plays a vital role in lung disease and regeneration after injury. In the mouse model of bleomycin-induced lung fibrosis, *Fgf10* overexpression during fibrosis formation or fibrosis resolution demonstrated a protective and therapeutic effect, respectively (42).

Fgf10 is also involved in the regeneration of the bronchial lung epithelium after naphthalene injury (43,44). Suggestive of a causative role in the bronchial airway manifestations in the context of chronic obstructive pulmonary disease, patients with heterozygous loss of function of *FGF10* exhibit a significant decrease in inspiratory vital capacity (IVC), forced expiratory volume in one second FEV1, and FEV1/IVC quota compared to non-carrier siblings and predicted reference values (45). This observation is supported by Fgf10-Hippo epithelial-mesenchymal crosstalk maintains and recruits lung basal stem cells in the conducting airways (46). While transient *Fgf10* expression by alveolar smooth muscle cells (ASMCs) is critical for proper airway epithelial regeneration in response to injury, sustained Fgf10 secretion by the ASMC niche, in response to chronic Ilk/Hippo inactivation, results in pathological changes in airway architecture (46). We also recently identified a new population of repair supportive mesenchymal cells (RSMCs), distinct from the ASMCs but which also secrete Fgf10 to restore the bronchial epithelium (44). Therefore, Fgf10/Fgfr2b signaling is an interesting target for lung diseases targeting the bronchial epithelium.

Furthermore, we experimentally demonstrated in mice that decreased Fgf10 expression is causative for the lethality of newborn mice observed following hyperoxia exposure (47). Hyperoxia (HYX) exposure (85% O_2) to newborn mice for eight days is used to trigger arrested lung development, thereby mimicking the bronchopulmonary dysplasia (BPD) phenotype. Inhibition of Fgfr2b signaling postnatally in the context of HYX also leads to increased alveolar defects and a pulmonary hypertension phenotype (48).

In humans, the decrease in the levels of expression of FGF10 protein in the lungs of patients suffering from BPD suggests it plays a role for FGF10 in the etiology of this disease (18). FGF10 expression has been reported to be a target of the inflammatory process taking place in BPD (49). Interactions between NF-κB, Sp1, and Sp3 led to inhibition of *Fgf10* transcription (50). *Fgf10* inhibition is mediated by toll-like receptor 2 and 4 (Tlr2 or Tlr4) activation (18). Therefore, we hypothesize that the exogenous application of recombinant FGF10 could potentially represent a solid therapeutic approach.

1.5 The mouse model used to study BPD

Exposing mice to O_2 (85%) is a well-established model mimicking the BPD model in premature infants. In multiple studies, different levels of O_2 were used to establish different levels of injury in the model representing other conditions happening in neonatal infants. Mice and rats are the standard used animal models to study BPD. Pups in both species are normally born during the saccular stage of lung development. As mentioned above, this stage begins *in utero* and will be completed on day P5.

In contrast, premature infants at risk for BPD are born in the saccular stage, a stage that takes place exclusively *in utero*. Therefore, premature infants suffer from complications due to immature lungs and surfactant insufficiency. Even though rodents are born surfactant-sufficient, there is a well-suited model to study some of the BPD features observed in human neonates. Figure 4 details the mouse model used in this study.

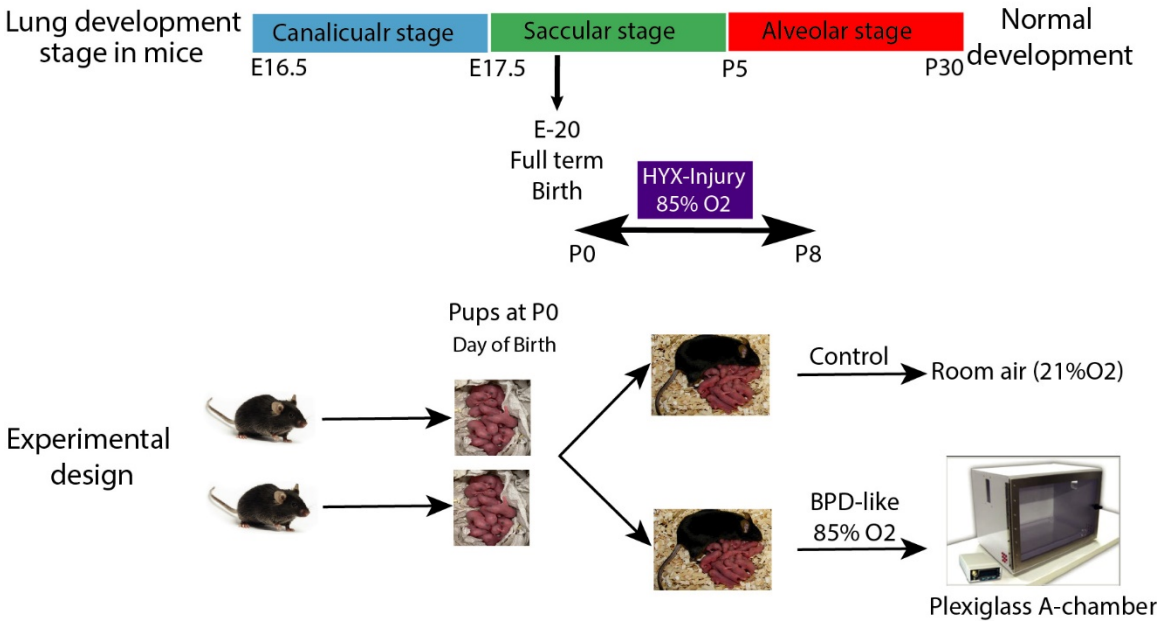

Figure 4: Established mouse model to study BPD.

In experimental design, C57BL6 pups from the experimental group were exposed to HYX (85% O_2) from P0 to P8. In parallel, Pups from control group were maintained under room air (21% O_2).

1.6 Organoid model definition and different applications

Organ modeling as a novel technology opens promising avenues to study organ development, disease modeling *in vitro,* cell-cell interactions, and drug screening. Organoids are self-organizing three-dimensional (3D) cellular structures that resemble organs in form and function. 3D organoids can be driven from two main types of stem cells: (1) pluripotent embryonic stem (ES) cells and their synthetic induced pluripotent stem (iPS) cell counterparts and (2) organ restricted adult stem cells (aSCs) (51,52). iPSCs can be generated from reprogrammed somatic cells isolated from healthy individuals or people who suffer from respiratory diseases. The reprogramming process is performed by overexpressing the Yamanaka factors OCT3/4, SOX-2, KLF4, and C-MYC in somatic cells and expanding individual iPSC colonies under conditions that support PSC self-renewal (53). With the development of robust differentiation protocols, iPSCs can be used to generate airway and alveolar epithelial cells.

Due to the complexity of working with *in vivo* models and some drawbacks of 2D cell culture, 3D models are becoming a model of interest to fill the gaps. Numerous 3D *in vitro* cell culture protocols have been established during the last ten years to produce organoids from different organs. For example, there are protocols to grow organoids from the lung, heart, liver, mammary glands, kidney, bone, brain, colon, stomach, and thyroid. Since organoids are forming following the interaction of multiple cell types, it is possible to study how the stromal niche supports epithelial stem/progenitor cells in terms of stem cell self-renewal and differentiation to other cell types.

Technically, 3D organoids are grown within gels made of a complex mixture of different extracellular matrix (ECM) proteins, including laminin, fibronectin, collagen, and heparin sulfate proteoglycans. The leading commercial gel used to grow organoids is Matrigel, a protein mixture secreted by Engelbreth–Holm–Swarm mouse sarcoma cells, liquid at low temperature and solidifies into a relatively soft gel at 37°C. In addition to ECM proteins, Matrigel contains a mixture of growth factors such as transforming growth factor (TGF)-β, epidermal growth factor (EGF), and fibroblast growth factor (FGF), which can impact the differentiation and proliferation of many cell types. Usually, Matrigel, where most of the growth factors have been removed, is used for organoid assays.

The ECM gels can mimic the in vivo extracellular environment in part and allow some of the cells to display characteristics of stem cells, namely self-renewal and multipotency. Once grown, these organoids can be reseeded for prolonged periods without changes in their karyotype. Additionally, these organoids can be cryopreserved without apparent alterations of the stem cells characteristics. When exposed to differentiating media, organoids give rise to specific cell types observed in the corresponding adult tissue in vivo.

Regarding the respiratory field, different types of organoids are known depending on which stem/progenitor cells are seeded in the combination of stromal cells (Figure 5). The epithelium undergoes extensive branching morphogenesis during lung development, leading to highly specialized epithelial cells along the proximal-distal axis. Using a lung injury model combined with exploiting lineage-tracing techniques, various epithelial cells as epithelial stem/progenitor cells have been identified. These epithelial cells are region-specific from the trachea to the alveoli. The pseudostratified epithelial cells lining the conducting airway are composed mainly of multiciliated and secretory cells, including Club and goblet cells. In the larger airways of the mouse lung and throughout most of the human lung, basal cells serve as progenitor cells. Two other distinct cell types line alveolar sacs: specialized alveolar type II cells (AT2s) that secrete surfactants and other proteins; and very thin, delicate type I cells (AT1s) that provide an extensive surface area for gas exchange with the surrounding capillaries (54).

Depending on the origin of the stem cell population used, organoids are called tracheospheres (trachea), bronchospheres (large airways), or alveolospheres (alveolar region). AT2s serve as stem cells in the distal part of the lung. As mentioned above, alveoli contain AT2, AT1, capillary endothelial cells, and associated mesenchymal cells.

In addition to the epithelial-based organotypic cultures mentioned, mesenchymal-based 3D cultures have been generated using fetal lung tissue or hPSCs and cultured in bioreactors. This approach formed a structural phenotype similar to that of native alveolar regions in vivo (55).

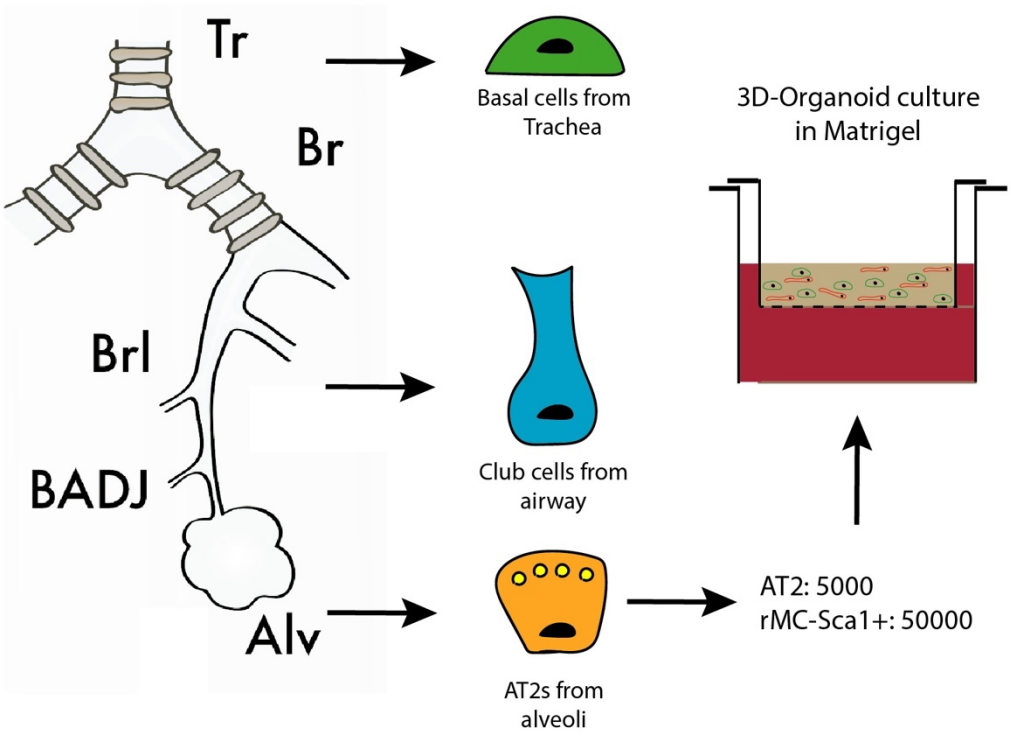

Figure 5: Overview of mouse lung organoid culture. At least three different stem/progenitor cell populations present in the adult lung are able to form organoids. Each cell type can be isolated by FACS or magnetic-activated cell sorting based on surface markers, fluorescent protein uptake or fluorescent protein expression in reporter mice. Isolated cells are cultured in Matrigel (light brown) with or without supporting stromal cells (depending on cell type). The stem/progenitor cells form organoids 2 weeks after plating. The cell and Matrigel mixture (typically 2000–5000 cells in 100 µL of gel) can be added to Transwell inserts (Corning Life Sciences) and the culture medium (red) is added to the bottom well.

In the future, organoid biobanks of healthy and diseased lung tissues will be established. These biobanks could be a significant source of organoids covering the range of genetic mutations that lead to respiratory disorders.

Lung-on-a-chip systems have been generated from differentiated cells, such as airway and alveolar epithelial cells, fibroblasts, and endothelial cells derived from primary cultures or isolated from healthy or diseased human or mouse tissue. It remains to be tested whether human (h)PSC-derived cells can mimic human biology and human disease in the lung-on-a-chip approach. Both organoids and lung-on-a-chip systems are amenable to high-throughput set-ups. Therefore, they have immediate application to model respiratory diseases in identifying new drugs which can normalize the disease phenotype. In addition, they contribute to evaluating the potency and toxicity of candidate drugs, and identifying biomarkers of drug interactions and drug-induced injury in the lung. Furthermore, both approaches have possible applications in personalized medicine, revealing which patients may benefit from treatment with a specific drug.

Cell turnover is usually very low during adult lung homeostasis, and the existing airway progenitor cells are quiescent. However, remarkably, numerous animal studies have shown that several progenitor cells can proliferate and differentiate into one or more cell types in response to various injuries, including exposure to infectious agents, tobacco smoke, high levels of oxygen, and chemotherapy Bleomycin (6).

The regenerative ability of these progenitor cells has triggered the scientific community to search for drugs that could activate them in vivo or establish cell-based therapies, which would enable the treatment of patients suffering from respiratory disease arising from lung injury or aging. Unfortunately, the translational transfer of the results obtained using animal models, primarily mice, has been limited so far and is probably due to unappreciated differences in lung anatomy and physiology between mice and humans. Altogether, these observations emphasize the unmet need for lung model systems that can complement animal models and validate the results obtained in animals to humans and improve our understanding of human lung physiology, regeneration, and disease. Figure 6 shows different applications of the 3D organoid model in stem cell differentiation, regenerative medicine, respiratory disease modeling, and drug screening.

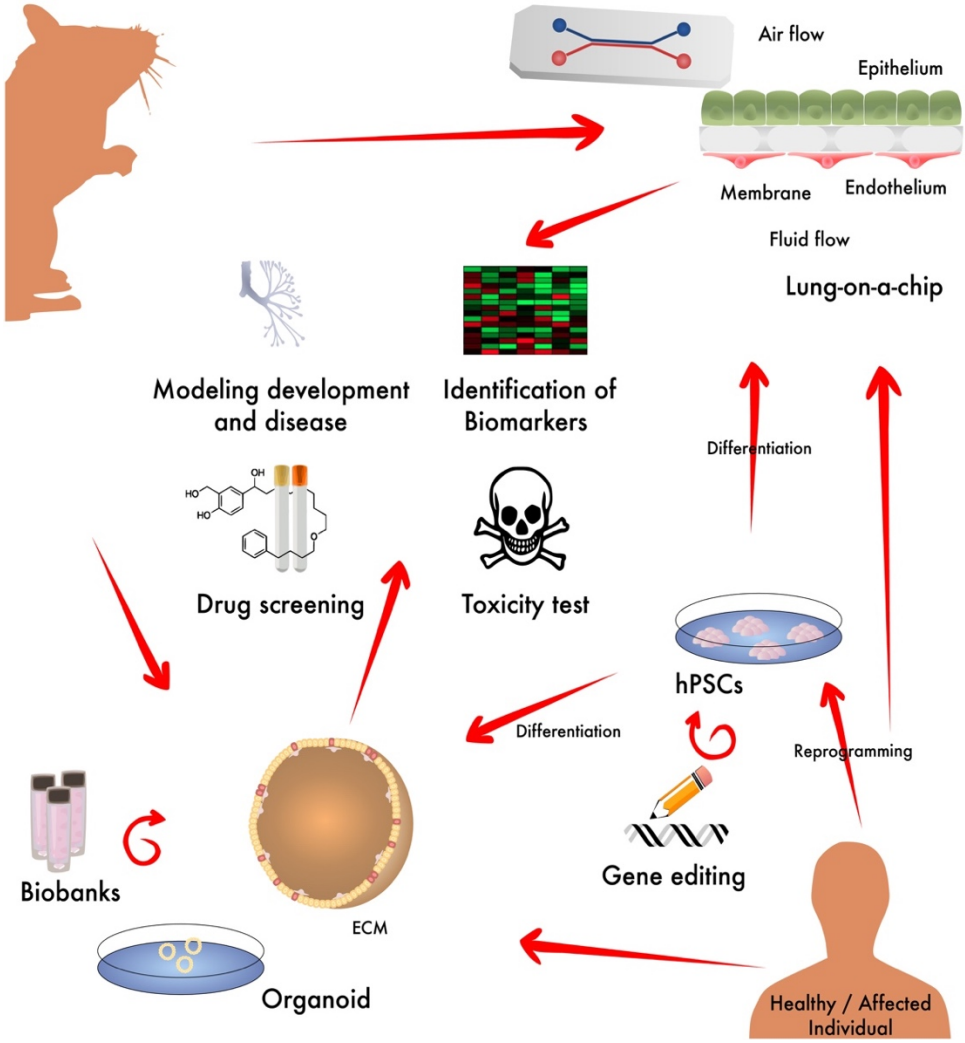
Air flow
Epithelium
Membrane
Endothelium
Fluid flow
Lung-on-a-chip
Modeling development and disease
Identification of Biomarkers
Differentiation
Drug screening
Toxicity test
hPSCs
Differentiation
Reprogramming
Gene editing
Biobanks
ECM
Organoid
Healthy / Affected Individual

Figure 6. Derivation and use of organoids and lung-on-a-chip.

Human and mouse organoids have been generated from stem cell populations isolated from **A.** healthy or diseased lung tissue and pluripotent stem cells (PSCs). **B.** PSCs, such as embryonic stem cells or induced pluripotent stem cells (iPSCs) can be maintained in culture for a number of passages and differentiate into derivatives of the three germ layers. **C.** Gene editing approaches such as the CRISPR/Cas9 technology enable the generation or correction of mutations leading to respiratory disease, providing appropriate control cells for these studies. **D.** Further culture in Matrigel and specific growth factor cocktails can give rise to organoids, which resemble distinct spatial regions of the lung. In addition, organoids can be grown from mouse stem cells isolated from the adult lung as well as from mouse PSCs. **E.** Organoid biobanks of healthy and diseased lung tissues. **F.** Lung-on-a-chip systems have been generated from differentiated cells. ECM: extracellular matrix (modified from Gkatzis et al., *ERJ*.2018).

2. Objectives

The lung is a complex organ containing different types of interconnected epithelial cells stromal cells, including vascular cells, immune cells, and extracellular matrix that maintain lung integrity. Since cell turnover in the adult lung usually is low, it is critical to investigate which sub-lineage of mesenchyme has a supportive function in terms of regeneration of tissue after injury. Resident mesenchymal cells (rMCs defined as $Cd31^{Neg}Cd45^{Neg}Epcam^{Neg}$) control the proliferation and differentiation of alveolar epithelial type 2 (AT2) stem cells in vitro. Some sub-lineages have been proposed in multiple studies to act as a niche for AT2 cell maintenance. However, the identity of this rMCs is still elusive. Here, we, therefore, combined two state-of-the-art techniques: 3D organoid model and single-cell RNA sequencing to address the following questions:

1) To investigate mesenchymal heterogeneity in the adult lung
2) To identify which mesenchyme sub-lineage could efficiently support AT2 stem cells in terms of proliferation and differentiation to AT1 cells
3) To optimize FACS protocol gating strategy, and establish a reproducible 3D organoid model
4) To investigate the difference between LIF-$Fgf10^{pos}$ sub-lineage and MANC ($Axin2^{pos}$) sub-lineage
5) To evaluate the impact of gender, metabolic dysfunction, hyperoxia injury on the niche activity of rMC-$Sca1^{Pos}$ cells
6) To monitor the effect of recombinant FGF10 administration on de novo alveologenesis following hyperoxia exposure in neonates (BPD model).
7) To investigate the impact of HYX injury on rMCs using the alveolosphere assay and scRNA-seq

3. Materials and methods

3.1 Mice

Sftpc$^{CreERT2/+}$ knock-in (gift from Harold Chapman, UCSF), *tdTomato*^{flox} reporter (Stock 007908, Jacksonlab), *Fgf10*^{LacZ} reporter (Mailleux et al., 2005), *Axin2*^{LacZ} reporter (stock 009120, Jackson lab), *Lep*$^{ob/ob}$ (aka *ob/ob*) mutant (stock 000632, Jackson lab) and wild type mice were maintained on the C57BL/6 background. All animal studies were performed according to protocols approved by the Animal Ethics Committee of the Regierungspraesidium Giessen (permit numbers: G7/2017-No. 844-GP and G11/2019-No. 931-GP).

3.2 Lung dissociation and fluorescence-activated cell sorting

Lungs from C57BL6 (WT) mice were collected at 6-8 weeks of age and processed into a single-cell suspension using collagenase type IV (0.5%ml per lung) and DNase I. Cd45^{Neg}Cd31^{Neg}Epcam^{Neg}Sca1^{Pos} cells were collected to establish an organoid model combined with AT2 cells. The total AT2 population (Sftpc^{Pos}Tom^{Pos} cells) was isolated from lungs of 6-8 weeks old *Sftpc*$^{CreERT2/+}$; *tdTomato*$^{flox/flox}$ mice. For the single-cell preparation, lungs were inflated intratracheally with 3 mL dispase and for further digestion, each lung was incubated in 3 mL dispase solution (5 U/mL) at room temperature for 30 minutes. For the isolation of epithelial cells from the *Sftpc*^{Tom} lungs, we first sorted a population of Cd45^{Neg}Cd31^{Neg}Epcam^{Pos} cells. To isolate enriched population of mature AT2 cells, we additionally used Lysotracker (100 µM; Green) and collected Lyso^{Pos}Tom^{Pos} cells. In general, we have considered the fluorescence values higher than 10^3 as a positive selection to gate cells of interest. The values around 0 were gated as a negative selection. In all experiments, we used the negative control to adjust gating to distinguish negative and positive populations.

3.3 FluoReporter *lacZ* flow cytometry

Fluorescein di (b-D-galactopyranoside) (aka FDG) was used to isolate by FACS, cells expressing ß-galactosidase from *Fgf10*^{LacZ} and *Axin2*^{LacZ} reporter lines. Lungs were collected from 6-8 weeks old *Fgf10*^{LacZ} and *Axin2*^{LacZ} reporter mice. According to manufacturer's

instruction, single-cell suspension and FDG working solution were prewarmed and the cells were resuspended with chloroquine followed by loading by FDG.

After incubation for 20 minutes, FDG loading is stopped by adding ice cold staining medium containing propidium iodide and chloroquine. Cells are then placed on ice and incubated with antibodies against Cd45, Cd31, Sca1, and Epcam (for details see Lung dissociation and Fluorescence-Activated Cell Sorting) before sorting using the FACSAria III (BD Bioscience) cell sorter. Cells were sorted through a flow chamber with a 100-µm nozzle tip under 25 psi sheath fluid pressure. Cells were collected in sorting media (advanced DMEM:F12 [Gibco#12634-010] plus 10% FBS and 1% P/S).

Table 2: Materials and antibodies used for flow cytometry

Materials and Antibodies	Cat Number& company	Dilution
APC anti-mouse Cd31	102410-Biolegend	1:50
APC anti-mouse Cd45	103112-Biolegend	1:50
APC/Cy7 anti-mouse Cd 326	118218-Biolegend	1:50
Pacific Blue anti-mouse Ly-6a	108120-Biolegend	1:50
LysoTracker- DND-26	L7526-Invitrogen	100 µM
FluoReporter *lacZ*	F1930-Thermo Fischer Scientific	Invitrogen protocol
DNase I	DN25-SIGMA	1:10
collagenase type IV	9001-12-1-Gibco	0.5% ml per lung
Dispase	354235-BD Biosciences	5 U/ ml
HCS LipidTOX Red neutral	H34476-Invitrogen	1:50

3.4 Alveolar organoid assay

Five thousand $Lyso^{Pos}Tom^{Pos}$ cells (AT2s from adult *Sftpc*$^{CreERT2/+}$; *tdTomato*$^{flox/+}$ lungs) and 50 000 rMCs cells were resuspended in 100 µL culture medium (sorting media plus 1% ITS [Gibco # 41400-045]) and mixed 1:1 with 100 µL growth factor-reduced phenol Red-free Matrigel (Corning #356231). Cells were seeded in individual 24-well 0.4 µm Transwell inserts (Falcon, SARSTEDT). After incubation at 37°C for 15 minutes, 500 µL of culture was placed in the lower chamber and the plate was placed at 37°C in 5% CO_2/air. The culture medium was changed every other day. ROCK inhibitor (10 µM, Y27632

STEMCELL#72304) was included in the culture medium for the first 2 days of culture. Organoids were counted and measured at day 14. Colony-forming efficiency (CFE) is calculated as the ratio between the numbers of spheres observed over the initial number (5000) of AT2 cells. At day 14, organoids were processed for whole-mount immunofluorescence staining.

3.5 Whole-mount immunofluorescence staining of organoids

Organoids were fixed in 4% paraformaldehyde for 30 minutes followed by 3× washing steps with PBS and incubation in 0.1% Triton X-100 for 30 min. After washing 3× with PBST, organoids were blocked with 1× TBS, 3% BSA. 0.4% Triton X-100 for 1 hour at room temperature. Organoids were washed and then incubated at 4°C overnight with 1× TBS, 1.5% BSA, 0.2% Triton X-100, and primary antibody against Hopx (1:250 SIGMA #HPA030180). The next day, after 3× washing with TBST for 10 minutes, organoids were incubated with secondary antibodies (AlexaFlour 488 goat anti-Rabbit IgG Green [1:500] Cat. #11034 Invitrogen) at RT and washed three times with TBST before being mounted with Prolong Diamond Anti-fade Mountant with DAPI (Invitrogen 4′,6-diamidino2-phenylindole). Photomicrographs of immunofluorescence staining were taken using a Leica DMRA fluorescence microscope with a Leica DFC360 FX camera (Leica, Wetzlar, Germany). Figures were assembled using Adobe Illustrator.

3.6 Quantitative RT-PCR

Total RNA was extracted from FACS-sorted $Sca1^{Pos}LT^{hi}$ and $Sca1^{Pos}LT^{Neg}$ cells using RNeasy plus Micro kit (Cat. # 74034 QIAGEN). cDNA was synthesized using QuantiTect Reverse Transcription kit (Cat. #205314 QIAGEN). Quantitative real-time PCR (qRT-PCR) analysis was performed using LightCycler 480 II machine (Roche AppliedScience). Data were presented as expression relative to hypoxanthine-guanine phosphoribosyltransferase (Hprt) for mouse genes. Primers:

Table 3: Primer sequences used for qRT-PCR

Primers	Forward	Reverse
mFgf10	ATGACTGTTGACATCAGA	CACTGTTCAGCCTTTTGA
mPdgfra	GTCGTTGACCTGCAGTGGA	CCAGCATGGTGATACCTTTG

3.7 Co-staining: RNA in situ hybridization assay and IF

Murine lungs were perfused with PBS and fixed in 4% paraformaldehyde according to standard procedures. Next, they were embedded in paraffin and sectioned at 5 μm thickness. RNAscope Mutiplex Fluorescent Reagent Kit v2 assay (document Nr:323100-USM, Advanced Cell Diagnostic, Newark, California) was performed according to the manufacturer's instructions, however, with slight changes in applying standard pretreatment conditions and target retrieval antigen. The pretreatment time was reduced to 7 minutes and the amplification steps were increased to 1 hour. Specific probes were used for the detection of *Fgf10* and *Fgf7* gene expression (*Mm-Fgf10* Cat. #446371, *Mm-Fgf7* Cat. #443521-C3). 3-plex Positive control (Cat. #320881) and 3-plex negative control (Cat. #320871) were carried out using probes specific to murine housekeeping-genes. These samples were followed by IF for Sftpc. Samples were washed in TBST buffer then incubated at 4°C overnight with 1× TBS, 1.5% BSA, 0.2% Triton X-100, and primary antibody against Sftpc (Anti-Pro-Surfactant Protein C, polyclonal Ab Cat. # AB3786). The next day, after 3× washing with TBST for 10 minutes, samples were incubated with secondary antibodies (AlexaFlour 488 goat anti-Rabbit IgG Green [1:250] Cat. #11034 Invitrogen) at RT and washed three times with TBST before being mounted with Prolong Diamond Anti-fade Mountant with DAPI (Invitrogen 4′,6-diamidino2-phenylindole). Photomicrographs of immunofluorescence staining were taken using a Leica DMRA fluorescence microscope with a Leica DFC360 FX camera (Leica, Wetzlar, Germany). Figures were assembled using Adobe Illustrator.

3.8 Microarray analysis

Gene expression profiles of two sub-lineages of the resident mesenchymal niche cells were carried out. Purified total RNA was amplified using the Ovation PicoSL WTA System V2 kit (NuGEN Technologies, Bemmel, Netherlands). Per sample, 2 μg amplified cDNA was Cy5-labeled using the SureTag DNA labeling kit (Agilent, Waldbronn, Germany). Hybridization to 8x60K 60mer oligonucleotide spotted microarray slides (Agilent-074809: Catalog gene expression microarray for Mouse, v2 8x60K) and subsequent washing and drying of the slides was performed following the Agilent hybridization protocol in Agilent hybridization chambers, with following modifications: 2 μg of the labeled cDNA were hybridized for

22 hours at 65°C. The cDNA was not fragmented before hybridization. Each sample was processed and hybridized twice (technical replicates).

The dried slides were scanned at 2 µm/pixel resolution using the InnoScan is 900 (Innopsys, Carbonne, France). Image analysis was performed with Mapix 6.5.0 software, and calculated values for all spots were saved as GenePix results files. Stored data were evaluated using the R software and the limma package from BioConductor. Log_2 mean spot signals were taken for further analysis. Data was background corrected using the NormExp procedure on the negative control spots and quantile-normalized before averaging. Log_2 signals of replicate spots were averaged, and from several different probes addressing the same gene only the probe with the highest average signal was used. Data from technical replicates was averaged. The data were deposited in a public database (GEO accession: GSE162859). Genes were ranked for differential expression using a moderated *t*-statistic. Pathway analyses were done using gene set tests on the ranks of the *t*-values. Pathways were taken from the KEGG database (**http://www.genome.jp/kegg/pathway.html**). Heatmaps are generated from the normalized log_2 spot intensities (I) and show the gene-wise z-values (where $z_j = (I_j - \text{mean}(I))/\text{SD}(I)$ for $j = 1,...,n$).

3.9 Experimental approach for BPD model and rFGF10 administration

Pregnant C57BL/6J at embryonic day (E) 14 were purchased from Jackson through Charles Rivers Laboratory, Germany. Mice were housed by the Animal Care and Veterinary Service of the University of Justus-Liebig University in accordance with institutional guidelines. Newborn mouse pups from dams that delivered on the same day, were randomized at the day of birth [postnatal day P0] and divided to equal-sized litters of 6 to 8 pups. Following randomization, mice cages were either maintained in room air (normoxia, NOX, 21% O_2) or in normobaric hyperoxia (HYX, 85% O_2) from P0 until P8. The hyperoxic environment was maintained in sealed plexiglass A-chamber with continuous oxygen monitoring (BioSpherix Ltd, Parish, NY). In order to avoid oxygen toxicity and associated confounding factors, nursing dams were rotated between NOX and HYX groups every 24 hrs. All mice were maintained in 12/12 h light/dark cycle and received food ad libidum. At the end of the HYX exposure (P8), pups in HYX group were subsequently divided in two groups; HYX-PBS and HYX-FGF10. Pups in HYX-FGF10 group received 6µg (60 µl) intraperitoneal (i.p.) injection of hrFGF10 (Cat Nr # 345-FG, R&D systems, USA) at P8, P10, P12, P14 followed by having

one-week rest. At P22, P24, P26, P28, and P36, P38, P40, P42, mice received 10 µg (100 µl) of hrFGF10. Then at P45 all developing mice were sacrificed by using CO_2 and cervical dislocation. All animal studies were performed according to protocols approved by the Animal Ethics Committee of the Regierungspraesidium Giessen (permit numbers: G29/2020-No. 994_GP and G85/2019-No. 986_GP).

3.10 Alveolar morphometry

Mice at P45 sacrificed with CO_2 administration and cervical dislocation. Lungs inflated first with cold PBS and then with 4% paraformaldehyde (PFA) in phosphate-buffered saline (pH 7.0) at a vascular pressure of 20 cm H_2O. PBS followed by 4% PFA was infused into the lung via the trachea at a pressure of 20 cm H_2O. Investigations were performed using 5 µm sections of paraffin-embedded left lobe of the lungs. The mean linear intercept, mean air space, and mean septal wall thickness were measured after staining with hematoxylin and eosin (H&E). Total scans from the left lobe were analyzed using a Leica DM6000B microscope with an automated stage which was implemented into the Qwin V3 software (Leica, Wetzlar, Germany). Horizontal and vertical lines (distance 40 µm) were placed across each lung section.

The mean linear intercept (MLI) was estimated in a blinded Fashion using the same software. The corresponds to the total length of the horizontal (or vertical) lines present in the section divided by the number of times these lines cross a septal wall. Bronchi and vessels above 50 µm in diameter were excluded prior to the computerized measurement. The air space was determined as the non-parenchymatous non-stained area. The septal wall thickness was measured as the length of the line perpendicularly crossing a septum. From the respective measurements, mean values were calculated.

3.11 Lung function measurement

Mice were anaesthetized by intraperitoneal injection of a solution of 1.2 µl/g body weight of ketamine 10% and 0.6 µl/g body weight of Dormitor (1mg/ml). Deepness of anesthesia was assessed by toe pinching. Then, an incision of the skin was made at the level of the larynx to access the trachea without opening the chest cavity. A horizontal tracheal incision was made to intubate the mouse and connect it to the flexivent fx1 (Scireq, Montreal, Canada) for lung

function measurement (compliance, elastance, and resistance). Eight measurements of each 10 sec were performed for each mouse, and mean values were calculated.

3.12 scRNA-seq library preparation

Single-cell suspensions were processed using the 10x Genomics Single Cell 3′ v3 RNA-seq kit. Gene expression libraries were prepared according to the manufacturer's protocol. MULTI-seq barcode libraries were retrieved from the samples, and libraries were prepared independently.

3.13 Sequencing and processing of raw sequencing reads

Sequencing was done on Nextseq2000, and raw reads were aligned against the mouse genome (mm10, ensemble assembly 104) and mapped and counted by StarSolo (Dobin et al., DOI: 10.1093/bioinformatics/bts635) followed by secondary analysis in Annotated Data Format. Pre-processed counts were analyzed using Scanpy (Wolf et al., doi: 10.1186/s13059-017-1382-0). Basic cell quality control was conducted by taking the number of detected genes and mitochondrial content into consideration. We removed 232 cells in total that did not express more than 300 genes or had a mitochondrial content less than 20%. Further, we filtered genes if they were detected in less than 30 cells (<3%). Raw counts per cell were normalized to the median count over all cells and transformed into log space to stabilize variance. We initially reduced dimensionality of the dataset using PCA, retaining 50 principal components. Subsequent steps, like low-dimensional UMAP embedding (McInnes & Healy, https://arxiv.org/abs/1802.03426) and cell clustering via community detection (Traag et al., https://arxiv.org/abs/1810.08473), were based on the initial PCA. The cellxgene package did final data visualization.

3.14 Statistical analysis

Data are presented as means ± SD. All statistical analyses were performed with GraphPad Prism 8.0. ROUT method for outliers' identification was performed for each experimental group. A one-way analysis of variance (ANOVA) was made between three experimental groups.Comparison between HYX PBS and HYX FGF10 was done using Student′s t-test *P* values < 0.05 were considered as significant and depicted as following: *P* values < 0.05: *; *P* values < 0.01: **; *P* values < 0.001: ***; *P* values <0.0001: ****.

4. Results

4.1 The capacity of $Cd45^{Neg}Cd31^{Neg}Epcam^{Neg}$ resident mesenchymal cells (rMCs) to functionally support the proliferation and differentiation of alveolar epithelial type 2 (AT2) stem cells is associated with Stem cell antigen 1 (Sca1) expression

This study aims to refine the adult lung resident mesenchymal cell population, called after that rMC and defined by flow cytometry as $Cd45^{Neg}Cd31^{Neg}Epcam^{Neg}$ cells. It was already shown that the $Cd45^{Neg}Cd31^{Neg}Epcam^{Neg}Pdgfr\alpha^{Pos}$ cell population could sustain AT2 stem cell renewal using the so-called alveolosphere in vitro assay.[3] In this approach, the use of antibodies against Cd45 and Cd31 allowed removing, from the target subpopulation, the hematopoietic and endothelial cells, respectively. In the context of a previous milestone study generating organoids in Matrigel arising from a co-culture of $Epcam^{High}$ $Cd24^{Low}$ epithelial cells (previously called epithelial stem/progenitor cells or epiSPC) with rMC-$Sca1^{Pos}$ ($Cd45^{Neg}Cd31^{Neg}Epcam^{Neg}Sca1^{Pos}$), it was demonstrated that these cells were capable of sustaining the proliferation and differentiation of epiSPCs. However, in this study, the impact of the different subpopulations of rMCs on AT2 stem cell proliferation and differentiation was not analysed.

For this purpose, we have sorted an enriched population of mature AT2 cells from the $Sftpc^{CreERT2/+}$; $Tomato^{flox/+}$ lungs. We started first by isolating $Cd31^{Neg}Cd45^{Neg}Epcam^{Pos}$ cells and then applied two successive and stringent sorting approaches: first using LysoTracker, a fluorescent dye that labels acidic compartments found abundantly in the lamellar bodies of AT2 cells. And second, using the tomato reporter expressed specifically in AT2 cells (Figure 7A).

In addition, we sorted also rMCs-$Sca1^{Pos}$ ($Cd45^{Neg}Cd31^{Neg}Epcam^{Neg}Sca1^{Pos}$) as well as rMCs-$Sca1^{Neg}$ ($Cd45^{Neg}Cd31^{Neg}Epcam^{Neg}Sca1^{Neg}$). To have sufficient cells to carry out our assay, we pooled the lungs of four adults (6-8 weeks old) C57BL/6 mice. This allowed us to carry out six independent co-cultures. $Sca1^{Pos}$ cells represent around 25% of the total rMC population (Figure 7A). When co-cultured with sorted mature AT2s, rMC-$Sca1^{Pos}$ led to organoids formation with colony-forming efficiency of 5% (Figure 7C) which is in line with previously published alveolosphere experiments. Interestingly, rMCs-$Sca1^{Neg}$ fail to sustain

alveolosphere formation (Figure 7B). The difference in organoid size and CFE is highly significant between the two rMC subpopulations (Figure 7C, $P < .01$)

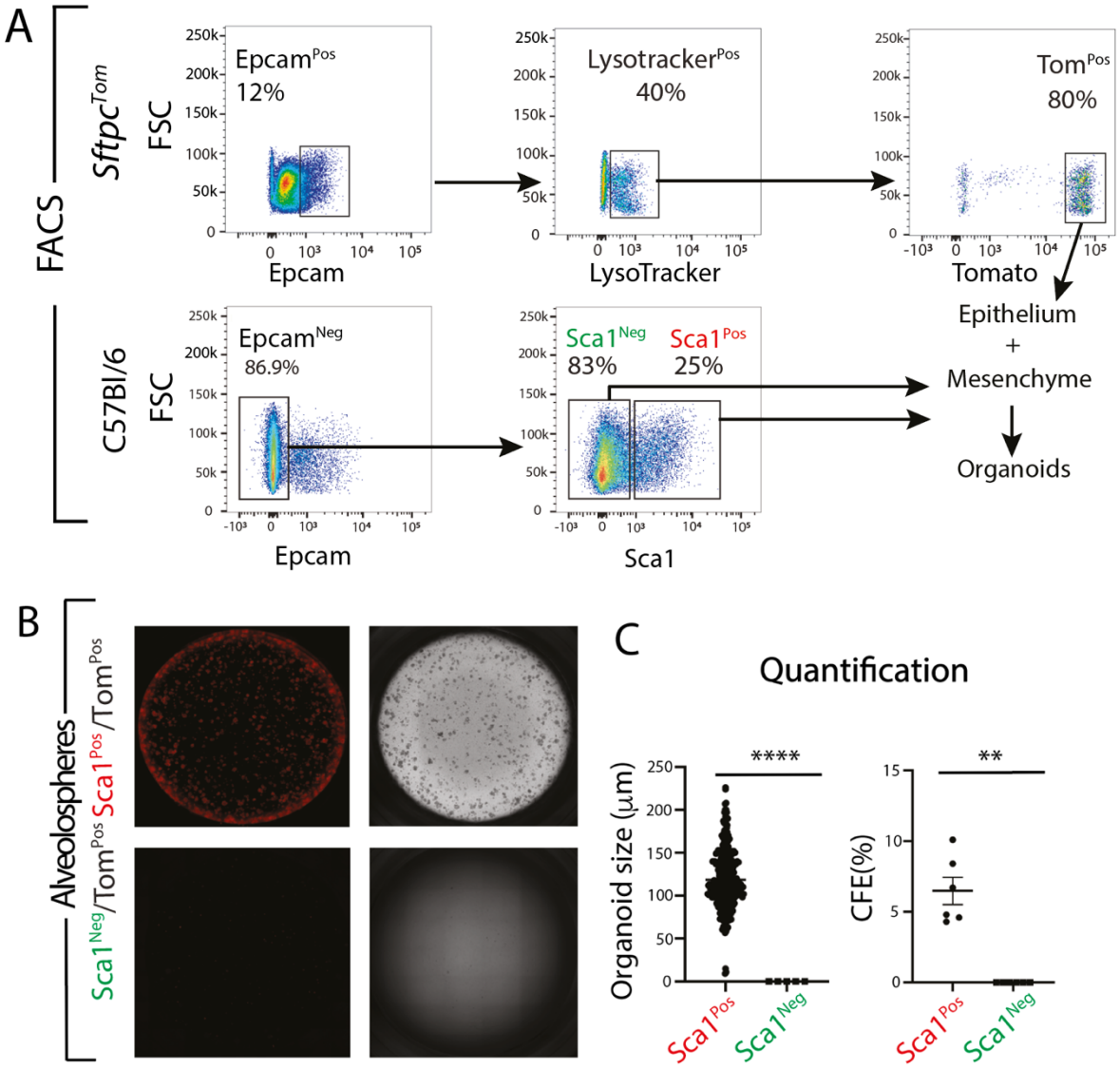

Figure 7. Sca1 expression in combination with the alveolosphere assay separates functionally the lung resident mesenchymal cells. A. Gating strategy to sort mature AT2 ($Epcam^{Pos}Lysotracker^{Pos}Tom^{Pos}$), rMc-$Sca1^{Pos}$ ($Cd31^{Neg}Cd45^{Neg}Epcam^{Neg}Sca1^{Pos}$) and rMC-$Sca1^{Neg}$ ($Cd31^{Neg}Cd45^{Neg}Epcam^{Neg}Sca1^{Neg}$) cells from C57BL6 (WT) mice. **B.** Alveolosphere assay at day 14: Co-culture of mature AT2 with rMC-$Sca1^{Pos}$ or rMC-$Sca1^{Neg}$ cells. **C.** Quantification of the organoids; organoid size, and colony forming efficiency of six independent experiments (n = 6). Scale bar = 50 µm (Taghizadeh et al,. *Stem Cells*, 2021)

4.2 rMCs-Sca1^{Pos} can be further functionally subdivided for the proliferation and differentiation of AT2 stem cells based on LipidTOX staining

To better characterize rMCs-Sca1^{Pos} lung cells and, in particular, whether this population may include the lipofibroblasts (LIFs), we used LipidTOX (LT), an efficient fluorescent stain for neutral lipid. As LIFs are abundant in neutral lipid droplets, LT has been previously used to quantify the LIF population during lung development. Sorted rMCs-Sca1^{Pos}LT^{High} and rMCs-Sca1^{Pos}LT^{Neg} were tested functionally in the alveolosphere model for their capacity to induce the proliferation and differentiation of AT2 stem cells (Figure 8A).

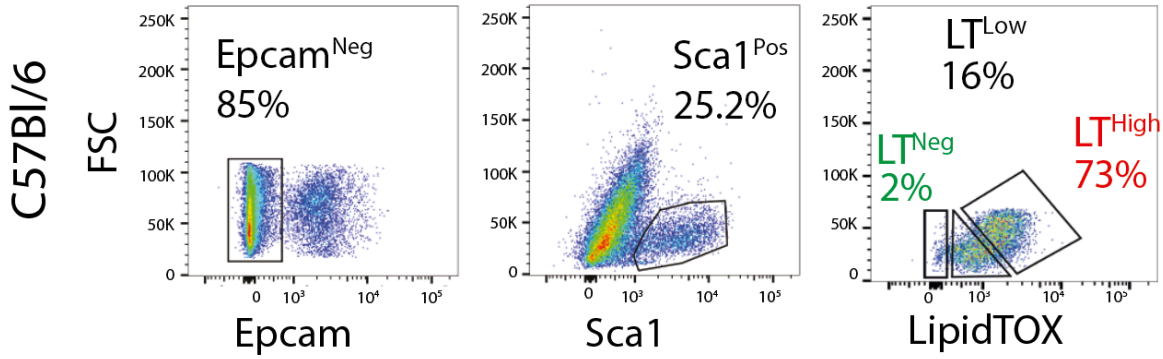

We pooled the cells from three mice and carried four independent co-cultures for this experiment. When co-cultured with sorted mature AT2s, rMCs-Sca1^{Pos}LT^{High} led to the formation of organoids (Figure 8B) with a colony forming efficiency of 2% (Figure 8C) while rMCs-Sca1^{Pos}LT^{Neg} failed to sustain organoid formation. We also carried out at day 14, Immunofluorescence (IF) for LT (LIF marker), Hopx (AT1 cell marker), and DAPI in conjunction with the detection of the endogenous tomato reporter (Figure 8B). Our results indicate that LT^{Pos} cells are located in the periphery of each organoid.

In addition, we observed abundant expression of Hopx within the organoid indicating proper AT2 to AT1 differentiation. RT-qPCR was also carried out to quantify the expression of *Fgf10* and *Pdgfra*, two well-known markers enriched in LIFs (Figure 8D).

Our results indicate a trend toward an increase in the expression of *Fgf10* and *Pdgfra* in rMCs-Sca1^{Pos}LT^{High} compared to rMCs-Sca1^{Pos}LT^{Neg} (n = 3 independent mice) (Figure 8D). These results are in line with the previous observation that *Fgf10* and *Pdgfra* are also expressed in cells other than LIFs. Therefore, our data support the previous conclusion that it is the LIF subpopulation of the rMCs that can preferentially support AT2 stem cell survival and differentiation.

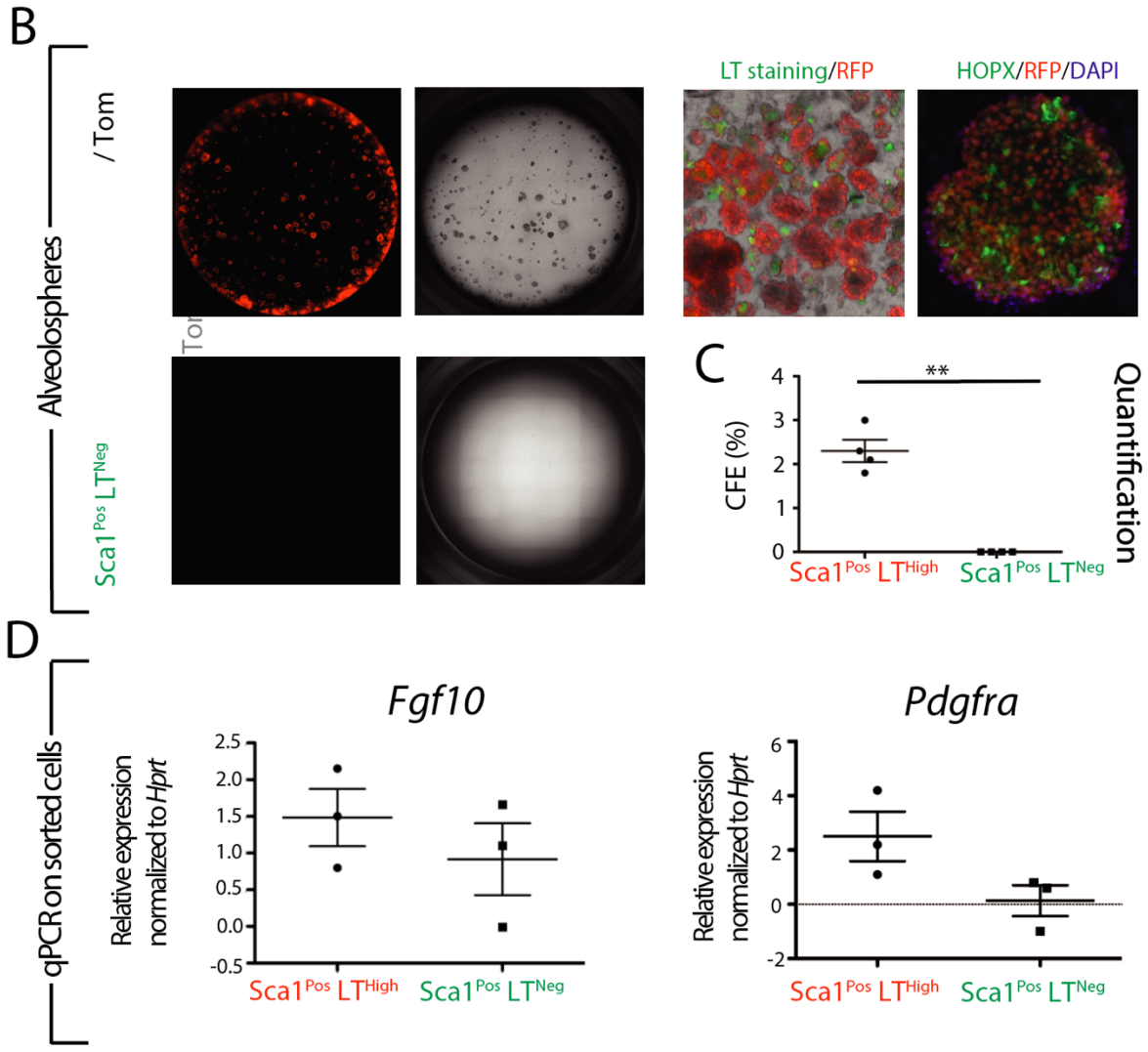

Figure 8. LipidTOX staining identifies a subpopulation of rMC-Sca1^{Pos} cells supporting the proliferation and differentiation of AT2 stem cells. A. *Sftpc^{Tom}* and C57BL6 (WT) mice in 6-8 weeks of age were used to sort Lyso^{Pos}Tom^{Pos} mature AT2 cells and rMC-Sca-1^{Pos}LT^{High} or rMC-Sca-1^{Pos}LT^{Neg} resident stromal cells. Mixture of cells were seeded in Matrigel in 24-well Transwell. **B.** Fluorescence and bright field picture of representative wells at day 14. IF staining of organoids for DAPI, RFP (surrogate for Sftpc, an AT2 cell marker), and Hopx (AT1 cell marker) indicating that lipofibroblasts (rMC-Sca-1^{Pos}LT^{High}) support AT2 stem cell differentiation into AT1 cells (Scale bar = 100 μm). **C**. Quantification of colony forming efficiency (2.3 vs 0 in rMC-Sca-1^{Pos}LT^{High} vs rMC-Sca-1^{Pos}LT^{Neg}, respectively (*P* value 0.001). **D**. *Fgf10* and *Pdgfra* gene expression were assessed by qRT-PCR in rMC-Sca-1^{Pos}LT^{High} vs rMC-Sca-1^{Pos}LT^{Neg}. Quantification of gene expression were normalized to *Hprt*. Scale bar = 50 μm.

4.3 Fgf10^{Pos} cells represent a niche for AT2 cells

We have previously reported that during development, a subset of Fgf10^{Pos} cells are progenitors for lipofibroblasts (LIFs) in the late stage of development and postnatally. We have also reported that during the early postnatal stage of lung development, only 28% of the LIFs express *Fgf10*, indicating that the LIFs, like Fgf10^{Pos} cells, are heterogeneous population. To functionally evaluate the difference between rMCs-Sca1^{Pos}Fgf10^{Pos} and rMCs-Sca1^{Pos}Fgf10^{Neg} cells, we used the *Fgf10^{LacZ}* reporter line in combination with the ß-galactosidase fluorescent substrate FDG to sort, from rMCs, enriched populations of FDG^{Pos} (Fgf10^{Pos}) and FDG^{Neg} (Fgf10^{Neg}) cells. We then isolated the Sca1^{Pos} fraction for each subpopulation. Our results indicate that rMCs-Sca1^{Pos}Fgf10^{Pos} represents around 33% of the rMCs-Fgf10^{Pos} and 25% of the rMCs-Sca1^{Pos}. These results indicate that the rMCs-Sca1^{Pos} and the rMCs-Fgf10^{Pos} subpopulation are indeed heterogeneous (Figure 9A). As previously described, we have co-cultured rMCs-Sca1^{Pos}Fgf10^{Pos} and rMCs-Sca1^{Pos}Fgf10^{Neg} cells with AT2 in our alveolosphere assay.

Our results indicate that organoids only form with rMCs-Sca1^{Pos}Fgf10^{Pos} with a CFE of 4% (n = 4 independent experiments) (Figure 9B, D). rMCs-Sca1^{Pos}Fgf10^{Neg} subset is not capable of eliciting organoid formation IF staining of the organoids for Hopx show that the AT2 cells properly differentiate into AT1 cells (Figure 9C).

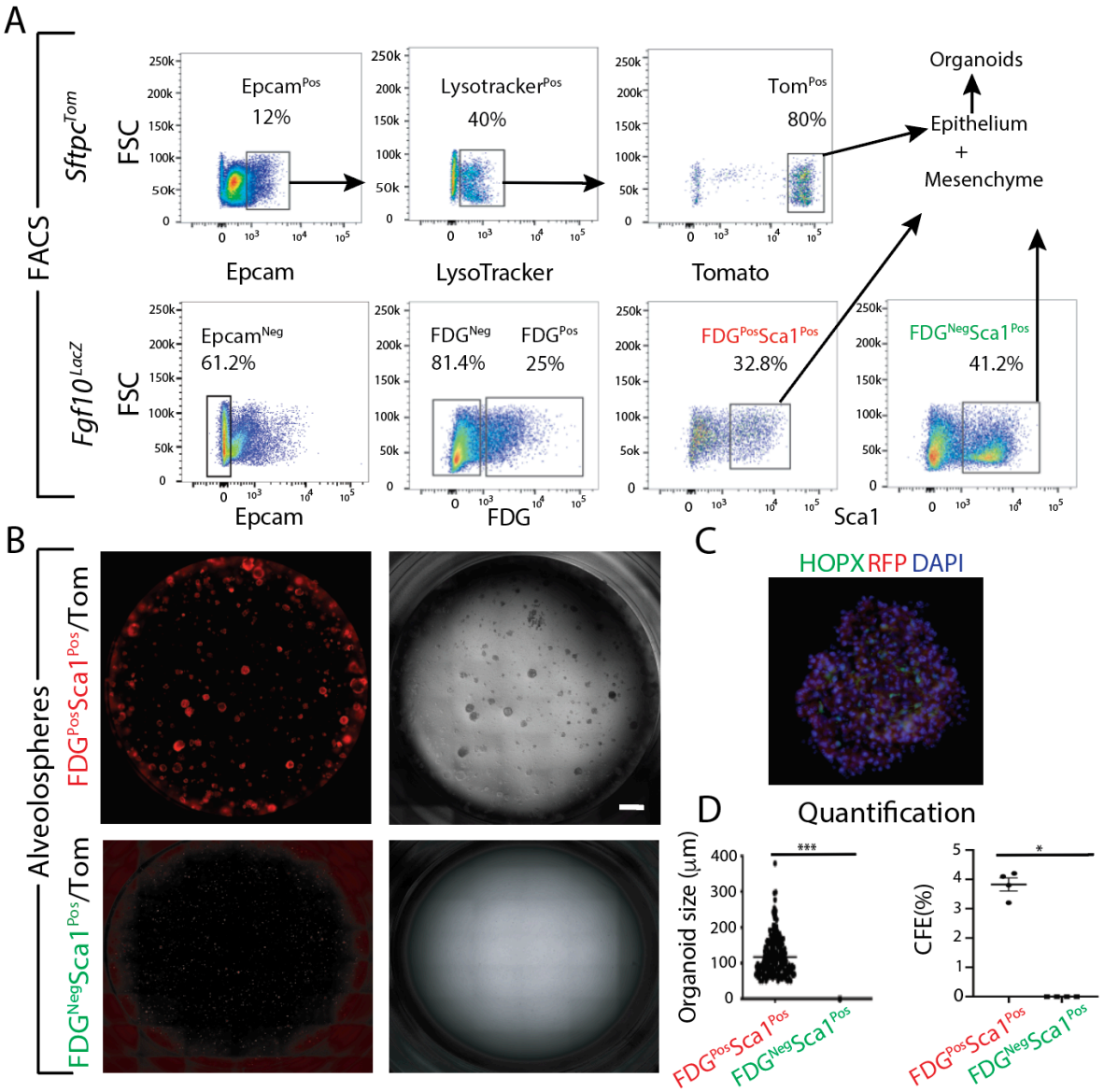

Figure 9. rMC-Sca1^{Pos}Fgf10^{Pos} cells are supporting the proliferation and differentiation of AT2 stem cells. A. Gating strategy to sort mature AT2 cells from *Sftpc^{Tom}* lungs as well as rMC-Sca1^{Pos}Fgf10^{Pos} and rMC-Sca1^{Pos}Fgf10^{Neg} cells from *Fgf10^{LacZ}* lungs using the FDG fluorescent substrate for ß-galactosidase. **B.** Alveolosphere assay showing that only co-culture with rMC-Sca1^{Pos}Fgf10^{Pos} leads to organoid formation. **C.** IF staining against for Hopx and DAPI. **D.** Quantification of organoid size and CFE with rMC-Sca1^{Pos}Fgf10^{Pos} or rMC-Sca1^{Pos}Fgf10^{Neg} (n = 4). Scale bar =100 µm.

4.4 Comparison of rMCs-Sca1^{Pos}Fgf10^{Pos} vs rMCs-Sca1^{Pos}Axin2^{Pos}

Fgf10^{Pos} cells are progenitor for lipofibroblast. LIF in the alveolar region is functionally necessary to support AT2 cells during lung development and postnatal stages. In addition, Axin2, a marker for Wnt signaling activation, is expressed in a subset of mesenchymal cells in the adult lung. It has been reported that 74% of Axin2^{Pos} cells in the alveolar region are also expressing Pdgfrα. Axin2^{Pos} Pdgfrα^{Pos} mesenchymal cells are called mesenchymal alveolar niche cells (MANC) and are located close to AT2 cells. Using the alveolosphere model, they have been reported to sustain AT2 stem cell proliferation and differentiation. As these cells have been described to express *Fgf7* and not *Fgf10*, we propose that rMCs-Sca1^{Pos}Fgf10^{Pos} and rMCs-Sca1^{Pos}Axin2^{Pos} represent two independent pools of niche cells for AT2 stem cells.

To better characterize these two rMC subpopulations, we used specific reporter lines, *Fgf10^{LacZ}* and *Axin2^{LacZ}*, to monitor the distribution of LipidTOX staining in these two sub-lineages. Using FACSAria III cell sorter, we analyzed 100 000 events; each sample contained harvested lung from one mouse with the same age range (6-8 weeks old). Cd45^{Neg}Cd31^{Neg}Epcam^{Neg}Sca1^{Pos} sorted cells were processed for further analysis (Figure 10A). For *Fgf10^{LacZ}* lungs, we found 25% FDG^{Pos} (rMC-Sca1^{Pos}Fgf10^{Pos}) cells out of total rMC-Sca1^{Pos}. For *Axin2^{LacZ}* lungs, our results indicate around 10% FDG^{Pos} (rMC-Sca1^{Pos}Axin2^{Pos}) cells out of total rMC-Sca1^{Pos}.

Further analysis based on LipidTox staining indicate that 85% of Fgf10^{Pos} and 98% of rMC-Sca1^{Pos}Axin2^{Pos} cells were also LT^{High} cells (Figure 10B, C, respectively). Based on LT staining, we also report that most of the rMCs-Sca1^{Pos}Fgf10^{Neg} as well as rMCs-Sca1^{Pos}Axin2^{Neg} subpopulations contain a high percentile of LT$^{Low/High}$ cells suggesting again a functional heterogeneity at the level of the LIFs (in regards to the maintenance of AT2 stem cell proliferation) based on whether they express or not *Fgf10* or *Axin2*.

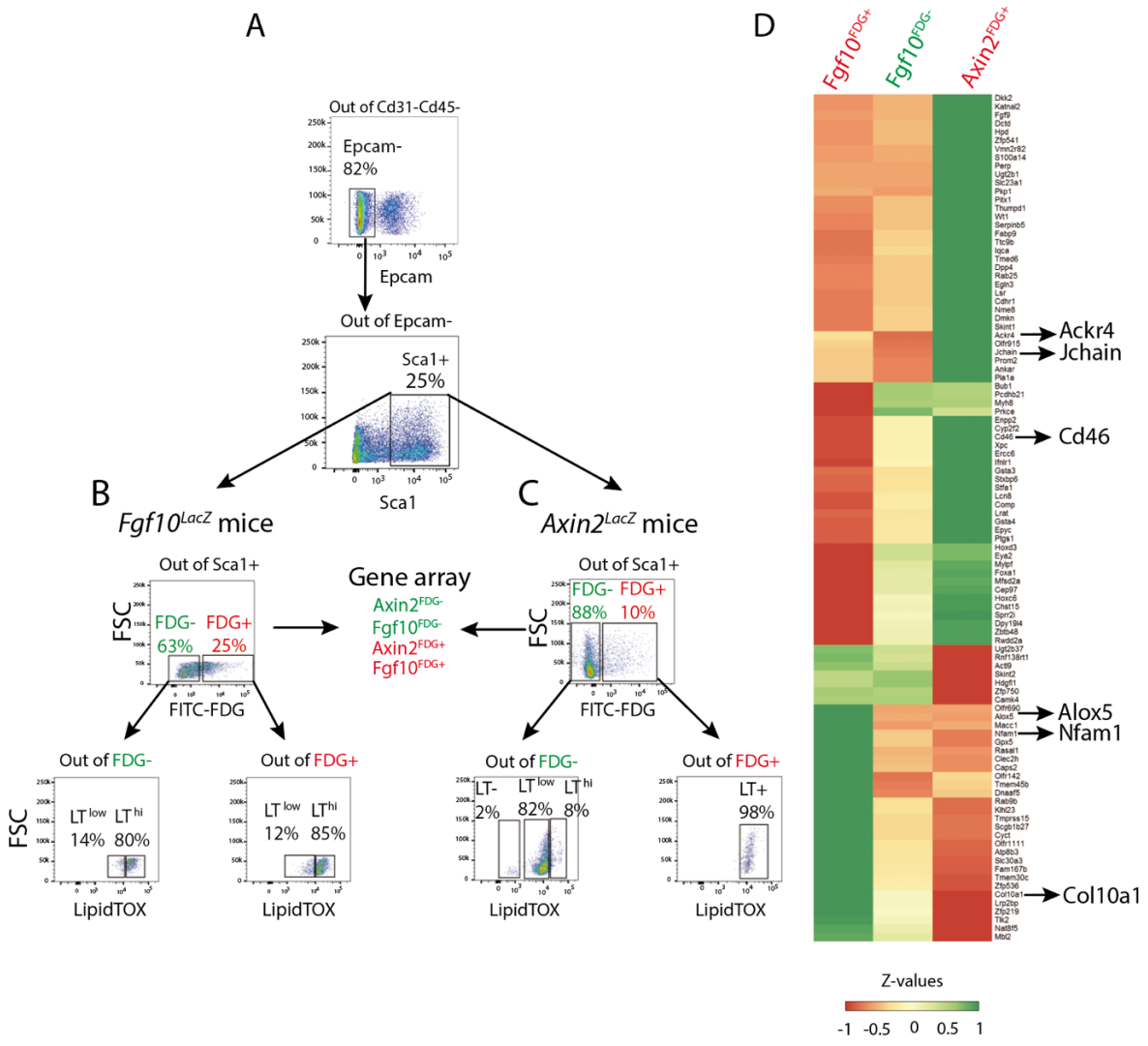

Figure 10. Comparison of rMC-Sca1^{Pos}Fgf10^{Pos} vs rMC-Sca1^{Pos}Axin2^{Pos}. A. Single cell suspension from the adult lungs of *Fgf10^{LacZ} and Axin2^{LacZ}* reporter lines were processed by flow for Cd31, Cd45, Epcam and Sca1 expression to isolate rMC-Sca1^{Pos}. **B,C.** Staining with the FDG fluorescent substrate for ß-galactosidase allowed to separate further the rMC-Sca1^{Pos} into rMC-Sca1^{Pos}Fgf10^{Pos} and rMC-Sca1^{Pos}Fgf10^{Neg} (B) as well as rMC-Sca1^{Pos}Axin2^{Pos} and rMC-Sca1^{Pos}Axin2^{Neg} (C). Further staining with LipidTOX allowed to quantify the abundance of LT^{High} in each subpopulation. **D**. Heatmap is representing top 100 genes which are differentially expressed between rMC-Sca1^{Pos}Fgf10^{Pos} and rMC-Sca1^{Pos}Fgf10^{Neg}. Note that the genes which are downregulated in rMC-Sca1^{Pos}Fgf10^{Pos} are upregulated in rMC-Sca1^{Pos}Axin2^{Pos} and vice versa. The arrows show some of the selected genes among the 100 genes.

To better define at the transcriptomic level the difference between rMCs-Sca1^{Pos}Fgf10^{Pos} and rMCs-Sca1^{Pos}Axin2^{Pos}, we performed gene array analysis using the Agilent platform. Figure 10D shows top 100 genes, which differentially expressed between rMCs-Sca1^{Pos}Fgf10^{Pos} and rMCs-Sca1^{Pos}Fgf10^{Neg} subsets. The genes differentially regulated between these two subsets were evaluated in rMCs-Sca1^{Pos}Axin2^{Pos} cells.

Our results indicate that several markers such as *Ackr4*, *Jchain*, *Cd46*, *Alox5*, *Nfam1,* and *Col10a1* are differentially expressed between rMCs-Sca1^{Pos}Fgf10^{Pos} and rMCs-Sca1^{Pos}Axin2^{Pos} and therefore could be used in the future to label these mesenchymal subpopulations.

KEGG analysis of rMCs-Sca1^{Pos}Axin2^{Pos} vs. rMCs-Sca1^{Pos}Fgf10^{Pos} indicates an upregulation of metabolic pathways, RNA transport, DNA replication as well as cell cycle, indicating that the Axin2^{Pos} cells are metabolically active and proliferative (Table S1). Altogether, our data notably suggest that rMCs-Sca1^{Pos}Fgf10^{Pos} cells are likely different from rMCs-Sca1^{Pos}Axin2^{Pos} cells.

4.5 *Fgf10* expressing cells are located close to Sftpc^{Pos} cells

To investigate the relative interaction between *Fgf10* expressing cells and AT2 cells, we combined the in-situ hybridization technique for detecting *Fgf10* mRNA expression with immunofluorescence staining for pro-SPC in adult wild type lungs. We found that 28% ± 0.5% (n = 3) of total *Fgf10* expressing cells are close to pro-SPC expressing cells (Figure 11A). This number is very similar to the one we reported before in the newborn lung using the *Fgf10*^{LacZ} reporter. This observation suggests that a subset only of the *Fgf10* expressing cells constitutes a critical component of the alveolar niche that may robustly communicate with AT2 cells.

To better define the heterogeneity of the AT2 stromal niche, we have also performed co-staining of *Fgf7* mRNA and Sftpc. *Fgf7* expression has been proposed to be a hallmark of the MANC population.

To validate the *Fgf7* mRNA probe, we used *Fgf7* KO adult lungs. While a clear signal was obtained with a positive control probe, the *Fgf7* mRNA probe failed to generate a signal in the *Fgf7* KO lungs (Figure S1), indicating that the signal observed in wild-type lung is specific (Figure 11B). We found that around only 2.0% ± 0.2% (n = 3) of *Fgf7* expressing cells are in the vicinity of Sftpc^{Pos} cells (Figure 11B).

Finally, we performed a co-staining for *Fgf7* and *Fgf10* mRNA using different fluorescent-labeled probes. Our results indicate that 15.7% ± 1.3% (n = 3) of total cells are *Fgf7* expressing cells vs. 25.4% ± 0.9% (n = 3) for *Fgf10* expressing cells. Finally, 4.0% ± 0.3% (n = 3) of total cells are double-positive *Fgf10/Fgf7* cells (Figure 11C). Taken together, these data suggest that the rMCs-Sca1^{Pos}Fgf10^{Pos} are distinct from Fgf7^{Pos} MANC, while both subpopulations are close to AT2 cells.

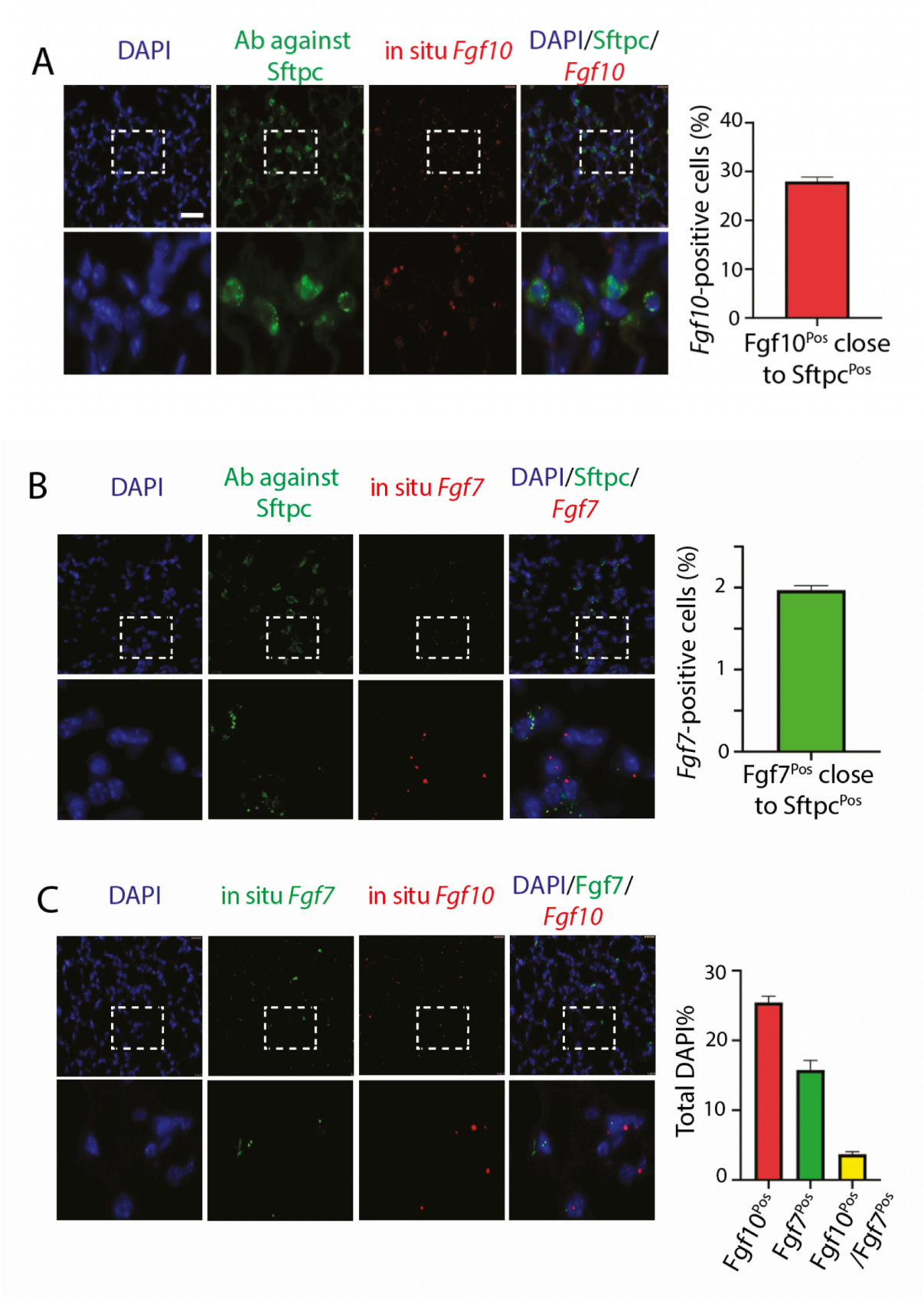
A
DAPI
Ab against Sftpc
in situ Fgf10
DAPI/Sftpc/ Fgf10
Fgf10-positive cells (%)
40
30
20
10
0
Fgf10Pos close to SftpcPos
B
DAPI
Ab against Sftpc
in situ Fgf7
DAPI/Sftpc/ Fgf7
Fgf7-positive cells (%)
2
1
0
Fgf7Pos close to SftpcPos
C
DAPI
in situ Fgf7
in situ Fgf10
DAPI/Fgf7/ Fgf10
Total DAPI%
30
20
10
0
Fgf10Pos
Fgf7Pos
Fgf10Pos /Fgf7Pos

Figure 11. Analysis and comparison of *Fgf10* and *Fgf7* mRNA expression in relation to pro-Sftpc^{Pos} cells in the adult mouse lung. A. In situ hybridization for *Fgf10* mRNA (in red) and IF staining against for pro-Sftpc (in green). Low and high magnification. Quantification of *Fgf10* expressing cells close to Pro-Sftpc^{Pos} cells. **B.** In situ hybridization for *Fgf7* mRNA (in red) and IF staining against for pro-Sftpc (in green). Low and high magnification. Quantification of *Fgf7* expressing cells close to Pro-Sftpc^{Pos} cells. **C.** Co-staining of *Fgf10* and *Fgf7* expressing cells. Quantification of *Fgf7*, *Fgf10* as well as *Fgf7/Fgf10* expressing cells compared to total cells. Scale bar for low magnification: 50 µm and Scale bar for high magnification 200 µm.

4.6 rMCs-Sca1^{Pos} are impacted by obesity and gender

Massive damages to the AT2s occur following various injuries such as viral infection. Consequently, the transdifferentiation of the LIFs into activated MYFs has been proposed, thereby leading to fibrosis formation. Obesity/diabetes and gender are thought to be aggravating pre-existing conditions predicting the severity of the disease. To explore the impact of obesity/diabetes and gender on the functionality of the rMCs-Sca1^{Pos} cells, we used 6-8 weeks C57BL6 males and females as well as *Leptin*-deficient *ob/ob* (aka *ob/ob*) mutant male and female mice (n = 3 for each gender; WT and mutant).

Figure 12A shows the analysis by flow cytometry of rMCs-Sca1^{Pos} in C57BL/6 mice vs. C57BL/6 Leptin-deficient *ob/ob* mice. Interestingly, a drastic reduction of the percentile of rMCs-Sca1^{Pos} is observed in *ob/ob* mice compared to wild-type mice (27.7% vs. 9%, respectively). We also functionally tested the rMCs-Sca1^{Pos} from these different mice by co-culturing them with sorted AT2 cells using the alveolosphere assay. When the rMCs-Sca1^{Pos} are isolated from *ob/ob* male mice presenting the two risk factors, obesity and male (Figure 12B), we observed a complete absence of organoid formation (n = 3). However, when rMCs-Sca1^{Pos} are isolated from female *ob/ob* mice presenting only obesity as a risk factor, a significant number of organoids are present (3% CFE, n = 3). However, this CFE is lower than the one observed in non-obese C57BL6 female wild type mice (5% CFE, n = 3), indicating that obesity alone is already impacting the functionality of the rMCs-Sca1^{Pos}.

Interestingly, non-obese C57BL6 male wild type mice also display a reduced CFE compared to non-obese C57BL6 female wild-type mice (2% vs. 5%, respectively, n = 3), indicating that the gender alone is also impacting the functionality of the rMCs-Sca1^{Pos}. We also observed that age was also having the same effect than obesity and gender on the capacity of the rMCs-Sca1^{Pos} to maintain the proliferation of the AT2 stem cells (data not shown).

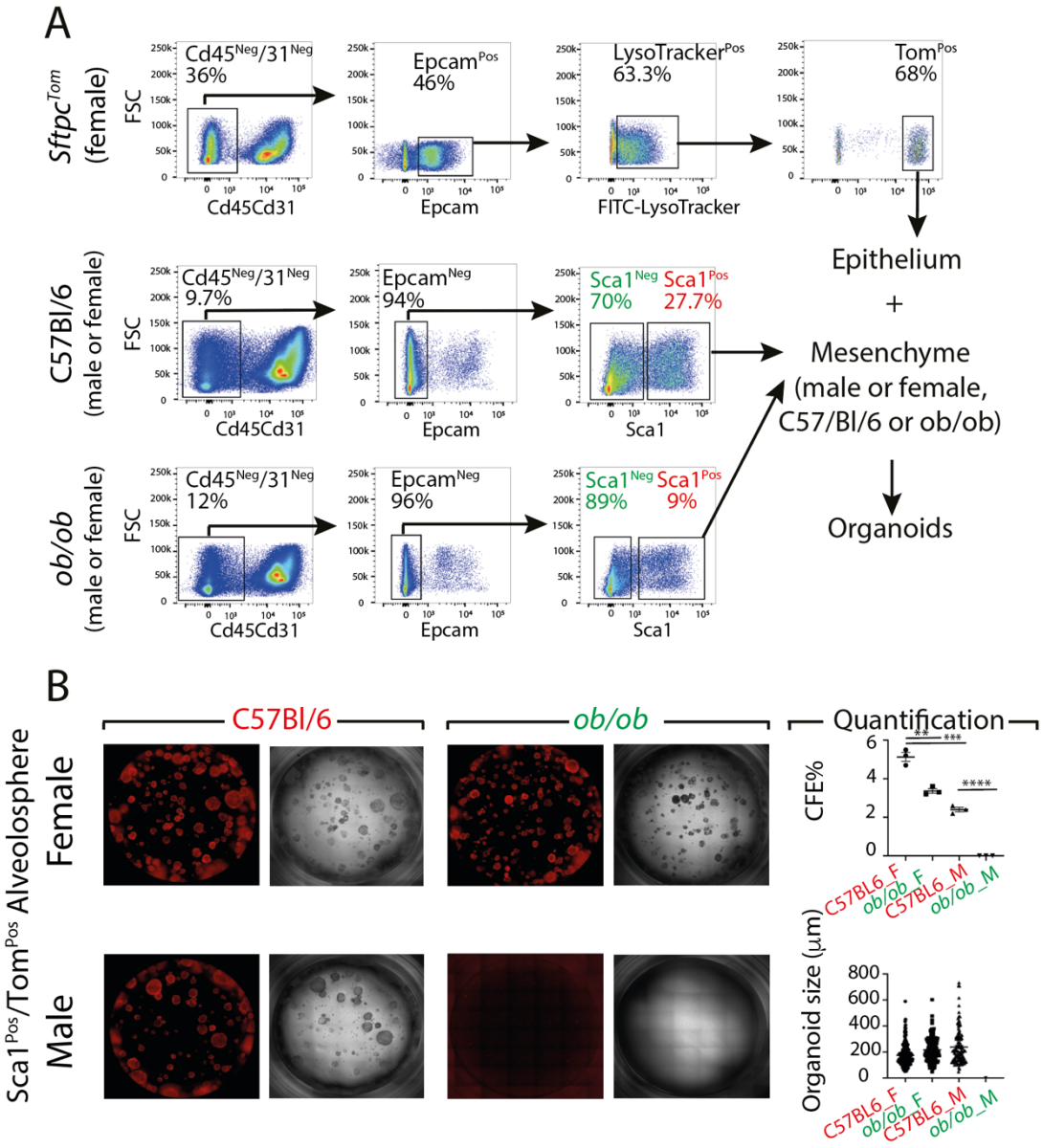

Figure 12: **rMC-Sca1^{Pos} cells are affected by obesity and gender.**
A. Flow cytometry analysis and gating strategy to sort mature AT2 cells from *Sftpc^{Tom}* as well as rMC-Sca1^{Pos} from male and female C57BL/6 mice, and male and female *ob/ob* mice (n = 3 for each genotype and gender). **B.** Alveolosphere culture after 14 days and corresponding quantification of organoid size and colony forming efficiency (n = 3 animals per condition). Scale bar = 50 µm.

4.7 Human recombinant FGF10 rescues the lung structure following hyperoxia induced-arrest in alveologenesis

To test the therapeutic potential of human recombinant FGF10 (rFGF10) in the repair process after HYX injury, we delivered rFGF10 to wild type mice. Figure 13A shows the experimental scheme depicting the injury period and time points of rFGF10 administrations. C57BL6 pups from the experimental group were exposed to HYX (85% O_2) from P0 to P8. In parallel, newborn mice belonging to the control group were maintained under room air (21% O_2). At P8, pups from HYX experimental group were re-exposed to NOX and subsequently divided into two groups, either receiving PBS (HYX+PBS) or rhFGF10 (HYX+FGF10) via intraperitoneal injections (i.p) at three different intervals every other day (P8-P14, P22-P28, and P36-P42). The dose of rFGF10 was six µg/g at the first period a ten 10 µg /g for the second and third treatment periods. Mice were sacrificed at P45. Echocardiography to assess heart function as a surrogate for pulmonary arterial hypertension and morphometry analysis to assess architectural defects were carried out.

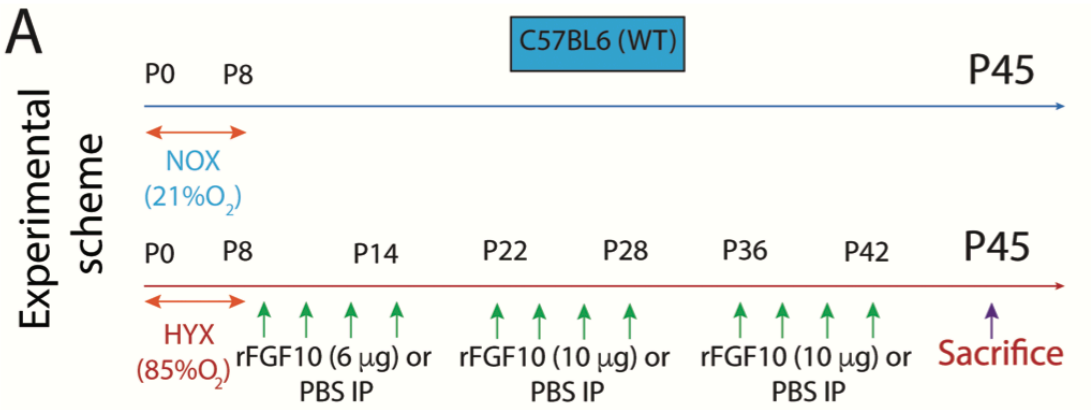

Histological and morphometric (n= NOX:16, HYX PBS: 11, HYX FGF10:13) analysis indicates arrested lung development between the HYX+PBS and NOX lungs. Increased airspace (p=0,0021), decreased wall thickness (p=0,048), and increased MLI (both horizontal and vertical) (p=0,0175, p=0,0066) are observed in HYX+PBS vs. NOX lungs (Fig 13B, C) indicating that hyperoxia led to the expected damages.

Supporting the role of FGF10 in de-novo alveologenesis, an obvious recovery of the lung structure was observed in HYX+FGF10 vs. HYX+PBS lungs (Fig 13B). Interestingly, ANOVA analysis did not indicate significant changes for morphometric parameters between these two groups (Fig 13C). However, a direct comparison between the HYX-PBS and HYX-FGF10 group by student T-test showed a statistically significant difference in air space (p=0,03). A trend towards significance for wall thickness (p=0,064), and MLI-H (p=0,522) and MLI-V (p=0,369) was also noted (Supp Fig 1).

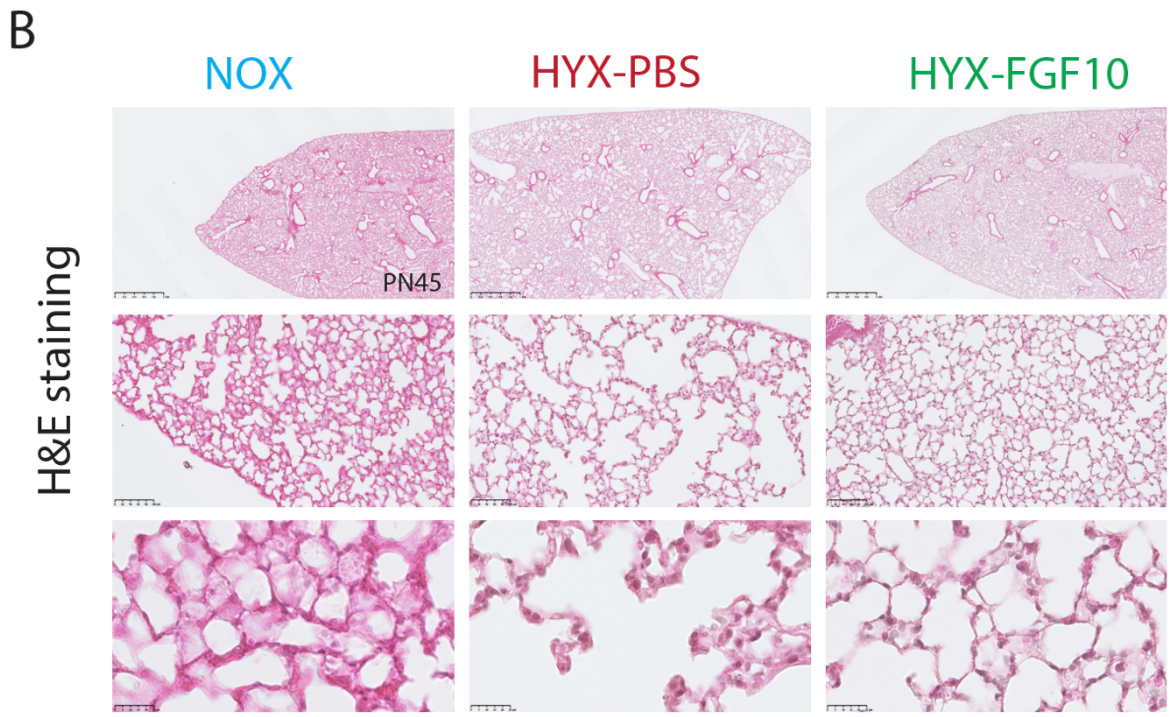

BPD is correlated with abnormalities in the right ventricular (RV). These heart defects are usually associated with PAH formation. RV function was evaluated by using echocardiography. In particular, we measured the tricuspid annular plane systolic excursion (TAPSE, n= NOX:21, HYX PBS:11, HYX FGF10:11) value <1.6 mm, as this was reported to be a sensitive method to estimate RV systolic dysfunction. In HYX+PBS vs. NOX, we observe a significant decrease in TAPSE ($p<0,00001$). As the TAPSE value is highly correlated with the body weight, we also monitored the weight of the pups between the two groups. No significant difference was found between them (Fig 13D).

Comparison between the HYX-FGF10 vs. the HYX-PBS groups indicates an increase of the TAPSE value ($p=0,028$). No significant difference was found between the HYX-FGF10 vs. the NOX groups ($p=0,1925$), indicating a normalization of the RV function. This difference between the HYX-FGF10 and HYX-PBS groups was not due to changes in body weight ($p=0,959$). Taken together, these observations support the therapeutic potential of rFGF10 delivered IP in the *de novo* alveologenesis process after hyperoxia injury.

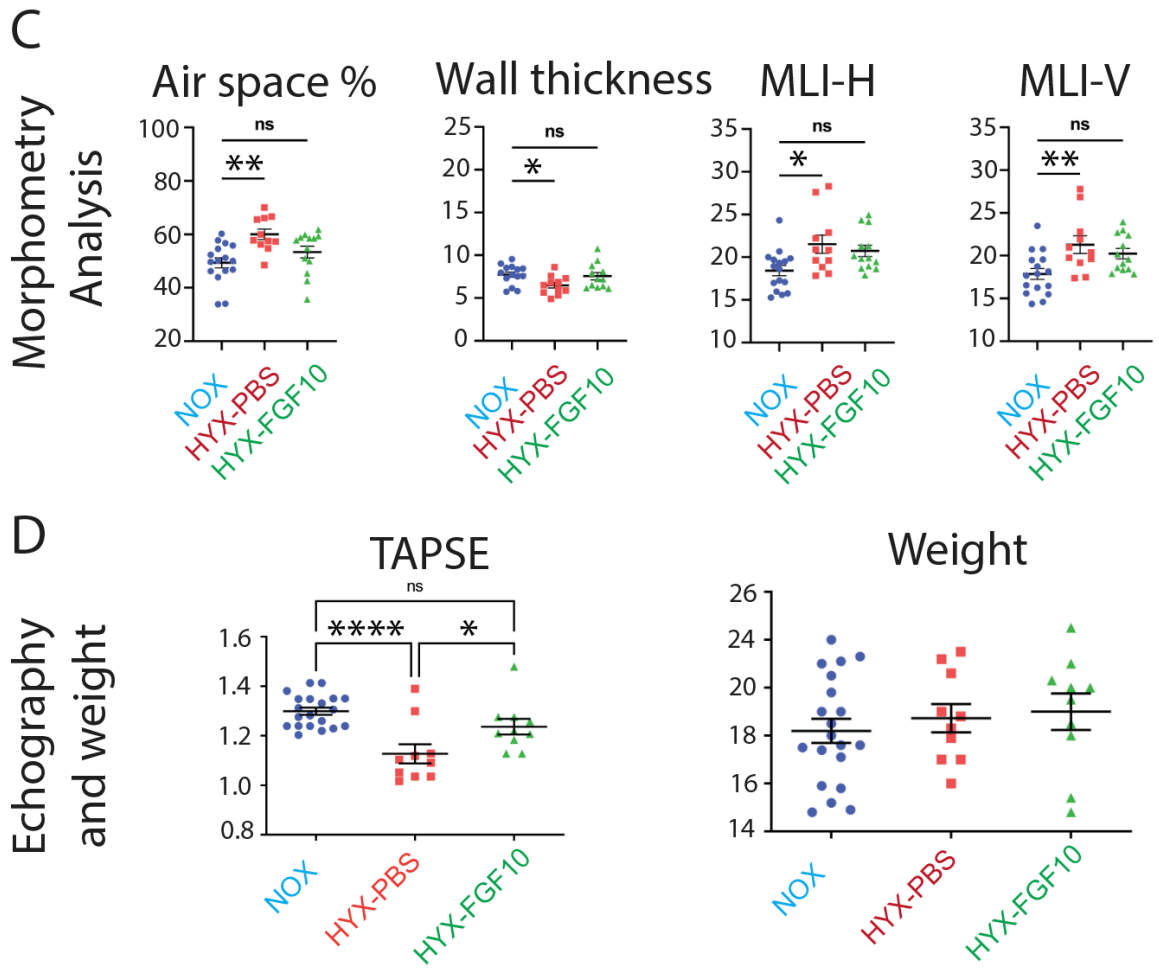

Figure 13: Recombinant FGF10 rescues the lung architecture following hyperoxia induced-arrest in alveologenesis A. Experimental approach depicting the regimen of rFGF10 administration to C57BL6 mice. **B.** H&E staining at P45 of three groups. **C.** Morphometry analysis at P45. Scale bar: 2.5x: 1mm, 20x: 100 µm, 80x: 25 µm. ns: non-significant. **D.** Echography was monitored at P45 and body weight was assessed regularly from P8 to P45. Representative graph shows the weight of the mice before sacrifice.

4.8 Alveolospheres assays indicate that HYX and FGF10 pre-treatments impact FACS-isolated rMC activity to sustain AT2 stem cell proliferation and differentiation

Alveolar epithelial type 2 cells (AT2), the quiescent stem/progenitor epithelial cells, are capable of proliferating and differentiating to alveolar epithelial type 1 (AT1) cells following exposure to injury. Resident mesenchymal cells (rMC) have been previously defined as $Cd45^{Neg}Cd31^{Neg}Epcam^{Neg}$ population and represent at large a niche for AT2 stem cells. In particular, rMC-$Sca1^{Pos}$ cells are very efficient in triggering organoid formation using the alveolosphere assay.

To perform this assay, we have collected lungs at P45 from NOX, HYX+PBS, and HYX+FGF10 mice and sorted the $Cd45^{Neg}Cd31^{Neg}Epcam^{Neg}$ $Sca1^{Pos}$ cells (rMC-$Sca1^{Pos}$). The rMC-$Sca1^{Pos}$ cells belonging to these three groups were individually co-cultured in Matrigel with $Epcam^{Pos}Lyso^{Pos}$ cells representing mature AT2 cells and analyzed after 14 days in culture (Fig 14A). Comparison between rMC-$Sca1^{Pos}$ (HYX+PBS) and rMC-$Sca1^{Pos}$ (NOX) indicates a decreased both in organoid formation (n=3 *P-value* < 0.0001) and in organoid size (n=3 *P* value < 0.0001). We could detect Sftpc and Pdpn expression in both organoids of both groups indicating normal AT2 and AT1 differentiation (Figure 14 B and C). Comparison between rMC-$Sca1^{Pos}$ (HYX+FGF10) and rMC-$Sca1^{Pos}$ (HYX+PBS) indicates a significant increase both in organoid formation (n=3 *P-value* < 0.0001) and in organoid size (n=3 *P-value* < 0.0001). Normal AT2 and AT1 differentiation was noted (Figure 14 B and C).

In conclusion, the activity of the rMC-$Sca1^{Pos}$ niche is negatively impacted by HYX, and human rFGF10 treatment restores its activity.

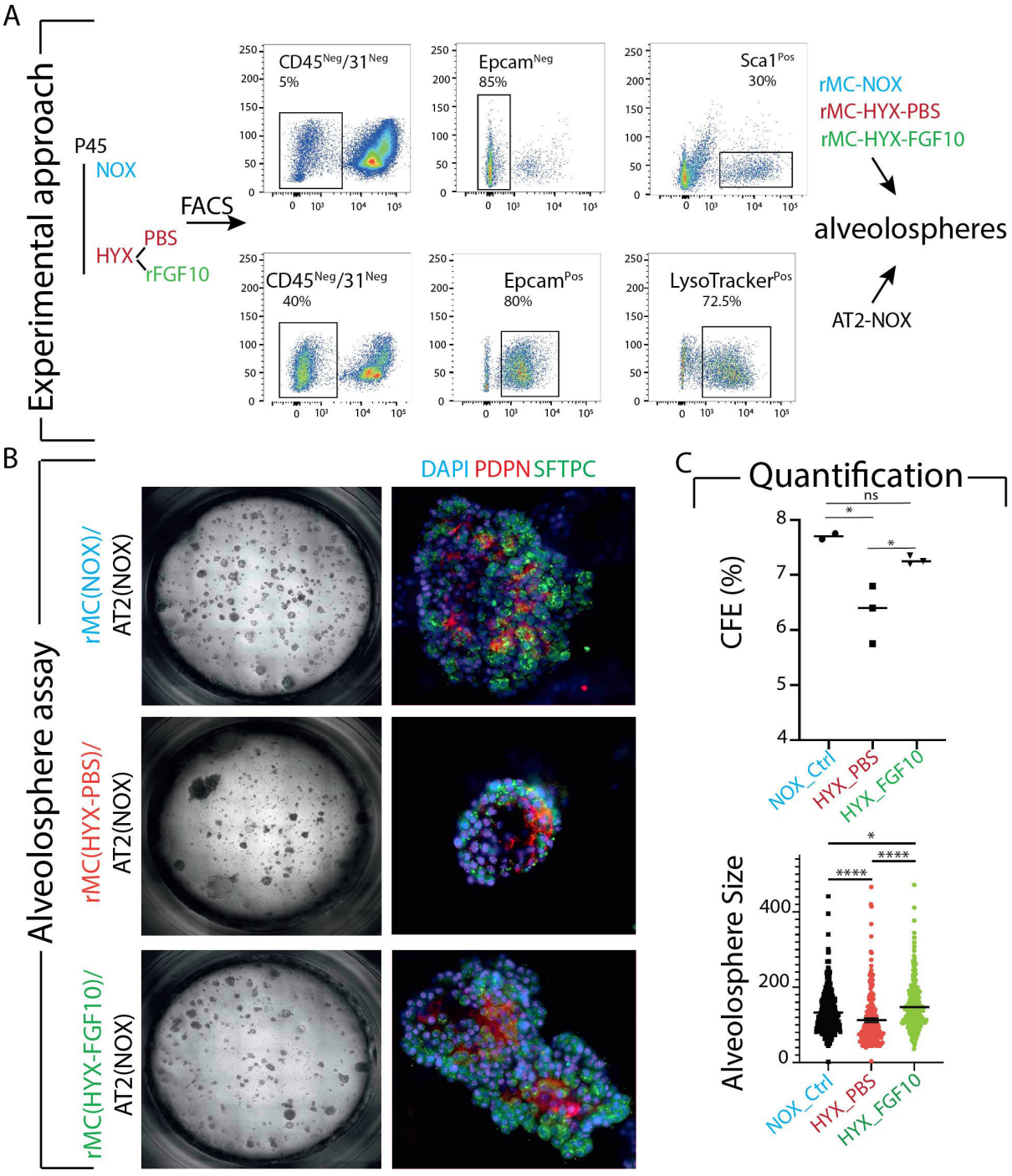

Figure 14: HYX and FGF10 treatments impact the rMC activity to sustain AT2 stem cell proliferation in vitro using alveolospheres A. Quantification of rMC Sca1^{Pos} by using flow cytometry and gating strategy for cell sorting**. B.** 3D organoid model by co-culturing rMC Sca1^{Pos} and mature AT2 (Lysotracker positive cells). Scale bar: 100 µm **C.** Quantification of CFE and organoid size between the three groups.

4.9 rMC-Sca1^{Pos} cells are quantitatively impacted by HYX and FGF10

The number of rMC-Sca1Pos cells in NOX, HYX+PBS, and HYX+FGF10 was quantified by flow cytometry analysis. Comparison between HYX+PBS vs. NOX indicate a decrease (12±8 vs. 25±5, P value <0.001, n=3). Comparison between HYX+FGF10 vs. HYX+PBS indicate an increase (40 ±4 vs. 12±8, P value <0.001, n=3) (Fig 15A).

To confirm our results by flow cytometry, we have performed IF staining against Sftpc in the three groups (Fig 15B). Quantification of AT2 cell number in HYX+PBS vs. NOX and HYX+FGF10 vs. HYX+PBS indicated that there is no significant change in total SftpcPos cells per total counted cell number (Fig 15C). We also found a significant decrease of DAPI+ cells in HYX-PBS group vs. NOX supporting the alveolar simplification phenotype trigger by HYX. This indicates that it is mostly the mesenchyme and not the epithelium where HYX quantitatively impacts. These changes in the number of DAPI+ cells are partially reversed upon human rFGF10 treatment. In conclusion, we demonstrated that the mesenchymal compartment represents a major target of HYX, both qualitatively (Fig 14) and quantitatively (Fig 15).

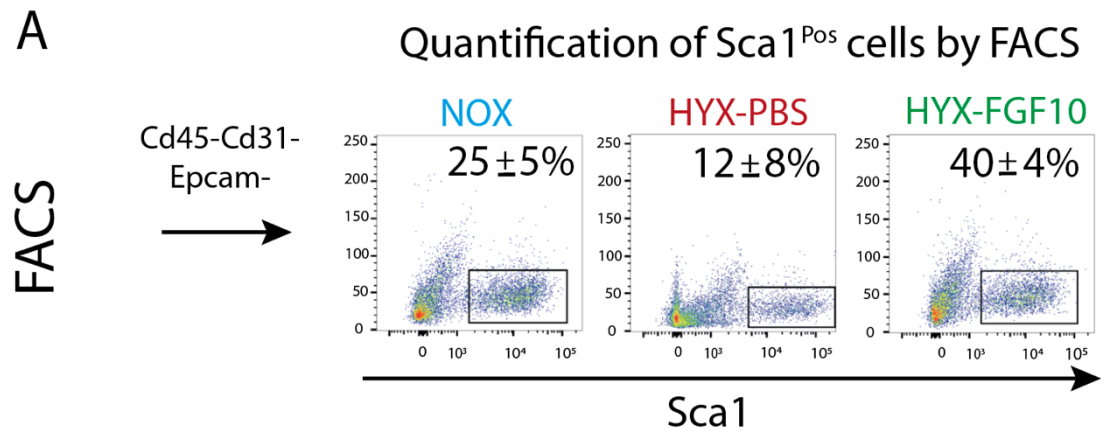

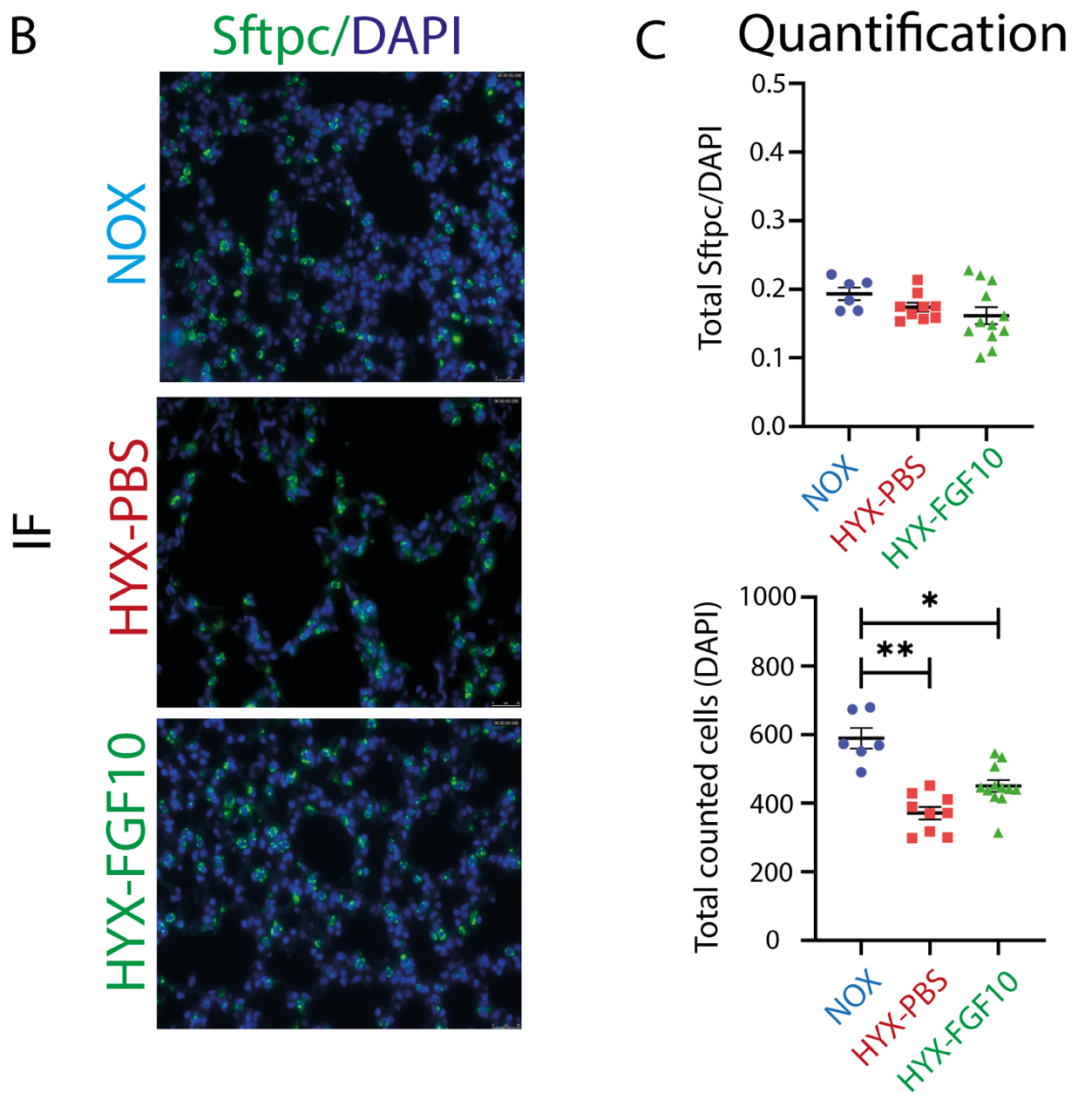

Figure 15: rMC-Sca1^{Pos} cells are impacted by HYX and FGF10 A. Flow cytometry analysis of rMC-Sca1^{Pos} cells in three groups. **B.** IF staining against for Sftpc. **C.** Quantification of total Sftpc out of total counted cells and total counted cells (DAPI) in three groups. Scale bar: 50 µm

4.10 Characterization rMC-Sca1^{Pos} by scRNA-seq in NOX and HYX+PBS

To define different subsets of rMC-Sca1^{Pos} cells, we sorted the Cd45^{Neg}Cd31^{Neg}Epcam^{Neg}Sca1^{Pos} cells after HYX+PBS or NOX at P45 and loaded 9000 cells per group on 10X RNAseq chips (Fig 16A). Quality control was performed independently on each library to find the appropriate filtering thresholds. Poor quality cells with a high percentage (>20%) of UMIs mapped to mitochondrial genes were removed (Fig 16B). We selected 877 cells in the NOX and 900 in HYX. We detected an average of 2271 and 2389 genes in NOX and HYX with the median number of reads per cell in NOX and HYX of 38.383 and 33.531, respectively. Performing UMAP embeddings identified 18 clusters, which were generated based on initial PCA (Fig 16C). As expected, Ly6a expression was expressed throughout all the different clusters at variable levels, and the epithelial marker Epcam was essentially absent from this data set (Supp Fig. 3A). The genes characterizing these different clusters are shown in Supp Fig. 3B.

These clusters correspond to three major cell groups: lipofibroblasts (LIFs, clusters 2, 6, 7, 11, and 12) (Fig 16D), myofibroblasts (MYF clusters 1 and 4), and extracellular matrix (ECM) cells (clusters 3 and 13). Next, we analyzed the expression level of published known markers for the rMC niche (Fig 16E and Supp fig 5). *Fgf10* and *Fgf7* are mainly expressed in the LIF group (clusters 2, 6, and 7). *Tgfbi* and *Lum* mainly label the LIF group (clusters 2 and 6). *Axin2* is found throughout the rMC-Sca1^{Pos} groups, which indicates that it does not represent a specific marker for the specialized niche cells within this mesenchymal population. *Pdgfra* is mainly expressed in clusters 2, 6, and 7. Finally, *Lumican* is found almost exclusively in clusters 2, 6, and 11-12. Fig 16G and Supp fig 3B display the genes characteristic of each LIF subcluster. Cluster 7, defined as LIF subset 1, significantly expresses *Fgf10*, *Limch, Inmt*, and *Col13a1*.

Cluster 2 as LIF subset 2 expresses Dcn, Nbl1, Lum, and Col1a1 preferentially. Cluster 6, identified as LIF subset 3 is highly enriched for *Apoe*, *Prrx1*, *Socs3*, *Col14a1*. Cluster 11, defined as LIF subset 4 highly express *Ly6a* (Sca1), *Igfbp7*, *Cd34*, *Col4a1*, Cluster 12 defined as LIF subset 5 is enriched in *Dner*, *IL6*, *Tagln,* and *Col14a1.*

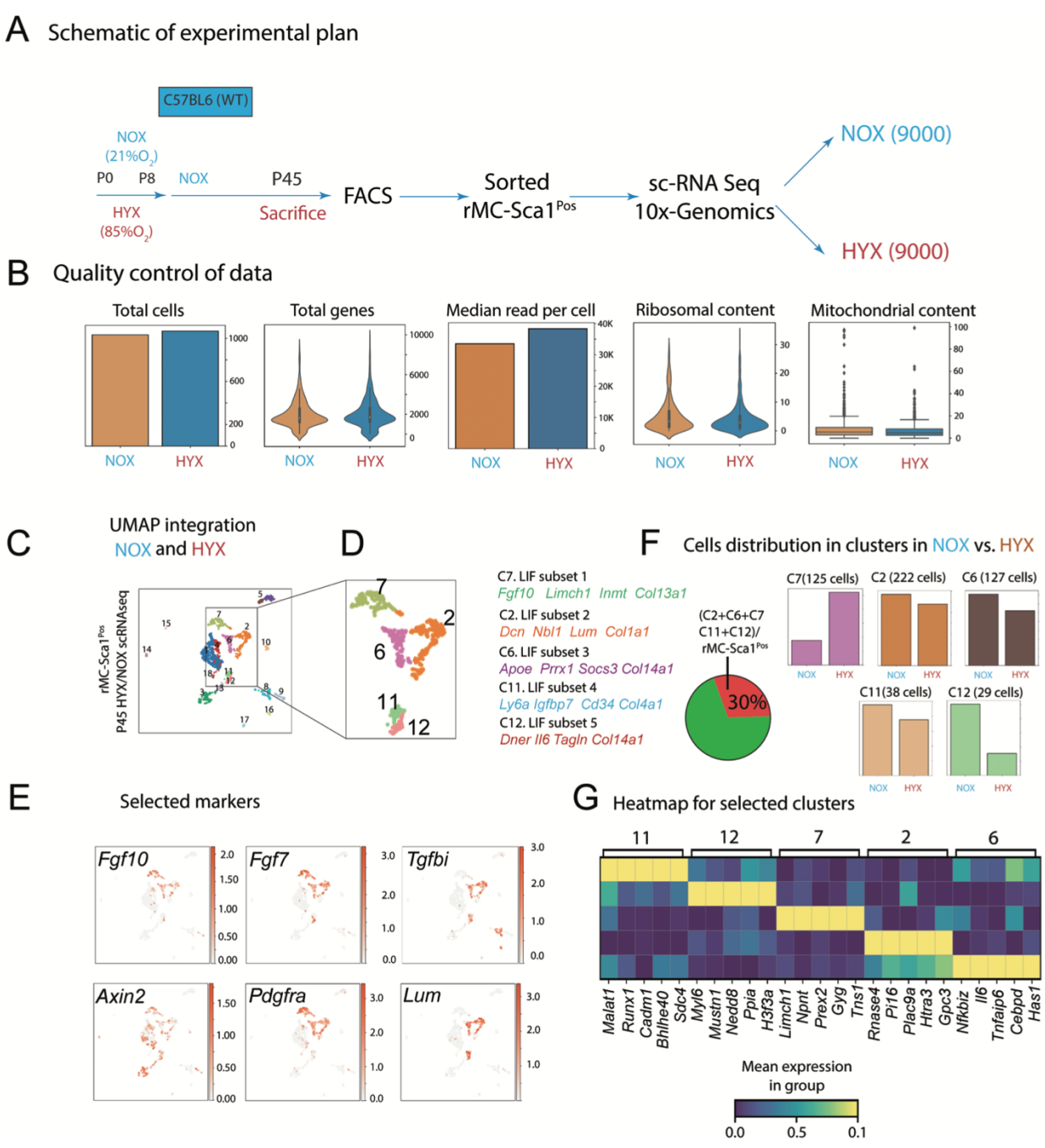
A Schematic of experimental plan
C57BL6 (WT)
NOX (21%O2)
P0
P8
NOX
P45
Sacrifice
HYX (85%O2)
FACS
Sorted rMC-Sca1Pos
sc-RNA Seq 10x-Genomics
NOX (9000)
HYX (9000)
B Quality control of data
Total cells
Total genes
Median read per cell
Ribosomal content
Mitochondrial content
NOX
HYX
C
UMAP integration
NOX and HYX
rMC-Sca1Pos P45 HYX/NOX scRNAseq
D
F Cells distribution in clusters in NOX vs. HYX
C7. LIF subset 1
Fgf10 Limch1 Inmt Col13a1
C2. LIF subset 2
Dcn Nbl1 Lum Col1a1
C6. LIF subset 3
Apoe Prrx1 Socs3 Col14a1
C11. LIF subset 4
Ly6a Igfbp7 Cd34 Col4a1
C12. LIF subset 5
Dner Il6 Tagln Col14a1
(C2+C6+C7 C11+C12)/ rMC-Sca1Pos
30%
C7(125 cells)
C2 (222 cells)
C6 (127 cells)
C11(38 cells)
C12 (29 cells)
E Selected markers
Fgf10
Fgf7
Tgfbi
Axin2
Pdgfra
Lum
G Heatmap for selected clusters
11
12
7
2
6
Malat1 Runx1 Cadm1 Bhlhe40 Sdc4 Myl6 Mustn1 Nedd8 Ppia H3f3a Limch1 Npnt Prex2 Gyg Tns1 Rnase4 P116 Plac9a Htra3 Gpc3 Nfkbiz Il6 Tnfaip6 Cebpd Has1
Mean expression in group
0.0
0.5
0.1

Figure 16: Characterization rMC-Sca1^{Pos} by scRNA-seq in NOX and HYX

A. Experimental approach: mice belonging to the NOX or HYX+PBS groups were sacrificed at P45 and rMC-Sca1^{Pos} cells were isolated by FACS and processed for scRNAseq on the 10X Genomic platform. **B.** Quality control data. **C.** UMAP integration of NOX and HYX scRNAseq dataset identifies 18 clusters. **D.** Selected clusters expressing previously reported LIF genes. **E.** Expression of selected mesenchymal cell markers on the UMAP representation. **F.** Cell distribution in clusters C7, C2, C6, C11, and C12 in NOX and HYX. **G.** Heatmap of top 25 genes differentially expressed between the five LIF clusters based on mean expression in the group.

In our previous study, we found by flow that around 25% of rMC-Sca1^{Pos} cells are Fgf10^{Pos} (56). rMC-Sca1^{Pos} Fgf10^{Pos} cells are the cells that display the rMC niche activity for AT2 stem cells. Our scRNAseq analysis found that the LIF group represents 30% of the rMC-Sca1^{Pos} cells, suggesting that the scRNAseq process conserved the ratio present initially in terms of rMC-Sca1^{Pos} Fgf10^{Pos} over rMC-Sca1^{Pos} cells.

Among the five clusters contained in the LIF group, the most abundant clusters displaying the highest level of *Fgf10* expression, clusters 2 and 6, show a reduction in cell number after HYX (Fig 16F). An extended list of the genes capable of distinguishing subclusters 2 and 6 from the other LIF subclusters is shown in Supp Fig. 2B. Interestingly, cluster 6 is characterized by the expression of genes controlling inflammatory responses like *Cebpd* (57), *Tnfaip6* (58), *Il6* (59), and *Nfkbiz* (60).

We then determined the genes differentially expressed in HYX vs. NOX for subclusters 2 and 6 (Supp Fig. 4). In general, our analysis indicated that, in our experimental conditions, the range in the expression level for these genes between the 2 conditions is relatively small. Among the genes identified for cluster 2, we noticed *Vegfd,* which is highly expressed during vascular formation and correlates with pulmonary hypertension after hyperoxia injury (61,62).

We also found *Akap12* (A-kinase anchoring protein 12), a gene encoding a protein that functions to bind regulatory subunits of protein kinase A and C and control cell growth (63).

Among the genes identified for cluster 6, we found proto-oncogene such as *Fosb* and *Junb* (64). These genes are involved in the regulation of cell proliferation and differentiation. We also found that *Apoe*, a well-accepted LIF marker (34), is expressed more in HYX than NOX. Interestingly, *Nbl1,* a gene encoding an antagonist for BMP signaling (65), is described more in NOX than HYX.

Altogether, our analysis reveals subtle changes in gene expression in clusters 2 and 6 in HYX vs. NOX, which may be explained by the late time point (P45) chosen for the analysis and compensatory mechanisms at play.

5. Discussion

5.1 rMC-Sca1^{Pos}Fgf10^{Pos} are different from the rMC-Sca1^{Pos}Axin2^{Pos}

A major problem arising from key publications using flow cytometry as a primary experimental approach is the lack of independent studies reporting the reproducibility of the results. This is due partly to the type of flow sorter used, the sophisticated flow cytometry protocols, including the gating conditions used, and the lack of comparison with other endogenous populations at the time of the sort as internal controls. This is particularly crucial in the context of the lung mesenchyme, which is still a huge black box both in humans and in mice despite recent scRNA seq studies (34). Our study adopted an unbiased and reproducible FACS strategy to sort both epithelial and mesenchymal populations. We used Sca1 as a resident mesenchymal cell marker to refine the rMC population. In previous studies, Cd45^{Neg}Cd31^{Neg}Sca1^{Pos} cells were detectable by flow cytometry in the postnatal lung coincidently with the transition from the saccular to the alveolar stage of the lung development. This population also co-expressed Cd34, Thy1 (Cd90), as well as Pdgfrα and was proposed to mark LIFs (23). Interestingly, our gene array data shows that Cd90 is highly expressed in rMC-Sca1^{Pos}Fgf10^{Pos} compared to rMC-Sca1^{Pos}Axin2^{Pos} (data not shown). Another study, it was demonstrated that Cd45^{Neg}Cd31^{Neg}Epcam^{Neg}Sca1^{Pos} (rMC-Sca1^{Pos} cells) could be refined into two main subpopulations, namely Cd166^{Pos}Cd90^{Neg} and Cd166^{Neg}Cd90^{Pos}.

The Cd166^{Neg}Cd90^{Pos} subpopulation contained undifferentiated mesenchymal progenitors capable of differentiating toward the LIF and the MYF lineage, while the Cd166^{Pos}Cd90^{Neg} subpopulation contained more differentiated mesenchymal cells already committed to the MYF lineage. Additionally, the Cd166^{Neg}Cd90^{Pos} expressed high levels of *Fgf10*. Further organoid-based experiments indicated that Cd166^{Neg} compared Cd166^{Pos} displayed higher activity in supporting the proliferation of epiSPC. In vitro culture of rMC-Sca1^{Pos} cells showed that they lost their capacity to maintain epiSPC proliferation over time. This activity could be rescued entirely by co-culturing these rMC-Sca1^{Pos} cells with the TGFb1-inhibitor SB431542. Such treatment was associated with the upregulation of endogenous *Fgf10* expression in *in vitro* cultured rMC-Sca1^{Pos}.

Finally, a drastic increase in CFE was observed upon treatment of rMC-Sca1^{Pos}-epiSPC co-culture with recombinant FGF10 (24).

In these experimental conditions, FGF7 did not display such activity. Taken together, our results indicate that rMC-Sca1^{Pos}Fgf10^{Pos} correspond to a specifically enriched population of LIFs capable of maintaining AT2 stem cell proliferation and differentiation. A recent milestone study published in Cell described a mesenchymal cell subpopulation called MANC (Mesenchymal Alveolar Niche Cells), positive for *Axin2*, *Pdgfra*, *Wnt2*, *Il6*, and *Fgf7* (26). MANCs are located close to AT2s and sustain in vitro the proliferation and differentiation of AT2 stem cells. Before this study, the current knowledge was that the MANC were considered at the top of a hierarchy of mesenchymal niche cells and were likely to be essential for both homeostasis and repair after injury. The current study brings into light a novel challenger for this vital role. Our results indicate that rMC-Sca1^{Pos}Fgf10^{Pos} are likely different from the rMC-Sca1^{Pos}Axin2^{Pos} (aka the MANC, but isolated in our experimental conditions) has, nonetheless, a similar function in regards to the AT2 stem cells. In addition, we cannot exclude the possibility that AT2 stem/progenitor cells are also heterogeneous and that rMC-Fgf10^{Pos} and rMC-Axin2^{Pos} (MANC) may be targeting different AT2 stem/progenitor cell subsets.

5.2 Are the rMC-Sca1^{Pos}Fgf10^{Pos} more relevant than the rMC-Sca1^{Pos}Axin2^{Pos} for the repair process after an injury?

Given the fact that both subpopulations appear to sustain the proliferation and differentiation of AT2 stem cells in vitro, the natural question is, therefore, whether they have redundant functions or whether one population seems to be more crucial than the other. From the angle of Fgf signaling and based on the consequence of *Fgf7* vs. *Fgf10* gene inactivation in mice, we can conclude that rMC-Sca1^{Pos}Fgf10^{Pos} subset is likely necessary. *Fgf10* inactivation leads to lung agenesis, while *Fgf7* null mice are viable and display no obvious lung phenotype (66). Changes in endogenous *Fgf10* expression have been correlated with disease progression and/or repair after lung injury both in mice and humans (43,44,46). Evidence for such a role for Fgf7 in the embryonic or adult lung in humans or mice is still lacking despite the fact that Fgf7 was discovered seven years before Fgf10 (67,68).

Another critical question is whether it matters if mesenchymal niche cells express Fgf7 vs. Fgf10 as they are both ligands acting through Fgfr2b. Indeed, it does matter as Fgf7 and Fgf10, although belonging to the same Fgf subfamily of paracrine growth factors, elicit different biological activities on isolated lung epithelium grown in Matrigel in vitro (41). During the process of lung branching, Fgf10 induces the formation of new buds by process of chemotaxis. At the same time, Fgf7 triggers the proliferation of the epithelium leading to the shape of a cyst-like structure. Mass spectrometry studies demonstrated that Fgf10 differentially stimulated the phosphorylation of tyrosine 734 of Fgfr2b and the recruitment of the SH3-domain-binding protein 4 (SH3bp4) (69). Tyrosine 734 phosphorylation controlled the trafficking route of the receptor after internalization, allowing receptor recycling at the cell surface and sustained Akt and Shc phosphorylation. Knockdown of SH3bp4 or ectopic expression of a Y734F-mutated form of Fgfr2b in lung explants cultured in vitro modified the biological activity triggered by Fgf10 from chemotactic (bud formation) to proliferative (cyst-like structure).

5.3 The activity of the rMc-Sca1^{Pos} cells is impacted by obesity and gender

In the context of lung fibrosis, the accumulation of activated MYF-producing extracellular matrix components modifies the lung structure and negatively impacts gas exchange. The LIF to MYF reversible differentiation switch appears to be a critical process in fibrosis formation and resolution. Moreover, this transition was also shown in vitro in response to hyperoxia as an important event in bronchopulmonary dysplasia (BPD). AT2 cells express angiotensin-converting enzyme II (ACEII), the main receptor for SARS-CoV-2 (70). Interestingly, SARS-CoV-2 induces the expression of transforming growth factor β (TGF- β) (71), which has been described to trigger the LIF to activated MYF transition. Such transition can be reversed by administering a PPARγ agonist (Rosiglitazone) and the antidiabetic drug metformin (33,72).

Interestingly, metabolic dysregulation such as the one observed in obese patients has been associated with a worst prognostic in the case of COVID-19. A similar conclusion has been reached for gender as well as for age. Indeed, we can detect the impact of obesity and gender on the functionality of the rMC-Sca1^{Pos} cells to sustain AT2 stem cell proliferation and differentiation. Our findings open the way to screen for drugs capable of restoring the stromal niche capabilities.

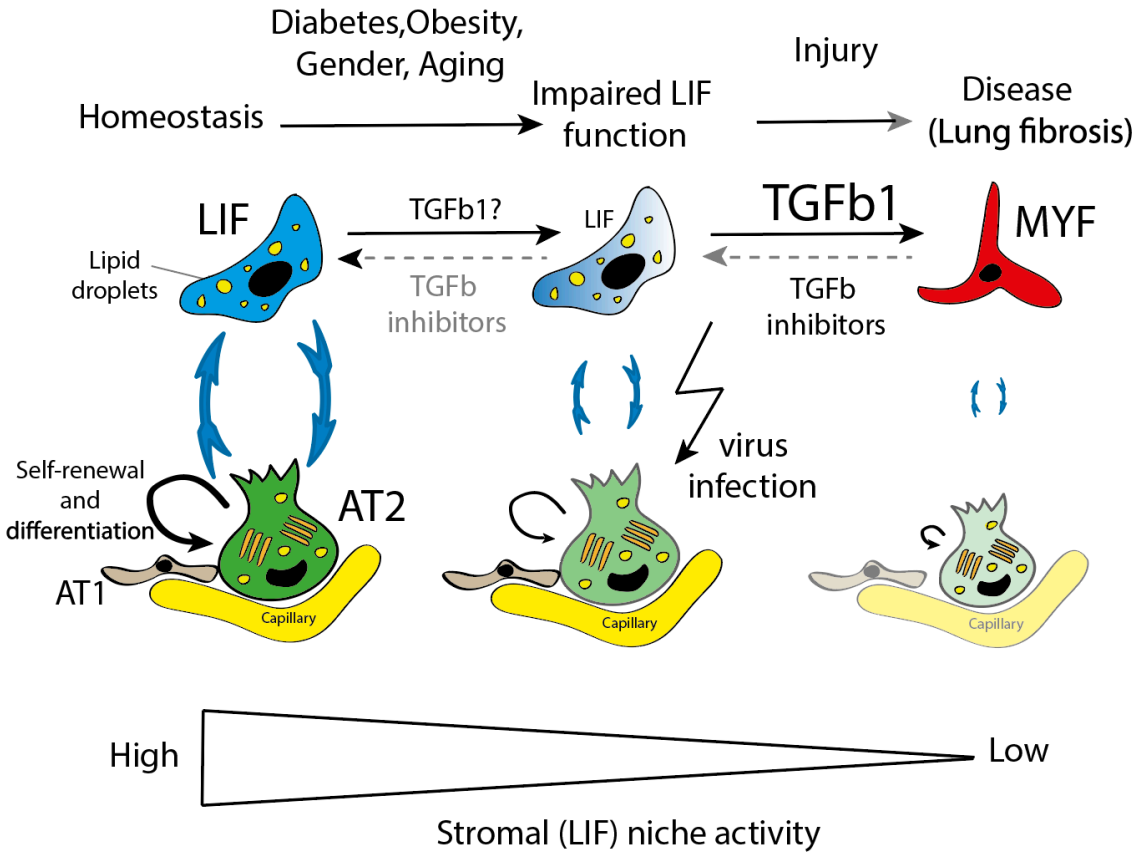

Figure 17: LIF is an important mesenchymal population supporting AT2 stem cells in terms of self-renewal and differentiation to AT1 cells. LIF cells provide lipid droplets to AT2 for the elaboration of surfactant. Diabetes, obesity, aging, and gender are proposed to be the main factors impacting negatively the stromal (LIF) niche activity. Following injury, impaired LIF will transdifferentiate to activated myofibroblast (MYF). Accumulation of MYF is a main characteristic of lung fibrosis which over time, in particular in old age, leads to failure of lung function. Moreover, AT2 cells are the main target of virus infection which drastically reduce their function in terms of surfactant protein production. TGFß is a causative growth factor for fibrosis induction and maintenance. We propose that TGFß inhibitors could be instrumental in restoring impaired LIF function in the context of diabetes, obesity, gender and aging as well as in the MYF to LIF transdifferentiation in the context of fibrosis.

5.4 The impact of rFGF10 on rMC in the BPD model

So far, there are no therapies for bronchopulmonary dysplasia (BPD), a respiratory disease occurring in preterm infants. As a high morbidity and mortality rate characterize this disease, such treatments are urgently needed. Symptomatic treatments for BPD include innovative ventilation strategies, corticosteroids, surfactant-replacement, caffeine, vitamin A, treatment with a bronchodilator, and stem cell therapy (73).

The holy grail in the field of lung regeneration is to identify drugs capable of jump-start alveoli formation after injury. In this context, the BPD model, with its permanent arrest in lung development at the saccular stage, is ideal for testing drugs that display this capability. The read-out for this de-novo alveologenesis process, primarily based on morphometry analysis, is reliable, easy to perform, and informative. In this context, we have confirmed, using translational approaches, that FGF10 can induce alveologenesis following HYX treatment. This original observation is in line with published evidence establishing that 1) FGF10 expression is decreased in lungs of patients with BPD and could therefore be causative for the diseases and that 2) decrease in *Fgf10* expression in mice leads, upon exposure to HYX, to a worsening of the structural defects and lethality. Fgf10 acts both on the epithelium and mesenchyme (31). Fgf10 acts on the alveolar progenitor during development to control their proliferation and differentiation along the alveolar type 2 lineage (14,16,74). Fgf10 also serves as lung mesenchymal progenitors to control their differentiation towards the lipofibroblast lineage (31). Suggesting a crucial role for Fgf10 in regulating the proliferation and differentiation of AT2 stem cells in the adult lung, we recently refined the resident mesenchymal cells (defined as $Cd45^{Neg}Cd31^{Neg}Epcam^{Neg}$), eliciting this activity in vitro using the alveolosphere model.

We found that rMC $Sca1^{Pos}Fgf10^{Pos}$ cells were the rMC subpopulation displaying most of the activity. These cells were defined as a niche for AT2 stem cells (56). Given our recent discovery that the niche activity of rMC $Sca1^{Pos}$ cells was impacted by metabolic dysfunction, gender (56).

We initially quantified the activity level of rMC Sca1^{Pos} cells in the context of NOX and HYX exposure at P45, one month after the HYX exposure. We found a significant drop in the niche activity in the HYX group, and interestingly, this activity could be partially restored by FGF10 administration. scRNAseq analysis of the rMC Sca1^{Pos} cells in the context of NOX and HYX allows to identify a subpopulation of the rMC Sca1^{Pos} cells, which co-expressed specifically *Fgf10* and *Fgf7*. Based on the expression of these two markers, we propose that these cells represent the *bona fide* niche for AT2 stem cells. Interestingly, these cells can be grouped in 2 sub-clusters (cluster 2 and 6) belonging to the Lipofibroblast cluster. As the analysis was done at P45, the difference in gene expression between the HYX and NOX groups was not noticeable. However, we did notice a shrinking in the respective number for these two sub-clusters in HYX compared to NOX, indicating that HYX could have a quantitative impact at the level of these 2 sub-clusters. Interestingly, a global effect on the rMC Sca1^{Pos} cells was observed upon HYX, and this impact was corrected upon FGF10 treatment.

In the future, more work will have to be done to better characterize these two sub-clusters at earlier time points following HYX exposure. In addition, a genetic model using dual Dre/Cre recombinase strategies will have to be established to specifically lineage-trace and characterize these two subpopulations. In that respect, the Fgf10^{CreERT2} line that we recently generated and validated (75) will be instrumental in targeting the rMC Sca1^{Pos}Fgf10^{Pos} cells. Other Dre lines with genes explicitly expressed in clusters 2 or 6 will be generated and validated.

5.5 The impact of hyperoxia injury on rMC-Sca1^{Pos}

Recently, scRNAseq data on total cells from HYX and NOX lungs at the different time points (3, 7, and 14) during HYX exposure (85%O_2) were reported (76). Dynamic changes triggered by HYX of the transcriptomic profiles in all subpopulations (including the alveolar epithelium, the resident mesenchymal cells, the endothelium and the macrophages) were observed. The authors concluded that HYX-induced inflammation was the main force behind these changes. Subsequently, using this dataset, the authors analyzed a minimal number of rMC Sca1^{Pos} cells (which in their paper are named Ly6a positive resident lung mesenchymal stromal cells or Ly6a^{Pos} L-MCSs).

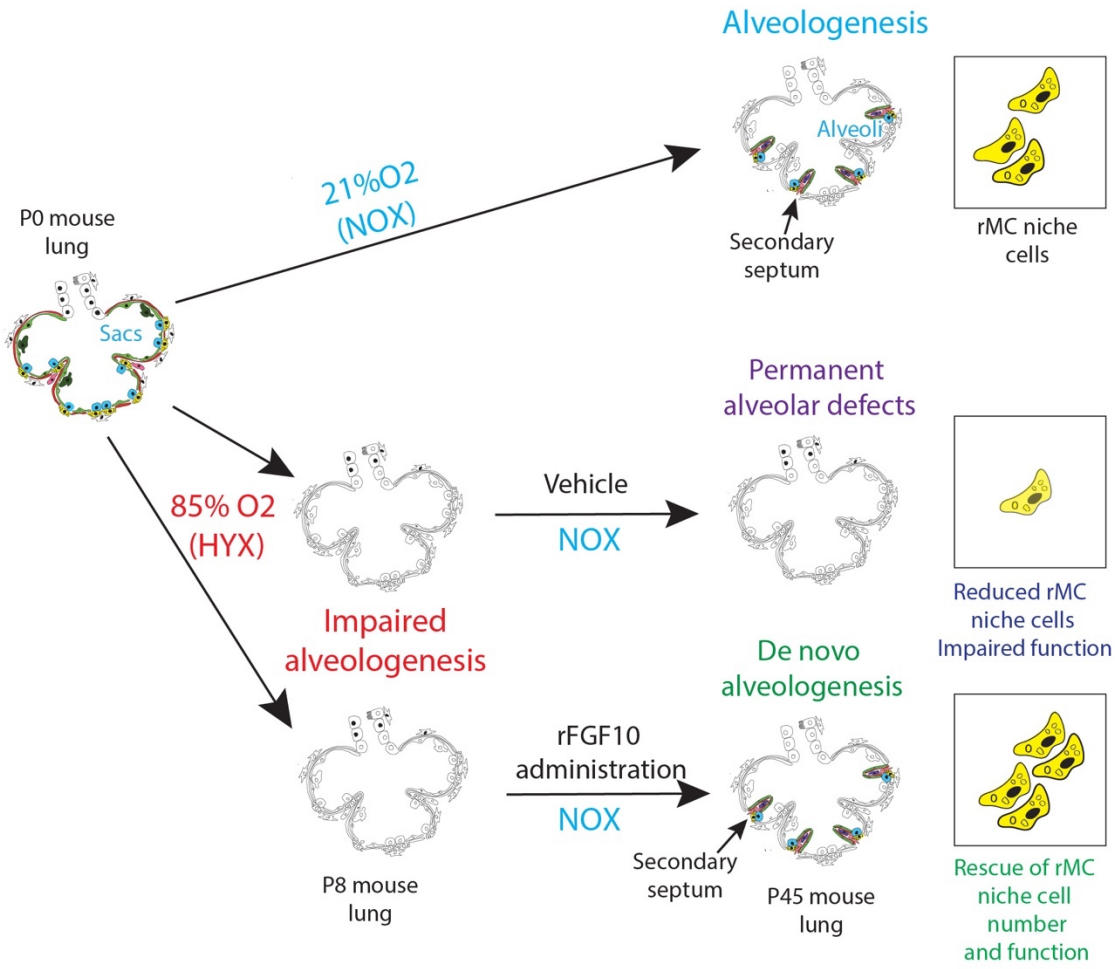

Figure 18. The impact of hyperoxia injury on resident mesenchymal (rMC) niche cells
C57BL6 pups belonging to the control group were maintained under room air (NOX 21% O_2). The lungs from these pups transition from the saccular to the alveolar stage with the formation of secondary septa characteristic of alveologenesis. In the experimental group, pups were exposed to HYX (85% O_2) from P0 to P8. At P8, pups were re-exposed to NOX and subsequently divided into two groups, either receiving vehicle (PBS) or rFGF10 via intraperitoneal injections (i.p). In the PBS group, injury results in permanent structural lung defects with reduced rMC niche cells and impaired function. In the FGF10 group, the lungs underwent de novo alveologenesis and displayed rescued rMC niche cells in terms of number and function thereby supporting the use of FGF10 as a therapy for BPD.

They found that these cells express Lumican and Ly6a at a high level and would therefore be matching clusters 2 and 6 in our study). The authors report that HYX exposure increases the number of these cells and alters their expression profile with the induction of pro-inflammatory, pro-fibrotic, and anti-angiogenic genes (77). While this analysis describes the behavior of the rMC Sca1^{Pos} cells during acute injury, our study focuses on the status of these cells during the following ”recovery” phase, as the animals are re-exposed to room air.

Our analysis also allowed us to further refine the rMC Sca1^{Pos} population into 18 clusters, from which only five belong to the LIF cluster. Due to the low number of rMC Sca1^{Pos} cells analyzed by Mizokova et al., it is challenging to state whether all the 18 clusters are increased or if this increase is differentially impacting the rMC Sca1^{Pos} clusters, with an increase in the MYF and ECM-producing cell clusters and a decrease in the LIF cluster. This is an essential aspect as only roughly 30% of the rMC Sca1^{Pos} cells corresponding to the LIF cluster display active niche activity (56).

In the future, a more detailed and powered analysis combining scRNAseq and functional assays of rMC Sca1^{Pos} cells at different time points during injury and recovery and FGF10 treatment will be crucial to nail down the impact of HYX on relevant rMC Sca1^{Pos} subpopulations. In conclusion, we demonstrate that FGF10 administration is curative for BPD and identified a subpopulation of rMC-Sca1^{Pos} niche cells representing its cellular target.

6. Summary

In mice's developing and mature lungs, the interaction between mesenchyme and epithelium is critical. Epithelial cells follow their fate during development and will either increase or decrease depending on the circumstances. On the other hand, the mesenchyme takes on varied roles and activities depending on its microenvironment. Considering this plasticity of fibroblasts, it is crucial to define the heterogeneity of lung mesenchyme. Furthermore, multiple studies have demonstrated the overlap of gene expression among mesenchyme and even in non-mesenchyme.

This study defined the resident mesenchyme stromal niche as rMC-Sca1^{Pos} (Cd45^{neg}Cd31^{neg}Epcam^{neg}Sca1^{Pos}). Co-culture of mature AT2 with rMC-Sca1^{Pos} and rMC-Sca1^{Neg} showed that only rMC-Sca1^{Pos} culture led to alveolosphere formation. In contrast, rMC-Sca1^{Neg} fails to support AT2 cells maintenance. Therefore, in further study, we used only rMC-Sca1^{Pos} to sort different subsets and test them in organoid culture. Using LipidTOX staining, we found three different levels of lipid-containing cells representing LIF subsets in the Sca1^{Pos} population. Among three subsets, we used rMCs-Sca1^{Pos}LT^{High} and rMCs-Sca1^{Pos}LT^{Neg} to combine with AT2 (Lyso^{Pos}Tom^{Pos}) to test these two subsets functionally. rMCs-Sca1^{Pos}LT^{High} shows organoid formation in comparison with rMCs-Sca1^{Pos}LT^{Neg}. Our results also indicate a trend toward an increase in the expression of *Fgf10* and *Pdgfra* in rMCs-Sca1^{Pos}LT^{High} compared to rMCs-Sca1^{Pos}LT^{Neg}.

To investigate the role of *Fgf10* positive cells to support AT2 cells, we used the *Fgf10^{LacZ}* reporter line to sort FDG^{Pos}Sca1^{Pos} and FDG^{Neg}Sca1^{Pos} subsets from rMCs. Our results indicate that rMCs-Sca1^{Pos}Fgf10^{Pos} represents around 33% of the rMCs-Fgf10^{Pos} and 25% of the rMCs-Sca1^{Pos}. We observed the organoid formation only in Sca1^{Pos}Fgf10^{Pos}, and this data indicates the heterogeneity in both Fgf10 and Sca1 populations. Another subset represents in the mesenchyme of the alveolar region is Axin2^{Pos}, which has previously shown that this subset. Axin2^{Pos}Pdgfra^{Pos} cells are playing a role as a niche for AT2 cells.

To refine better the heterogeneity in the alveolar region, this question will arise whether there is any overlap between rMCs-Sca1^{Pos}Fgf10^{Pos} and rMCs-Sca1^{Pos}Axin2^{Pos} subsets.

We, therefore, exploit two reporter lines, *Fgf10*^{LacZ} and *Axin2*^{LacZ} mice, to carry out gene array analysis. We found genes differentially regulated between these two subsets at the transcriptomic level. And in lipid-containing levels by using LipidTOX staining, we could quantify by flow cytometry that 85% of Sca1^{Pos}Fgf10^{Pos} and 100% of Sca1^{Pos}Axin2^{Pos} are representing LT^{High} in two subsets. This evidence confirms our previous results in this study in the context of mesenchymal heterogeneity.

We used *Fgf10* and *Fgf7* mRNA probes in the RNA Scope experiment, one marker for MANC (Axin2^{Pos}Pdgfra^{Pos}) combined with IF staining against Pro-SPC. We found that 28% ± 0.5% (n = 3) of total *Fgf10* expressing cells versus 2.0% ± 0.2% (n = 3) of *Fgf7* expressing cells are located close to pro-SPC expressing cells.

In the context of lung disease, we employed ob/ob and C57B/L6 mice to investigate rMC activity in the setting of organoid creation to show how pre-existing risk factors like obesity/diabetes and gender contribute to a chronic lung illness. We also functionally tested the rMCs-Sca1^{Pos} from these different mice by co-culturing them with sorted AT2 cells using the alveolosphere assay. When the rMCs-Sca1^{Pos} are isolated from *ob/ob* male mice presenting the two risk factors, obesity and male (Figure 12B), we observed a complete absence of organoid formation. However, rMCs-Sca1^{Pos} from female ob/ob culture mice shows organoid formation. Interestingly, we observed a drastic reduction in Sca1^{Pos} percentiles in flow cytometry analysis.

Next, we used the BPD model to investigate the regeneration capacity of rMCs after exposure to injury. Bronchopulmonary dysplasia (BPD) is a neonatal lung disease developing in premature babies characterized by arrested alveologenesis and associated with decreased Fibroblast growth factor 10 (FGF10) expression. One-week hyperoxia (HYX) exposure of newborn mice leads to a permanent arrest in alveologenesis. We used recombinant FGF10 to test the role of Fgf10 signaling to improve alveologenesis in the BPD model.

Key findings from the BPD model as read out from rFGF10 administration, alveolosphere 3D *in vitro* model, and scRNA-seq analysis show that:

- Recombinant FGF10 improved hemodynamic measurements and alveologenesis.

- Alveolosphere assays indicate that the activity of rMC-Sca1^{Pos} is negatively impacted by HYX and partially rescued by FGF10 treatment.

- Analysis by IF demonstrates that the significant impact of FGF10 is on the resident mesenchymal cells and not on AT2s.

- scRNAseq results identified clusters expressing *Fgf10*, *Fgf7*, *Pdgfra,* and *Axin2,* representing the rMC niche cells for the AT2 stem cells.

In conclusion, we demonstrate that FGF10 administration is curative for BPD and identified a subpopulation of rMC-Sca1^{Pos} niche cells potentially representing its cellular target.

7. Zussamungfassung

In der sich entwickelnden und reifen Lunge von Mäusen ist die Wechselwirkung zwischen Mesenchym und Epithel entscheidend.

Während der Entwicklung folgen Epithelzellen ihrer Schicksalsentscheidung und nehmen je nach den Umständen entweder zu oder ab. Das Mesenchym hingegen übernimmt je nach Mikroumgebung unterschiedliche Rollen und Aktivitäten. Angesichts dieser Plastizität von Fibroblasten ist es sehr wichtig, die Heterogenität des Lungenmesenchyms zu definieren. Mehrere Studien haben die Überschneidung der Genexpression zwischen Mesenchym und sogar in Nicht-Mesenchym gezeigt.

In dieser Studie haben wir die ansässige Mesenchym-Nische als rMC-Sca1Pos ($Cd45^{Neg}Cd31^{Neg}Epcam^{Neg}Sca1^{Pos}$) definiert. Die Kokultur von reifem AT2 mit rMC-$Sca1^{Pos}$ und rMC-$Sca1^{Neg}$ zeigte, dass nur die rMC-$Sca1^{Pos}$-Kultur zur Alveolosphärenbildung führte, im Gegensatz dazu konnte rMC-$Sca1^{Neg}$ die Aufrechterhaltung der AT2-Zellen nicht unterstützen. Daher haben wir in weiteren Studien nur rMC-$Sca1^{Pos}$ verwendet, um verschiedene Teilmengen zu sortieren und in Organoid kultur zu testen. Unter Verwendung von LipidTOX-Färbung fanden wir drei verschiedene Niveaus von lipidhaltigen Zellen, die LIF-Untergruppen in der $Sca1^{Pos}$-Population darstellen. Unter drei Teilmengen haben wir rMCs-$Sca1^{Pos}LT^{High}$ und rMCs-$Sca1^{Pos}LT^{Neg}$ verwendet, um sie mit AT2 ($Lyso^{Pos}Tom^{Pos}$) zu kombinieren, um diese beiden Teilmengen funktionell zu testen.

rMCs-$Sca1^{Pos}LT^{High}$ zeigt im Vergleich zu rMCs-$Sca1^{Pos}LT^{Neg}$ eine Organoidbildung. Unsere Ergebnisse zeigen auch einen Trend zu einer Zunahme der Expression von Fgf10 und Pdgfra in rMCs-$Sca1^{Pos}LT^{High}$ im Vergleich zu rMCs-$Sca1^{Pos}LT^{Neg}$.

Um die Rolle von Fgf10-positiven Zellen bei der Unterstützung von AT2-Zellen zu untersuchen, verwendeten wir die Fgf10LacZ-Reporterlinie, um FDGPosSca1Pos- und $FDG^{Neg}Sca1^{Pos}$-Untergruppen von rMCs zu sortieren. Unsere Ergebnisse zeigen, dass rMCs-$Sca1^{Pos}Fgf10^{Pos}$ etwa 33 % der rMCs-Fgf10Pos und 25 % der rMCs-$Sca1^{Pos}$ darstellt. Da wir die Organoidbildung nur in $Sca1^{Pos}Fgf10^{Pos}$ beobachtet haben, weisen diese Daten auf die

Heterogenität sowohl in Fgf10- als auch in Sca1-Populationen hin. Eine weitere Untergruppe, die im Mesenchym der Alveolarregion vertreten ist, ist Axin2Pos, von der zuvor gezeigt wurde, dass diese Untergruppe Axin2PosPdgfraPos-Zellen eine Rolle als Nische für AT2-Zellen spielt.

Um die Heterogenität in der Alveolarregion besser zu verfeinern, stellt sich die Frage, ob es eine Überlappung zwischen den Untergruppen rMCs-Sca1PosFgf10Pos und rMCs-$Sca1^{Pos}Axin2^{Pos}$ gibt. Wir nutzen daher zwei Reporterlinien aus; $Fgf10^{LacZ}$- und $Axin2^{LacZ}$-Mäuse, um eine Gen-Array-Analyse durchzuführen.

Auf transkriptomischer Ebene fanden wir Gene, die zwischen diesen beiden Untergruppen unterschiedlich reguliert wurden. Und im Lipidgehalt konnten wir mithilfe von LipidTOX-Färbung durch Durchflusszytometrie quantifizieren, dass 85 % von $Sca1^{Pos}Fgf10^{Pos}$ und 100 % von $Sca1^{Pos}Axin2^{Pos}$ LT^{High} in zwei Teilmengen darstellen. Dieser Beweis bestätigt unsere früheren Ergebnisse in dieser Studie im Zusammenhang mit mesenchymaler Heterogenität.

Im RNA-Scope-Experiment verwendeten wir *Fgf10*- und *Fgf7*-mRNA-Sonden, einen Marker für MANC ($Axin2^{Pos}Pdgfra^{Pos}$), kombiniert mit IF-Färbung gegen Pro-SPC. Wir fanden heraus, dass 28 % ± 0,5 % (n = 3) der gesamten Fgf10-exprimierenden Zellen gegenüber 2,0 % ± 0,2 % (n = 3) der Fgf7-exprimierenden Zellen in der Nähe von pro-SPC-exprimierenden Zellen lokalisiert sind.

Im Zusammenhang mit Lungenerkrankungen haben wir ob/ob- und C57B/L6-Mäuse eingesetzt, um die rMC-Aktivität im Rahmen der Organoidbildung zu untersuchen, um zu zeigen, wie bereits bestehende Risikofaktoren wie Fettleibigkeit/Diabetes und Geschlecht zu chronischen Lungenerkrankungen beitragen. Wir haben auch die rMCs-$Sca1^{Pos}$ dieser verschiedenen Mäuse funktionell getestet, indem wir sie mit sortierten AT2-Zellen unter Verwendung des Alveolosphären-Assays co-kultiviert haben. Wenn die rMCs-$Sca1^{Pos}$ aus männlichen Ob/Ob-Mäusen isoliert werden, die die beiden Risikofaktoren Fettleibigkeit und Männchen aufweisen (Abbildung 12B), beobachteten wir ein vollständiges Fehlen einer Organoidbildung. rMCs-$Sca1^{Pos}$ aus weiblichen ob/ob-Kulturmäusen zeigt jedoch eine Organoidbildung. Interessanterweise beobachteten wir bei der durchflusszytometrischen Analyse eine drastische Verringerung der $Sca1^{Pos}$-Perzentile.

Als nächstes verwendeten wir das BPD-Modell, um die Regenerationsfähigkeit von rMCs nach einer Verletzung zu untersuchen. Die bronchopulmonale Dysplasie (BPD) ist eine neonatale Lungenerkrankung, die sich bei Frühgeborenen entwickelt und durch eine angehaltene Alveogenese gekennzeichnet ist und mit einer verminderten Expression des Fibroblasten-Wachstumsfaktors 10 (FGF10) einhergeht. Eine einwöchige Hyperoxie (HYX)-Exposition neugeborener Mäuse führt zu einem dauerhaften Stillstand der Alveogenese. Wir verwendeten rekombinantes FGF10, um die Rolle der Fgf10-Signalgebung zur Verbesserung der Alveogenese im BPD-Modell zu testen.

Die wichtigsten Ergebnisse des BPD-Modells, die aus der rFGF10-Verabreichung, dem Alveolosphären-3D-In-vitro-Modell und der scRNA-seq-Analyse hervorgehen, zeigen Folgendes:

• Rekombinantes FGF10 verbesserte hämodynamische Messungen und Alveogenese.

• Alveolosphären-Assays weisen darauf hin, dass die Aktivität von rMC-Sca1^{Pos} durch HYX negativ beeinflusst und durch FGF10-Behandlung teilweise wiederhergestellt wird.

• Die Analyse von IF zeigt, dass der signifikante Einfluss von FGF10 auf die ansässigen mesenchymalen Zellen und nicht auf AT2s erfolgt.

8. References

1. Cardoso W V., Lü J. Regulation of early lung morphogenesis: Questions, facts and controversies. Development. 2006;133(9):1611–24.
2. (No Title). 2020 [cited 2020 Jun 17]; Available from: www.atsjournals.org.
3. Morrisey EE, Hogan BLM. Preparing for the First Breath: Genetic and Cellular Mechanisms in Lung Development. Dev Cell [Internet]. 2010;18(1):8–23. Available from: http://dx.doi.org/10.1016/j.devcel.2009.12.010
4. Warburton D. Conserved Mechanisms in the Formation of the Airways and Alveoli of the Lung. Front Cell Dev Biol. 2021 Jun 15;9.
5. Branchfield K, Li R, Lungova V, Verheyden JM, McCulley D, Sun X. A three-dimensional study of alveologenesis in mouse lung. Dev Biol [Internet]. 2016 [cited 2020 Aug 5];409(2):429–41. Available from: http://dx.doi.org/10.1016/j.ydbio.2015.11.017
6. Hogan BLM, Barkauskas CE, Chapman HA, Epstein JA, Jain R, Hsia CCW, et al. Repair and regeneration of the respiratory system: Complexity, plasticity, and mechanisms of lung stem cell function. Cell Stem Cell [Internet]. 2014;15(2):123–38. Available from: http://dx.doi.org/10.1016/j.stem.2014.07.012
7. Herriges M, Morrisey EE. Lung development: Orchestrating the generation and regeneration of a complex organ. Dev. 2014;141(3):502–13.
8. Ornitz DM, Yin Y. Signaling networks regulating development of the lower respiratory tract. Cold Spring Harb Perspect Biol. 2012;4(5):4.
9. Torday JS, Rehan VK. On the evolution of the pulmonary alveolar lipofibroblast. Exp Cell Res. 2016;340(2):215–9.
10. Zepp JA, Morley MP, Loebel C, Kremp MM, Chaudhry FN, Basil MC, et al. Genomic, epigenomic, and biophysical cues controlling the emergence of the lung alveolus. Science (80-). 2021;371(6534).
11. Mailleux AA, Kelly R, Veltmaat JM, De Langhe SP, Zaffran S, Thiery JP, et al. Fgf10 expression identifies parabronchial smooth muscle cell progenitors and is required for their entry into the smooth muscle cell lineage. Development. 2005;132(9):2157–66.
12. Weaver M, Batts L, Hogan BLM. Tissue interactions pattern the mesenchyme of the embryonic mouse lung. Dev Biol. 2003;258(1):169–84.

13. S. Bellusci JGHENIBLH. Fibroblast growth factor 10 (FGF10) and branching morphogenesis in the embryonic mouse lung.
14. Jones MR, Dilai S, Lingampally A, Chao CM, Danopoulos S, Carraro G, et al. A comprehensive analysis of fibroblast growth factor receptor 2b signaling on epithelial tip progenitor cells during early mouse lung branching morphogenesis. Front Genet. 2019;10(JAN):1–20.
15. Taghizadeh S, Jones MR, Olmer R, Ulrich S, Danopoulos S, Shen C, et al. Fgf10 Signaling-Based Evidence for the Existence of an Embryonic Stage Distinct From the Pseudoglandular Stage During Mouse Lung Development. Front Cell Dev Biol. 2020;8(October):1–13.
16. Jones MR, Lingampally A, Dilai S, Shrestha A, Stripp B, Helmbacher F, et al. Characterization of Tg(Etv4-GFP)and Etv5RFP reporter lines in the context of fibroblast growth factor 10 signaling during mouse embryonic lung development. Front Genet. 2019;10(MAR):1–12.
17. Chao CM, Yahya F, Moiseenko A, Tiozzo C, Shrestha A, Ahmadvand N, et al. Fgf10 deficiency is causative for lethality in a mouse model of bronchopulmonary dysplasia. J Pathol. 2017;241(1):91–103.
18. Benjamin JT, Smith RJ, Halloran BA, Day TJ, Kelly DR, Prince LS. FGF-10 is decreased in bronchopulmonary dysplasia and suppressed by Toll-like receptor activation. Am J Physiol - Lung Cell Mol Physiol. 2007;292(2):550–8.
19. Barkauskas CE, Cronce MJ, Rackley CR, Bowie EJ, Keene DR, Stripp BR, et al. Type 2 alveolar cells are stem cells in adult lung. J Clin Invest. 2013 Jul 1;123(7):3025–36.
20. Rock JR, Hogan BLM. Epithelial progenitor cells in lung development, maintenance, repair, and disease. Annu Rev Cell Dev Biol. 2011;27:493–512.
21. Rock JR, Barkauskas CE, Cronce MJ, Xue Y, Harris JR, Liang J, et al. Multiple stromal populations contribute to pulmonary fibrosis without evidence for epithelial to mesenchymal transition. Proc Natl Acad Sci U S A. 2011;108(52).
22. Ushakumary MG, Riccetti M, Perl AKT. Resident interstitial lung fibroblasts and their role in alveolar stem cell niche development, homeostasis, injury, and regeneration. Stem Cells Transl Med. 2021;10(7):1021–32.
23. McQualter JL, Brouard N, Williams B, Baird BN, Sims-Lucas S, Yuen K, et al. Endogenous Fibroblastic Progenitor Cells in the Adult Mouse Lung Are Highly Enriched in the Sca-1 Positive Cell Fraction. Stem Cells [Internet]. 2009 Mar [cited 2020 Apr 1];27(3):623–33. Available from:

http://www.ncbi.nlm.nih.gov/pubmed/19074419

24. McQualter JL, McCarty RC, Van der Velden J, O'Donoghue RJJ, Asselin-Labat ML, Bozinovski S, et al. TGF-β signaling in stromal cells acts upstream of FGF-10 to regulate epithelial stem cell growth in the adult lung. Stem Cell Res [Internet]. 2013;11(3):1222–33. Available from: http://dx.doi.org/10.1016/j.scr.2013.08.007
25. Chung M-I, Bujnis M, Barkauskas CE, Kobayashi Y, Hogan BLM. STEM CELLS AND REGENERATION Niche-mediated BMP/SMAD signaling regulates lung alveolar stem cell proliferation and differentiation. 2018;
26. Zepp JA, Zacharias WJ, Frank DB, Cavanaugh CA, Zhou S, Morley MP, et al. Distinct Mesenchymal Lineages and Niches Promote Epithelial Self-Renewal and Myofibrogenesis in the Lung. Cell. 2017 Sep 7;170(6):1134-1148.e10.
27. Lee JH, Tammela T, Hofree M, Choi J, Marjanovic ND, Han S, et al. Anatomically and Functionally Distinct Lung Mesenchymal Populations Marked by Lgr5 and Lgr6. Cell [Internet]. 2017;170(6):1149-1163.e12. Available from: http://dx.doi.org/10.1016/j.cell.2017.07.028
28. Ornitz DM, Itoh N. The fibroblast growth factor signaling pathway. Wiley Interdiscip Rev Dev Biol. 2015;4(3):215–66.
29. Sekine K, Ohuchi H, Fujiwara M, Yamasaki M, Yoshizawa T, Sato T, et al. Fgf10 is essential for limb and lung formation. Nat Genet. 1999;21(1):138–41.
30. El Agha E, Herold S, Alam D Al, Quantius J, MacKenzie BA, Carraro G, et al. Fgf10-positive cells represent a progenitor cell population during lung development and postnatally. Dev. 2014;141(2):296–306.
31. Al Alam D, El Agha E, Sakurai R, Kheirollahi V, Moiseenko A, Danopoulos S, et al. Evidence for the involvement of fibroblast growth factor 10 in lipofibroblast formation during embryonic lung development. Dev. 2015;142(23):4139–50.
32. Park J, Ivey MJ, Deana Y, Riggsbee KL, Sörensen E, Schwabl V, et al. The Tcf21 lineage constitutes the lung lipofibroblast population. Am J Physiol - Lung Cell Mol Physiol. 2019;316(5):L872–85.
33. El Agha E, Moiseenko A, Kheirollahi V, De Langhe S, Crnkovic S, Kwapiszewska G, et al. Two-Way Conversion between Lipogenic and Myogenic Fibroblastic Phenotypes Marks the Progression and Resolution of Lung Fibrosis. Cell Stem Cell. 2017;20(2):261-273.e3.
34. Travaglini KJ, Nabhan AN, Penland L, Sinha R, Gillich A, Sit R V., et al. A molecular cell atlas of the human lung from single-cell RNA sequencing. Nature.

2020;587(7835):619–25.

35. Li R, Bernau K, Sandbo N, Gu J, Preissl S, Sun X. Pdgfra marks a cellular lineage with distinct contributions to myofibroblasts in lung maturation and injury response. Elife. 2018;7:1–20.
36. Hwang JS, Rehan VK. Recent Advances in Bronchopulmonary Dysplasia: Pathophysiology, Prevention, and Treatment. Lung [Internet]. 2018;196(2):129–38. Available from: http://dx.doi.org/10.1007/s00408-018-0084-z
37. Kalikkot Thekkeveedu R, Guaman MC, Shivanna B. Bronchopulmonary dysplasia: A review of pathogenesis and pathophysiology. Vol. 132, Respiratory Medicine. W.B. Saunders Ltd; 2017. p. 170–7.
38. Stoll BJ, Hansen NI, Bell EF, Shankaran S, Laptook AR, Walsh MC, et al. National Institutes of Health Bethesda, Maryland Pediatrics. Pediatrics [Internet]. 2010;126(3):443–56. Available from: http://www.pediatrics.org/misc/reprints.shtml
39. Cerny L, Torday JS, Rehan VK. Prevention and treatment of bronchopulmonary dysplasia: Contemporary status and future outlook. Vol. 186, Lung. 2008. p. 75–89.
40. Choi J, Park JE, Tsagkogeorga G, Yanagita M, Koo BK, Han N, et al. Inflammatory Signals Induce AT2 Cell-Derived Damage-Associated Transient Progenitors that Mediate Alveolar Regeneration. Cell Stem Cell [Internet]. 2020;27(3):366-382.e7. Available from: https://doi.org/10.1016/j.stem.2020.06.020
41. Bellusci S, Grindley J, Emoto H, Itoh N, Hogan BLM. Fibroblast Growth Factor 10 (FGF10) and branching morphogenesis in the embryonic mouse lung. Development. 1997;124(23):4867–78.
42. Gupte V V., Ramasamy SK, Reddy R, Lee J, Weinreb PH, Violette SM, et al. Overexpression of fibroblast growth factor-10 during both inflammatory and fibrotic phases attenuates bleomycin-induced pulmonary fibrosis in mice. Am J Respir Crit Care Med. 2009;180(5):424–36.
43. Volckaert T, Campbell A, Dill E, Li C, Minoo P, De Langhe S. Localized Fgf10 expression is not required for lung branching morphogenesis but prevents differentiation of epithelial progenitors. Dev. 2013;140(18):3731–42.
44. Moiseenko A, Vazquez-Armendariz AI, Kheirollahi V, Chu X, Tata A, Rivetti S, et al. Identification of a Repair-Supportive Mesenchymal Cell Population during Airway Epithelial Regeneration. Cell Rep. 2020;33(12).
45. Klar J, Blomstrand P, Brunmark C, Badhai J, Håkansson HF, Brange CS, et al. Fibroblast growth factor 10 haploinsufficiency causes chronic obstructive pulmonary

disease. J Med Genet. 2011;48(10):705–9.

46. Volckaert T, Yuan T, Chao CM, Bell H, Sitaula A, Szimmtenings L, et al. Fgf10-Hippo Epithelial-Mesenchymal Crosstalk Maintains and Recruits Lung Basal Stem Cells. Dev Cell. 2017;43(1):48-59.e5.
47. Chao CM, El Agha E, Tiozzo C, Minoo P, Bellusci S. A breath of fresh air on the mesenchyme: Impact of impaired mesenchymal development on the pathogenesis of bronchopulmonary dysplasia. Front Med. 2015;2(APR).
48. Chao CM, Moiseenko A, Kosanovic D, Rivetti S, El Agha E, Wilhelm J, et al. Impact of Fgf10 deficiency on pulmonary vasculature formation in a mouse model of bronchopulmonary dysplasia. Hum Mol Genet. 2019;28(9):1429–44.
49. Klinger G, Sirota L, Lusky A, Reichman B. Bronchopulmonary dysplasia in very low birth weight infants is associated with prolonged hospital stay. J Perinatol. 2006;26(10):640–4.
50. Carver BJ, Plosa EJ, Stinnett AM, Blackwell TS, Prince LS. Interactions between NF-κB and SP3 connect inflammatory signaling with reduced FGF-10 expression. J Biol Chem [Internet]. 2013;288(21):15318–25. Available from: http://dx.doi.org/10.1074/jbc.M112.447318
51. Artegiani B, Clevers H. Use and application of 3D-organoid technology. Hum Mol Genet. 2018;27(2):R99–107.
52. Hofer M, Lutolf MP. Engineering organoids. Nat Rev Mater [Internet]. 2021;6(5):402–20. Available from: http://dx.doi.org/10.1038/s41578-021-00279-y
53. Takahashi K, Tanabe K, Ohnuki M, Narita M, Ichisaka T, Tomoda K, et al. Induction of Pluripotent Stem Cells from Adult Human Fibroblasts by Defined Factors. Cell. 2007;131(5):861–72.
54. Barkauskas CE, Chung MI, Fioret B, Gao X, Katsura H, Hogan BLM. Lung organoids: Current uses and future promise. Dev. 2017;144(6):986–97.
55. Surgery M, Hospital S, Surgery M, Key S, Processing F, Park G-Y, et al. Tissue Engineering and Regenerative Medicine T ISSUE E NGINEERING AND R EGENERATIVE M EDICINE Concise Review : Cell-Based Strategies in Bone Tissue Engineering and Regenerative Medicine. Stem Cells Transl Med. 2014;4:1–10.
56. Taghizadeh S, Heiner M, Vazquez-Armendariz AI, Wilhelm J, Herold S, Chen C, et al. Characterization in mice of the resident mesenchymal niche maintaining AT2 stem cell proliferation in homeostasis and disease. Stem Cells. 2021;39(10):1382–94.
57. Roos AB, Barton JL, Miller-Larsson A, Dahlberg B, Berg T, Didon L, et al. Lung

epithelial-C/EBPβ contributes to LPS-induced inflammation and its suppression by formoterol. Biochem Biophys Res Commun [Internet]. 2012;423(1):134–9. Available from: http://dx.doi.org/10.1016/j.bbrc.2012.05.096

58. Mittal M, Tiruppathi C, Nepal S, Zhao YY, Grzych D, Soni D, et al. TNFα-stimulated gene-6 (TSG6) activates macrophage phenotype transition to prevent inflammatory lung injury. Proc Natl Acad Sci U S A. 2016;113(50):E8151–8.
59. Rincon M, Irvin CG. Role of IL-6 in asthma and other inflammatory pulmonary diseases. Int J Biol Sci. 2012;8(9):1281–90.
60. Chapman SJ, Khor CC, Vannberg FO, Rautanen A, Segal S, Moore CE, et al. NFKBIZ polymorphisms and susceptibility to pneumococcal disease in european and african populations. Genes Immun. 2010;11(4):319–25.
61. Voelkel NF, Gomez-Arroyo J. The role of vascular endothelial growth factor in pulmonary arterial hypertension: The angiogenesis paradox. Am J Respir Cell Mol Biol. 2014;51(4):474–84.
62. Sato T, Paquet-Fifield S, Harris NC, Roufail S, Turner DJ, Yuan Y, et al. VEGF-D promotes pulmonary oedema in hyperoxic acute lung injury. J Pathol. 2016;239(2):152–61.
63. Jo U, Whang YM, Kim HK, Kim YH. AKAP12α is AssoCiated with Promoter Methylation in Lung Cancer. Cancer Res Treat. 2006;38(3):144.
64. Lord KA, Abdollahi A, Hoffman-Liebermann B, Liebermann DA. Proto-oncogenes of the fos/jun family of transcription factors are positive regulators of myeloid differentiation. Mol Cell Biol. 1993;13(2):841–51.
65. Torgerson DG, Ballard PL, Keller RL, Oh SS, Huntsman S, Hu D, et al. Ancestry and genetic associations with bronchopulmonary dysplasia in preterm infants. Am J Physiol - Lung Cell Mol Physiol. 2018;315(5):L858–69.
66. Finch PW, Rubin JS, Miki T, Ron D, Aaronson SA. Human KGF is FGF-related with properties of a paracrine effector of epithelial cell growth. Science (80-). 1989;245(4919):752–5.
67. Yamasaki M, Miyake A, Tagashira S, Itoh N. Structure and expression of the rat mRNA encoding a novel member of the fibroblast growth factor family. J Biol Chem [Internet]. 1996;271(27):15918–21. Available from: http://dx.doi.org/10.1074/jbc.271.27.15918
68. Rubin JS, Osada H, Finch PW, Taylor WG, Rudikoff S, Aaronson SA. Purification and characterization of a newly identified growth factor specific for epithelial cells.

Proc Natl Acad Sci U S A. 1989;86(3):802–6.

69. Francavilla C, Rigbolt KTG, Emdal KB, Carraro G, Vernet E, Bekker-Jensen DB, et al. Functional Proteomics Defines the Molecular Switch Underlying FGF Receptor Trafficking and Cellular Outputs. Mol Cell. 2013;51(6):707–22.
70. Kruglikov IL, Scherer PE. The Role of Adipocytes and Adipocyte-Like Cells in the Severity of COVID-19 Infections. Obesity. 2020;28(7):1187–90.
71. Ferreira-Gomes M, Kruglov A, Durek P, Heinrich F, Tizian C, Heinz GA, et al. SARS-CoV-2 in severe COVID-19 induces a TGF-β-dominated chronic immune response that does not target itself. Nat Commun [Internet]. 2021;12(1). Available from: http://dx.doi.org/10.1038/s41467-021-22210-3
72. Kheirollahi V, Wasnick RM, Biasin V, Vazquez-Armendariz AI, Chu X, Moiseenko A, et al. Metformin induces lipogenic differentiation in myofibroblasts to reverse lung fibrosis. Nat Commun. 2019;10(1).
73. Muehlbacher T, Bassler D, Bryant MB. Evidence for the management of bronchopulmonary dysplasia in very preterm infants. Children. 2021;8(4).
74. Jones MR, Lingampally A, Wu J, Sedighi J, Ahmadvand N, Zhang J, et al. Evidence for Overlapping and Distinct Biological Activities and Transcriptional Targets Triggered by. 2020;9(1274):1–19.
75. Chu X, Taghizadeh S, Vazquez-Armendariz AI, Herold S, Chong L, Chen C, et al. Validation of a Novel Fgf10Cre–ERT2 Knock-in Mouse Line Targeting FGF10Pos Cells Postnatally. Front Cell Dev Biol. 2021;9(May):1–13.
76. Hurskainen M, Mižíková I, Cook DP, Andersson N, Cyr-Depauw C, Lesage F, et al. Single cell transcriptomic analysis of murine lung development on hyperoxia-induced damage. Nat Commun. 2021;12(1):1–19.
77. Mižíková I, Lesage F, Cyr-Depauw C, Cook DP, Hurskainen M, Hänninen SM, et al. Single-cell RNA sequencing-based characterization of resident lung mesenchymal stromal cells in bronchopulmonary dysplasia. bioRxiv. 2021;2021.06.18.448928.

9. Supplementary Material

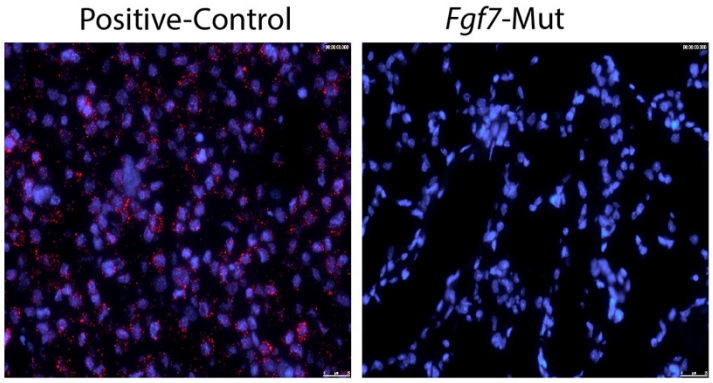

Figure S1. Validation of the *Fgf7* mRNA probe

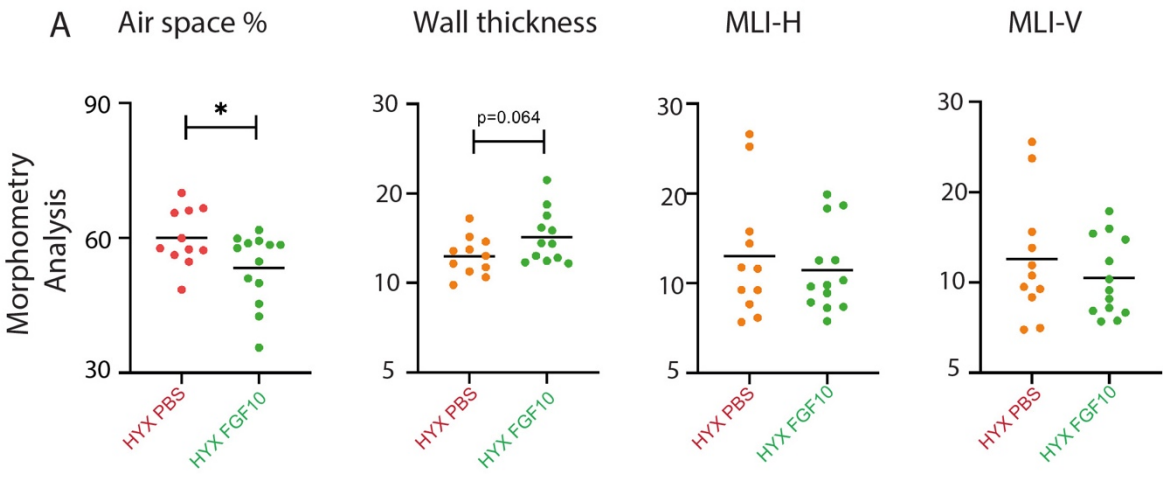

Figure S2: Morphometry quantification of impaired lung in HYX+PBS vs. HYX+FGF10. Student T-test was used to compare the two experimental groups.

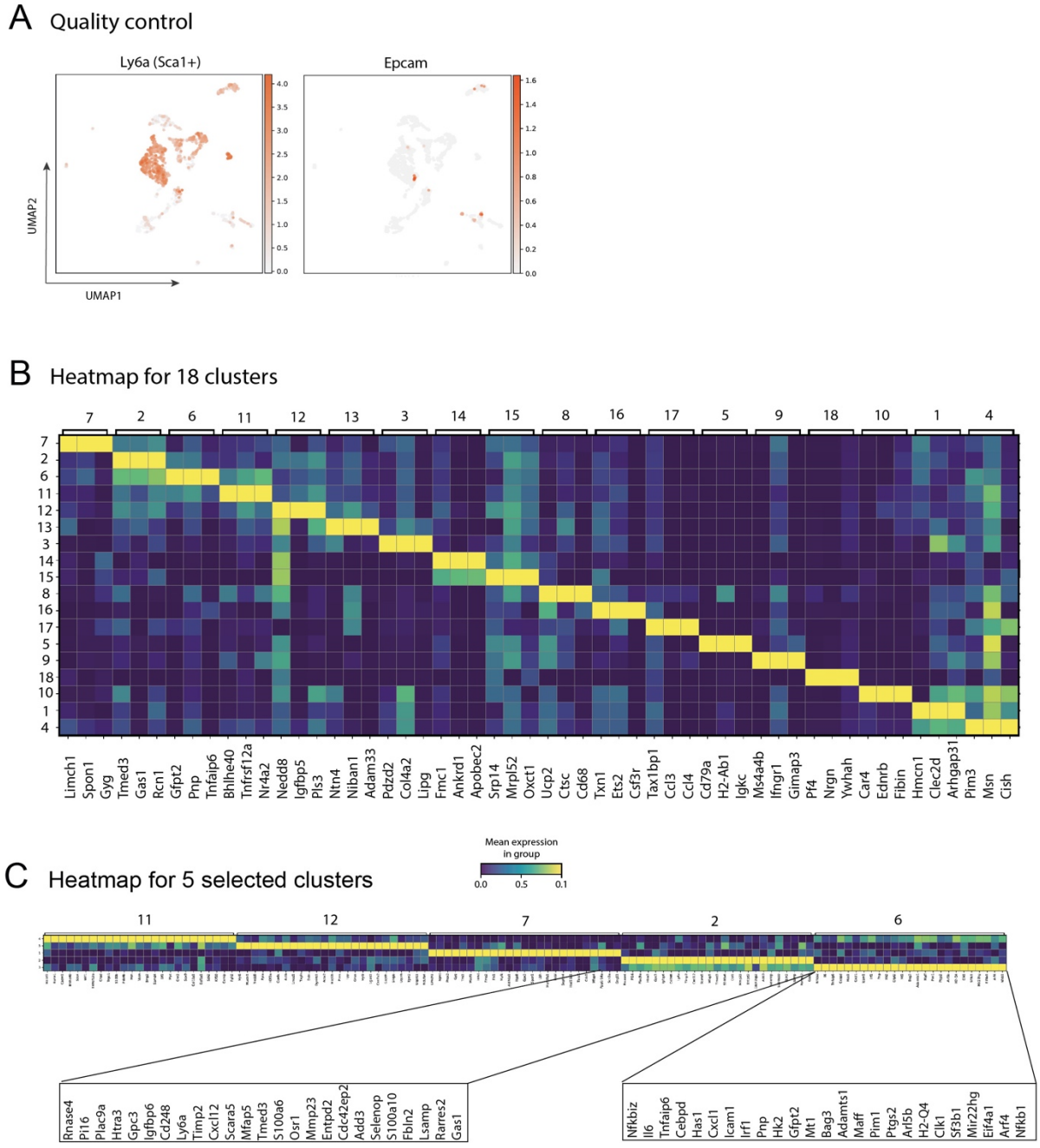

Figure S3: scRNAseq analysis of rMC-Sca1^{Pos} cells in NOX and HYX. A: Expression of Ly6a and Epcam in the UMAP. **B:** Heatmap from differentially expressed genes between the 18 clusters. **C.** Genes enriched in clusters 2 and 6

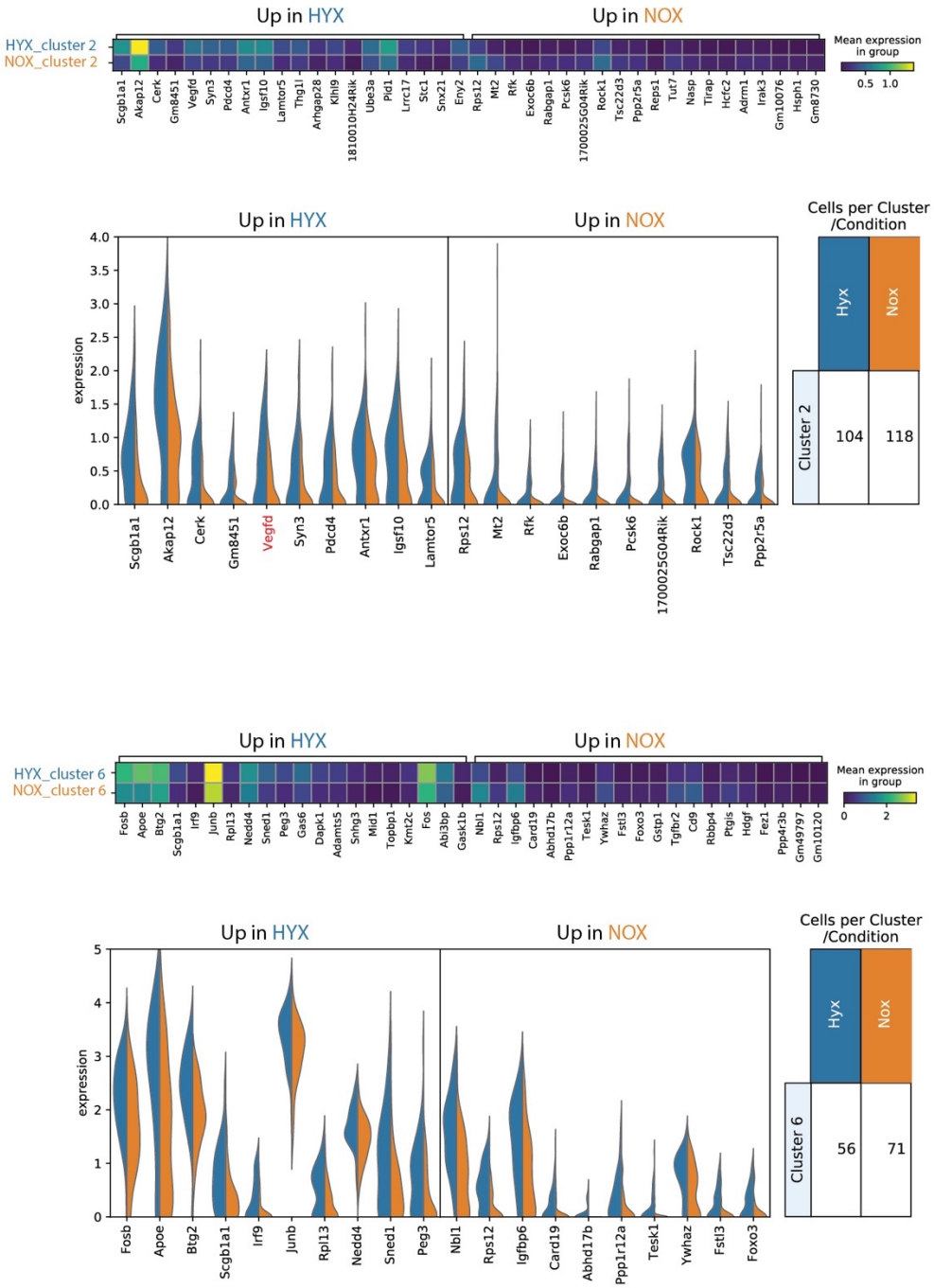

Figure S4: Impact of HYX treatment on cluster 2 and 6. Heatmaps and violin plots of altered gene expression in clusters 2 and 6 in HYX vs. NOX

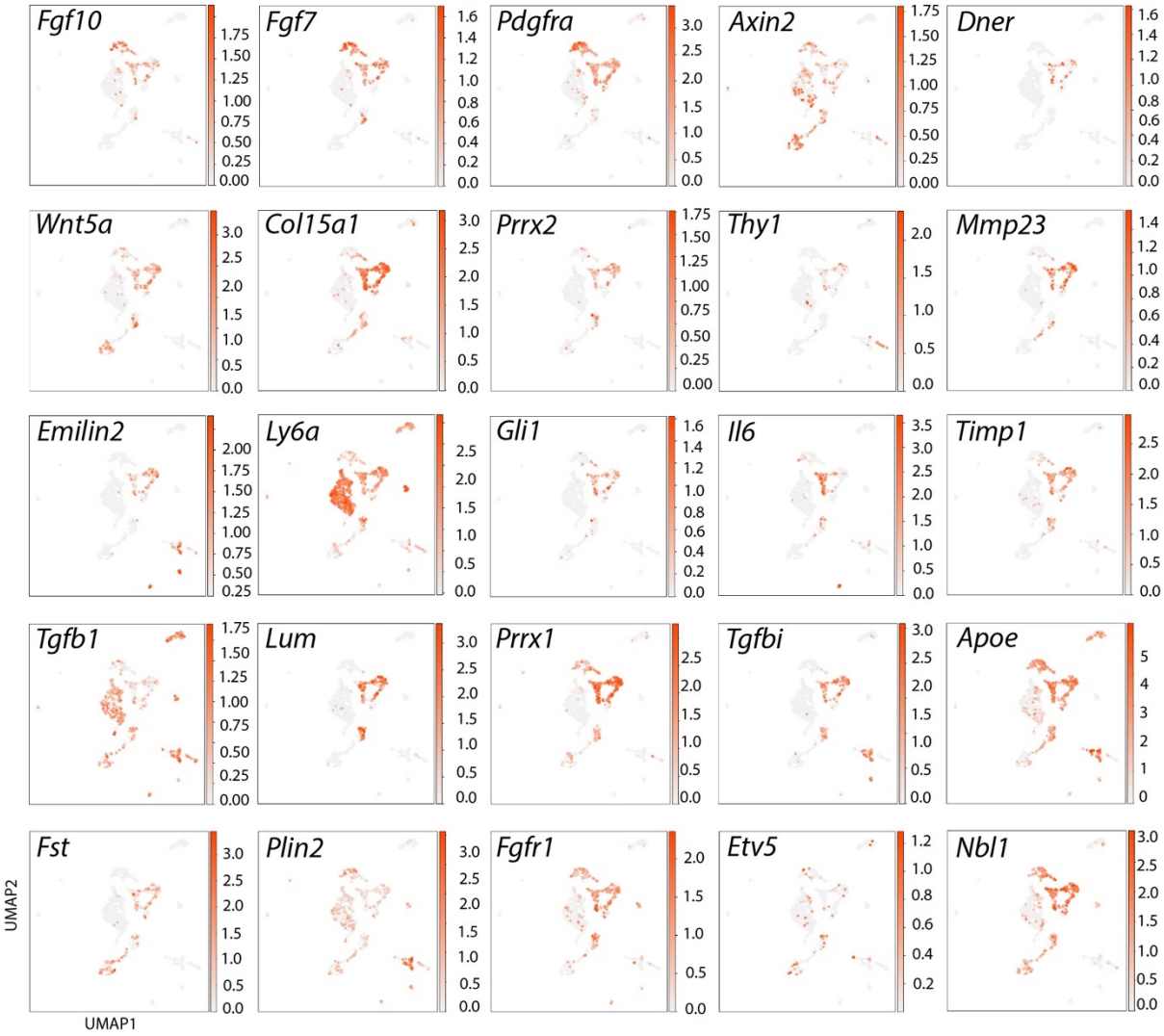

Figure S5: Expression of selected markers on the UMAP

Table S1: KEGG analysis of signalling pathways in Axin2^{Pos} cells vs. Fgf10^{Pos} cells

Name	*-log P*
Metabolic pathways	12.9
RNA transport	4.87
FoxO signaling pathway	3.13
DNA replication	2.50
Mismatch repair	2.07
Influenza A	1.73
ECM-receptor Interaction	1.87
MAPK signaling pathways	1.53
Antigen processing	1.36
Cell cycle	1.26
Fatty acid biosynthesis	1.21
Adipocytokine signaling pathway	1.08
VEGF signaling pathway	1.05

10. Acknowledgements

During my scientific journey, a lot of people gave me kindly their help, advice and encouragement to fulfil my PhD degree. Accomplishing this task without their help would have been very hard for me. Thus, I would like to express my gratitude and appreciation to them in this section.

First of all, I would like to express my deep gratitude to my professor, Saverio Bellusci, for allowing me to do my thesis in his lab. He taught kindly me science word by word. Furthermore, his scientific support, positive mentality, great vision and optimism, flat hierarchy in his lab, and inspiration were phenomenal. For sure, in the future, even now, when I look back and think about these five years, I notice how much I have learned from him and how invaluable this experience is.

Secondly, I would like to thank Heike Habermann and Kerstin Goth for the friendly atmosphere and their administrative help and ensuring that contracts are signed on time and that legal documents are translated. Also, I need to express my appreciation to Kerstin for giving help me with all animal experiments, including taking care of mice, scoring, and ordering animals during the five years of my Ph.D. degree. I would also like to thank Jessica for giving help with genotyping of mice.

I would also like to express my gratitude to Prof. Dr. Behjati who believed in me from the first time we met and continues to support me unconditionally.

I would also like to thank Prof. Werner Seeger, Prof. Rory E. Morty, and Prof. Elie El-Agha for providing me the invaluable experience of joining the Molecular Biology and Medicine of Lung (MBML). During my time in the program, I always enjoyed very productive and interesting seminars, lectures, and also tutorial sessions which provided me with ample opportunities to learn more and more, find new colleagues and even greater friends, participate in the annual retreats to present my work in front of high-level scientists coming from different parts of the world which altogether was a fantastic experience.

I would also like to thank the International Giessen Graduate School committee for the Life Sciences (GGL) and Prof. Baumgart-Vogt for great seminars and events and for establishing a vast social network of young scientists. I would like to thank you to Prof. Dr. Reinhard Dammann for his kind help as co-supervisor through GGL program during my PhD time.

I would like to thank all my colleagues, Negah, Esmeralda, Afshin, Xuran, Matthew, Arun, Stefano and Manuella, and Tayyeb in the Bellusci's lab, for giving me their kind help and contributing to a friendly atmosphere during work. I would also like to thank Prof. Susanne Herold's lab members, Dr. Monika Heiner and Dr. Ana Ivonne Vazquez-Armendariz their support for using the sorter in FACS core. I also acknowledge Dr. Daniel Zahner and animal caretakers Christian Eng, Viktoria Gutjahr, and Martin Stellwagen for their indispensable help. I would also like to thank Dr. Jochen Wilhelm for his assistance in performing the gene arrays and associated data analysis as well as Dr. Thomas Sonntag for his help in preparing the animal protocols.

Many thanks to our collaborators, Prof. Dr. Ulrich Martin (Hannover), Prof. Dr. Denise Al-Alam (USA), Prof. Dr. Laurent Boyer (Paris), Prof. Dr. Cho-Ming Chao (Rostock), and Dr. Stefan Guenther (Bad Nauheim), for their collaboration to complete different projects.

Finally, I would like to express my deep gratitude to my parents and brother Ali, who believed in me and always supported me through all difficulties. Also, I would like to give my special thanks to my sisters for always helping me with their emotional and spiritual support all the way. I would also like to thank my close friends living in Iran for their emotional support and my new friends here for the good times that we spent together. Lastly, I would like to thank Evelyn Bellusci, Prof. Dr. Behjati, and Andres Alberro Brage, who reviewed this dissertation.